

CHAPTER 5

Poisson Voronoi Diagrams

In Section 2.1 we introduced the idea of a generator set $P = \{p_1, \dots, p_n\}$ as a set of n distinct points (i.e. no two or more points were spatially coincident) which generates the ordinary Voronoi diagram \mathcal{V} . For a finite Voronoi diagram the only condition imposed on P was that n was finite and greater than one. Other than this, no other aspects of the locations of the points in m -dimensional Euclidean space, \mathbb{R}^m , were specified. In this chapter we consider \mathcal{V} , its dual Delaunay tessellation \mathcal{D} , and some generalizations of \mathcal{V} when P contains countably infinitely many distinct points which generate the *infinite* Voronoi diagram. To avoid pathological cases, we assume that P is locally finite (i.e. there are only finitely many points inside a bounded region) and its points are *in the general quadratic position*, i.e. the points satisfy:

The Non-collinearity Assumption No $k+1$ points lie on a $(k-1)$ -dimensional hyperplane of \mathbb{R}^m , $k = 2, \dots, m$, and

The Non-cosphericity Assumption No $m+2$ points lie on the boundary of a sphere in \mathbb{R}^m .

(See Assumption D1 in Section 2.2 and Assumption V2 in Section 2.3). In particular, we concentrate on the case when the members of P are located in \mathbb{R}^m according to the homogeneous Poisson point process Θ_P discussed in Section 1.3.3, and refer to the resulting tessellation as the *Poisson Voronoi diagram* \mathcal{V}_P , and the *Poisson Delaunay tessellation* \mathcal{D}_P . We use the terms *Poisson Voronoi cell* (PVC) and *Poisson Delaunay cell* (PDC) to refer to the individual m -dimensional random polytopes ($m \geq 2$) of the respective tessellations. With probability 1, all PVCs and PDCs are bounded polygons (cf. Property V2 in Section 2.3). Most results concerning the Voronoi diagram and Delaunay tessellation generated by Θ_P or other random point processes discussed in this chapter hold only *almost surely* (i.e. they hold with probability 1). Nevertheless, for ease of presentation in what follows we omit the phrase ‘almost surely’.

Figure 5.0.1 shows a portion of \mathcal{V}_P in \mathbb{R}^2 , while a *typical* PVC in \mathbb{R}^3 is illustrated in Figure 5.0.2. A *typical* Voronoi cell refers to a random polytope which, loosely speaking, has the same distribution as a randomly chosen cell

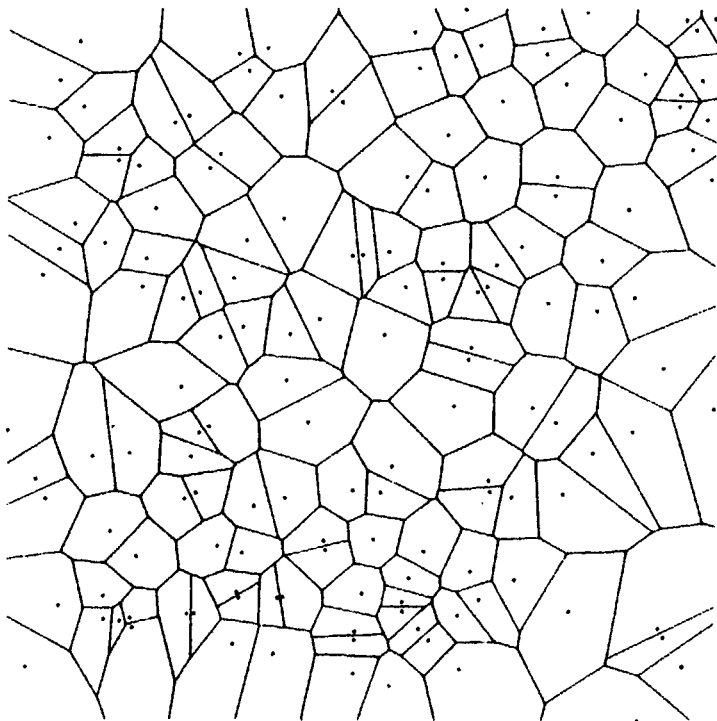


Figure 5.0.1 A portion of a planar Poisson Voronoi diagram.

from \mathcal{V} selected in such a way that every cell has the same chance of being sampled. However, such a uniform sampling scheme is in fact impossible to perform if P contains infinitely many distinct generators. The reason is that we are not able to choose with ‘equal probability’ from infinitely many cells. Nevertheless, a typical cell can be defined by using the ergodic theorem (Cowan, 1978, 1980) or the Palm distribution (Mecke, 1980; Møller, 1989, 1994) (see Section 1.3.3). If the generator set P is a realization of a simple stationary ergodic point process in \mathbb{R}^m , then these two methods are equivalent (see Section 1.3.3).

We first present the general properties of an infinite Voronoi diagram in \mathbb{R}^m in Section 5.1, and then begin our treatment of \mathcal{V}_P by considering its properties in Section 5.2. Some of these properties are inherited from properties of Θ_P by which the members of P are generated. Other properties of \mathcal{V}_P make it very attractive for use in a number of ways in an extensive range of empirical circumstances which are described in Section 5.3. In view of this widespread use of \mathcal{V}_P (and \mathcal{D}_P), there is great interest in obtaining information on both PVCs and PDCs. Such information includes moments, distributions and correlations of various characteristics such as the number of sides, area, perimeter (in \mathbb{R}^2), number of faces, volume and total edge

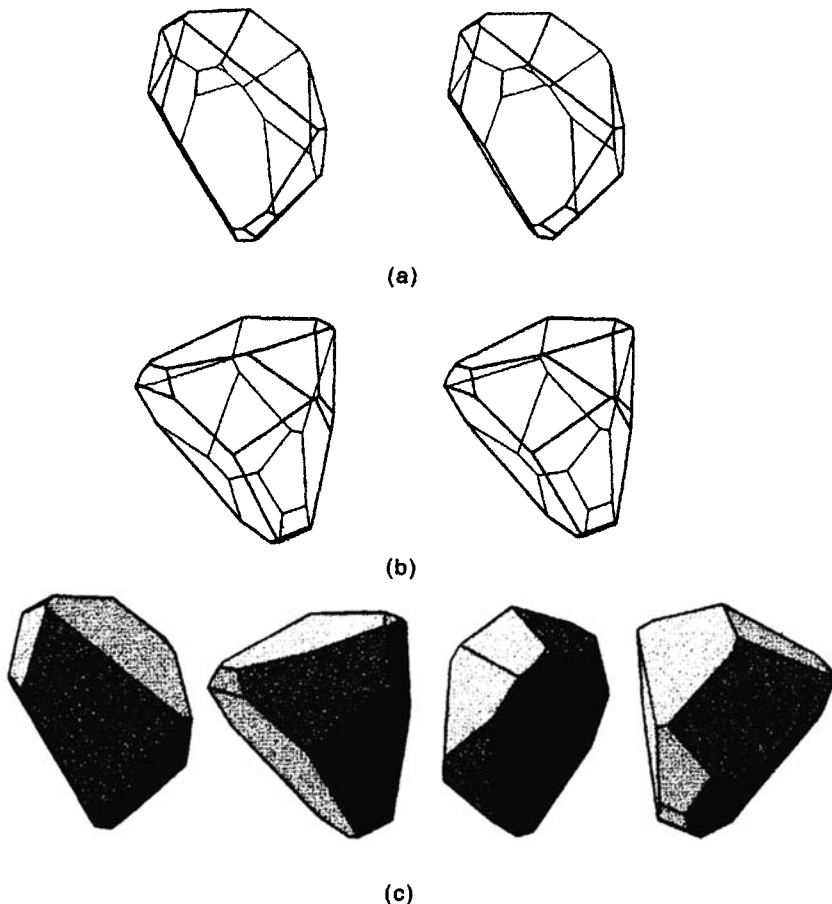


Figure 5.0.2 (a) Stereo pair of typical Poisson Voronoi cells in \mathbb{R}^3 . (b) The stereo pair after rotation of 90° about a fixed axis. (c) Cell shown after rotation of 0°, 90°, 180°, 270° about the fixed axis. (Source: Møller et al., 1989.)

length (\mathbb{R}^3) of a typical cell. Considerable success has been achieved in deriving analytically the first-order moments of a variety of PVC and PDC characteristics, and these are reported in Sections 5.5.1 and 5.11, respectively. There is considerable interest in the conditional moments of PVC characteristics. Most of the 'equalities' are empirical laws obtained from simulation only. These are summarized in Sections 5.5.2 and 5.5.3.

In the first edition we stated that '*In principle it is also possible to derive integral formulae to obtain other moments of cell characteristics but often these are notoriously complicated, especially for PVCs. Consequently, many researchers have resorted to Monte Carlo approaches where the characteristics of cells are estimated by simulation*'. However, the scenery has changed. Integral formulae which are numerically tractable for the distributions of quite

a number of characteristics have been derived. These will be reported in Section 5.5.4. Nevertheless, the distributions of some important characteristics are still numerically intractable and have to be estimated by simulation. Several different simulation approaches are possible for both \mathcal{V}_P and \mathcal{D}_P and these are outlined in Section 5.4. Estimates obtained from such simulations of PVCs and PDCs are reported in Sections 5.5 and 5.11, respectively.

Poisson Voronoi diagrams induce many interesting stochastic processes, such as the point process of vertices. Some of these processes are discussed in Section 5.6.

In many applications involving \mathcal{V}_P in \mathbb{R}^3 , information concerning \mathcal{V}_P is not directly available but instead is acquired from planar sections or linear probes. Thus, such applications require information on sections of PVCs rather than the PVCs themselves. This information is reported in Section 5.7.

In Chapter 3 we described various ways of generalizing \mathcal{V} . Many of these generalizations can also be pursued when the generator set is a realization of a stationary point process. In fact, as noted in Section 3.1.5, the sectional Voronoi diagram of Section 5.7 can be considered as a type of weighted Voronoi diagram. Section 5.8 considers a particular type of additively weighted Poisson Voronoi diagram, more commonly known as the Johnson–Mehl model. This creates a dynamic version of the Poisson Voronoi model by associating with each generator point a weight which reflects the arrival time of the point in \mathbb{R}^m . Order- k and ordered order- k Voronoi diagrams and Voronoi diagrams on the surface of a sphere are discussed in Sections 5.9 and 5.10, respectively.

In general our knowledge of PDCs, particularly that derived by analytical methods, is greater than that of PVCs. This information, together with a brief treatment of sections of \mathcal{D}_P and \mathcal{D}_P on the surface of a sphere, is reported in Section 5.11.

For some applications the conditions involved in generating \mathcal{V}_P are inappropriate, perhaps because there are additional conditions influencing the locations of the members of P or because there are constraints on the sizes of the cells. In such circumstances modifications may be undertaken which produce other random tessellations. A selection of such tessellations is briefly surveyed in Section 5.12.

In view of the widespread interest in \mathcal{V}_P in empirical circumstances, considerable effort has been extended in many different disciplines in the pursuit of information on PVCs and PDCs and consequently the results of such endeavours are widely dispersed over a far-flung range of publications. In light of this it is not surprising that much duplication or near duplication has occurred because individual researchers (and reviewers and editors!) have been ignorant of similar, previous work of others. To reduce further duplication and in an attempt to synthesize previous activity, Sections 5.5–5.11 emphasize the reporting and reconciliation of the results of many previously disparate studies. Reviews on the mathematical theory for Poisson Voronoi diagrams can be found in Møller (1994, 1998, 1999).

5.1 PROPERTIES OF INFINITE VORONOI DIAGRAMS

As indicated in Section 2.1, no matter if P is finite or infinite, an m -dimensional Voronoi diagram, \mathcal{V} , constitutes a tessellation of \mathbb{R}^m ($m = 1, 2, \dots$) since the interiors of the individual cells of \mathcal{V} are non-overlapping and together with their boundaries are collectively space-filling. Denote by x_i the location vector of p_i and by $V(p_i)$ the Voronoi cell of p_i . The intersection of $k+1$ cells,

$$F(p_0, \dots, p_k) = \bigcap_{i=0}^k V(p_i),$$

lies on the hyperplane

$$G(p_0, \dots, p_k) = \{x \in \mathbb{R}^m \mid \|x - x_0\| = \dots = \|x - x_k\|\}.$$

The non-collinearity assumption is equivalent to one that such an affine subspace $G(p_0, \dots, p_k)$ is of $m-k$ dimensions for $k = 1, \dots, m$. The non-cosphericity assumption is equivalent to that $G(p_0, \dots, p_k) = \emptyset$ whenever $k > m + 1$. The general quadratic position and the local finiteness of the generator set P imply that $F(p_0, \dots, p_k)$ is either empty or of dimension $m-k$. A non-empty $F(p_0, \dots, p_k)$ is called an $(m-k)$ -face of the tessellation, and a cell an m -face. The boundary of an m -face consists of a hierarchy of s -dimensional polyhedra ($s = 0, 1, \dots, m$) which we term s -faces of a cell. In general, an s -face of a cell is not the same as an s -face of a tessellation. An s -face of a cell in a tessellation is the union of all s -faces of the tessellation which is contained in this s -face of a cell. For example, in \mathbb{R}^3 the 0-faces, 1-faces and 2-faces of a cell are the vertices, edges and faces of a cell. If an m -face is a polytope (i.e. a convex and bounded polyhedron), then all the s -faces on its boundary are s -dimensional polytopes. The 0-faces and m -faces of a tessellation coincide with the 0-faces and m -faces of the individual cells, respectively, but faces of other dimensions may not. A tessellation is called *regular* if the s -faces of the individual cells coincide with those of the tessellation for all s , $s = 0, \dots, m$. A typical s -face ($0 \leq s \leq m$) can be defined in the same way as a typical cell by using the ergodic theorem or the Palm distribution (see Sections 1.3.3 and 5.0). Note that a typical s -face ($0 \leq s < m$) and an s -face of a typical cell have different distributions.

Property IV1 (Møller, 1994, Proposition 2.1.2) The set of faces of cells is locally finite, i.e. there are only finitely many s -faces intersecting a bounded subset of \mathbb{R}^m , $s = 0, \dots, m$. Moreover, if P contains at least $m+1$ points, then \mathcal{V} contains faces of any dimensions s , $s = 0, \dots, m$.

Thus, if a Voronoi cell is bounded, then Property IV1 implies that it has only finitely many neighbours. This finiteness is essential for the discussion of the so-called *Aboav's law* and *Lewis' law* in Section 5.5.

Property IV2 (Møller, 1994, Proposition 2.1.3) A Voronoi cell $V(p_i)$ is bounded if and only if for all x_u (location vectors) on the surface of the unit

sphere in \mathbb{R}^m , there exists a generator $p \neq p_i$ with location vector \mathbf{x} such that $(\mathbf{x} - \mathbf{x}_i)^T \mathbf{x}_u > 0$.

(Cf. Property V2 in Section 2.3.) If $P = \{p_0, p_1, \dots\}$ is a realization of a non-empty stationary point process, then the condition of Property IV2 holds for all p_i (Møller, 1994, Proposition 3.1.1).

Property IV3 (Møller, 1994, Proposition 2.1.4) If a Voronoi cell $V(p_i)$ is bounded, then all its s -faces on the boundary coincide with those s -faces ($s = 0, \dots, m$) of the tessellation which are included in $V(p_i)$. Moreover, if all cells are bounded, then \mathcal{V} is regular.

A *normal* tessellation is one in which every s -face of the tessellation lies in the boundaries of $(m-s+1)$ cells ($0 \leq s \leq m-1$).

Property IV4 Every Voronoi diagram \mathcal{V} generated by points which are in the general quadratic position is a normal tessellation.

Equivalent terms to normal are ordinary or natural or in equilibrium state, all of which are used because empirical tessellations (for $1 \leq m \leq 3$) frequently possess this property. In terms of Section 2.1 (Assumption V1), \mathcal{V}_p is non-degenerate. Because of Property IV3 we may also express Property IV4 in terms of the constituent cells of the Voronoi diagram. Each s -face of a Voronoi cell lies in the s -dimensional hyperplane the points of which are equidistant from a set of $(m-s+1)$ generators in P . Thus, in \mathbb{R}^2 each vertex is shared by three cells and each edge is common to two cells. In \mathbb{R}^3 four cells meet at each vertex, each edge is shared by three cells and each face is common to two cells.

If in addition to the local finiteness and the general quadratic position assumptions, P is a realization of a stationary simple point process Θ in \mathbb{R}^m , then the Voronoi diagram generated, \mathcal{V}_Θ , is a random tessellation of \mathbb{R}^m . In view of Properties IV2, IV3 and IV4, we obtain an important property of such a random Voronoi diagram:

Property IV5 \mathcal{V}_Θ is a regular and normal random tessellation.

Reviews of theory and applications of general random tessellations can be found in Santaló (1988), Møller (1989, 1994) and Stoyan *et al.* (1995, Chapter 10). The most important class of random tessellations is the Poisson Voronoi diagram discussed in detail later in this chapter.

Once \mathcal{V}_Θ is generated by Θ , other point processes can be constructed from \mathcal{V}_Θ . Of particular interest are the stationary point processes Θ_s with intensities λ_s of the centroids of the s -faces of the cells of \mathcal{V}_Θ ($s = 0, \dots, m$) (see Section 5.6.1).

Property IV6 (Møller, 1989, Corollary 5.4) The intensity λ_s of the stationary point process Θ_s ($s = 1, \dots, m$) constructed from \mathcal{V}_Θ satisfies

$$[1 - (-1)^s] \lambda_s = \sum_{t=0}^{s-1} (-1)^t \binom{m-t+1}{s-t} \lambda_t. \quad (5.1.1)$$

Denote by λ the intensity of Θ . By definition, $\lambda = \lambda_m$ and so equation (5.1.1) yields

$$\begin{aligned} \lambda_0 &= 2\lambda, & \lambda_1 &= 3\lambda, & \lambda_2 &= \lambda, & \text{if } m = 2, \\ \lambda_1 &= 2\lambda_0, & \lambda_2 &= \lambda + \lambda_0, & \lambda_3 &= \lambda, & \text{if } m = 3. \end{aligned}$$

In fact, equation (5.1.1) holds for all regular and normal random tessellations.

For each $s = 0, 1, \dots, m$, the union of all s -faces of \mathcal{V}_Θ forms a stationary manifold process (see Section 1.3.3). In particular, it is known as a fibre process (consisting of the set of edges of \mathcal{V}_Θ) if $s = 1$ and a surface process (consisting of the set of facets of Voronoi cells) if $s = m - 1$ and $m \geq 3$. A Voronoi diagram is determined uniquely by its fibre or surface process.

Other relationships which hold for all stationary tessellations and which may be derived by either the ergodic theorem (see Section 1.3.3) (Miles, 1972a; Cowan, 1978, 1980) or the Palm distribution (see Section 1.3.3) (Radecke, 1980; Mecke, 1980, 1984; Møller, 1989), relate to the mean values of the cell characteristics. For \mathbb{R}^m general expressions are given by Møller (1989, Section 5) while specific relationships for $m = 2$ or $m = 3$ are given by Stoyan *et al.* (1995, pp. 317–318 and pp. 322–323, respectively). Furthermore, Mecke (1984) shows that for \mathbb{R}^2 these relationships can be expressed in terms of three parameters, λ_0 , λ_2 and L_A (the intensity of the fibre process of edges of the tessellation in \mathbb{R}^2 , i.e. the mean total edge length per unit area), while for \mathbb{R}^3 seven parameters are required (λ_0 , λ_3 , $\lambda_1 + \lambda_2$, L_V , S_V , T_V and Z_V , where L_V and S_V are the intensities of the fibre and surface processes of edges and facets, respectively, and T_V and Z_V are the intensities of the weighted vertex point process and the edge fibre process where the vertices and edges are weighted by the number of adjacent cells). In particular, for \mathcal{V}_Θ only two parameters $\lambda = \lambda_2$ and L_A and four parameters $\lambda = \lambda_3$, λ_0 , L_V and S_V are needed in \mathbb{R}^2 and \mathbb{R}^3 , respectively. The results are given in Table 5.1.1.

Both Miles (1972a) and Møller (1989) exploit these relationships in deriving many of the properties of PVC characteristics reported in Section 5.5. Møller also derives a series of relationships between the mean values of face and tessellation characteristics. Finally, since the intersection between an arbitrary p -dimensional hyperplane ($p = 1, \dots, m$) and \mathcal{V}_p in \mathbb{R}^m yields a random tessellation, the properties of such sections and their constituent cells can be generated from those of \mathcal{V}_p (Miles, 1972a, Section 2.5; 1972b; Møller, 1989, Section 6; Chiu *et al.*, 1996) and these are reported in Section 5.7.

The dual of an infinite Voronoi diagram is still a Delaunay tessellation. The non-empty intersection of Delaunay cells of dimension s is an s -face of

Table 5.1.1 The first moment of various characteristics of \mathcal{V}_Θ .

Characteristic	Mean
$m = 2$	
Area of a typical cell	$1/\lambda$
Perimeter of a typical cell	$2L_A/\lambda$
Number of vertices/edges of a typical cell	6
Length of a typical edge	$L_A/(3\lambda)$
$m = 3$	
Volume of a typical cell	$1/\lambda$
Surface area of a typical cell	$2S_V/\lambda$
Total length of all edges of a typical cell	$3L_V/\lambda$
Mean breadth (also known as the mean caliper diameter)*	$L_V/(4\lambda)$
Number of vertices of a typical cell	$4\lambda_0/\lambda$
Number of edges of a typical cell	$6\lambda_0/\lambda$
Number of faces of a typical cell	$2(1 + \lambda_0/\lambda)$
Area of a typical face	$S_V/(\lambda_0 + \lambda)$
Perimeter of a typical face	$3L_V/(\lambda_0 + \lambda)$
Number of vertices/edges of a typical face	$6/(1 + \lambda/\lambda_0)$
Length of a typical edge	$L_V/(2\lambda_0)$

L_A = intensity of the edge fibre process in \mathbb{R}^2 .

L_V = intensity of the edge fibre process in \mathbb{R}^3 .

S_V = intensity of the face, surface process in \mathbb{R}^3 .

λ_0 = intensity of the vertex point process.

λ = intensity of Θ .

* Mean length of the cell's projection onto an isotropic random line.

Source: Møller (1994, Proposition 3.3.1).

Table 5.1.2 The first moment of various characteristics of \mathcal{D}_Θ .

Characteristic	Mean
$m = 2$	
Area of a typical cell	$1/(2\lambda)$
Perimeter of a typical cell	L'_A/λ
Number of vertices/edges of a typical cell	3
Length of a typical edge	$L'_A/(3\lambda)$
$m = 3$	
Volume of a typical cell	$1/\lambda_0$
Surface area of a typical cell	$2S'_V/\lambda_0$
Area of a typical face	$S'_V/(2\lambda_0)$
Length of a typical edge	$L'_V/(\lambda_0 + \lambda)$

L'_A = intensity of the Delaunay edge fibre process in \mathbb{R}^2 .

L'_V = intensity of the Delaunay edge fibre process in \mathbb{R}^3 .

S'_V = intensity of the Delaunay face, surface process in \mathbb{R}^3 .

λ_0 = intensity of the Voronoi vertices/Delaunay cell centroids.

λ = intensity of Θ .

Source: Møller (1994, Remark 3.3.1).

the Delaunay tessellation ($s = 0, \dots, m$). An s -face of a Delaunay cell is the s -dimensional simplex which is the convex hull of $s+1$ distinct generators.

Property ID1 (Møller, 1994, Proposition 2.1.6) Delaunay tessellations are regular.

Denote by \mathcal{D}_Θ the dual of \mathcal{V}_Θ . \mathcal{D}_Θ is a stationary random Delaunay tessellation. The point processes of the centroids of the s -faces of \mathcal{D}_Θ are stationary and the intensities are simply λ_{m-s} ($s = 0, \dots, m$), because of the duality between \mathcal{D}_Θ and \mathcal{V}_Θ . The first moment of some characteristics, which depend on two and four parameters in \mathbb{R}^2 and \mathbb{R}^3 , respectively, are tabulated in Table 5.1.2.

5.2 PROPERTIES OF POISSON VORONOI DIAGRAMS

The results in Section 5.1 hold for any locally finite set P , the members of which are in the general quadratic position. In this section we discuss the Poisson Voronoi diagrams \mathcal{V}_P , which are generated by realizations of the homogeneous Poisson point process Θ_P .

Characteristics of \mathcal{V}_P and its constituent PVCs either derive from the procedure for generating Voronoi cells described in Section 2.1 or are inherited from the properties of Θ_P . The stationarity of \mathcal{V}_P yields the following two properties.

Property PV1 The cells of \mathcal{V}_P are polytopes (bounded and convex polyhedra).

(Cf. Property V1 in Section 2.3 and Property IV2 in Section 5.1.) Because all PVCs are bounded and the points of Θ_P are in the general quadratic position, by Property IV5 in Section 5.1 we have

Property PV2 \mathcal{V}_P is a regular and normal tessellation.

(See Møller, 1989, Example 1 and Proposition 7.1.) Thus, we need not distinguish an s -face of \mathcal{V}_P and an s -face of an individual cell of \mathcal{V}_P .

Properties which are inherited from Θ_P include the following.

Property PV3 \mathcal{V}_P is stationary and isotropic.

This means that its characteristics and those of its constituent PVCs are invariant under both translation and rotation about the origin in \mathbb{R}^m . Thus, \mathcal{V}_P can be considered a motion-invariant tessellation.

Property PV4 \mathcal{V}_P satisfies the strong mixing condition under the translation transformation.

The mixing condition means that spatially distant features of the tessellation are asymptotically independent as the distance tends to infinity (see Section 1.3.3).

5.3 USES OF POISSON VORONOI DIAGRAMS

Given the way in which the Poisson Voronoi diagram, \mathcal{V}_p , is generated and its resulting properties, there has been widespread interest in its use in a variety of empirical situations. Such uses of \mathcal{V}_p take two main forms. The most straightforward is as a model of a given empirical structure, while the other use is as a normative model against which other tessellations can be evaluated. Sometimes the distinction between these two uses becomes blurred because, once established as a structural model, \mathcal{V}_p is often subsequently used in a normative way.

An example of the direct use of \mathcal{V}_p is provided by Kumar and Kurtz (1994a) and Kumar and Singh (1995) who use the three-dimensional form as a microstructural model of a dense, single phase polycrystalline material in their investigations of thermal conductivity. They justify this by noting that the two structures are topologically equivalent and that the mean dihedral angle of 120° and the mean bond angle (i.e. the angle between edges) of 111.11° in \mathcal{V}_p are very close to those required by the minimum surface energy (120° and $109^\circ 28' 16''$, respectively), while the mean number of edges per face (5.228) is very similar to experimentally observed values. Further support for the use of \mathcal{V}_p as a model of single phase microstructures is provided by considering industrial standards. For single phase microstructures these deal only with the mean grain size as determined from the mean number of intercepts per unit length of test line or by the mean number of grain sections per unit area of test area. Mücklich *et al.* (1997) show that for the German standard DIN 50 601 these mean values are consistent with those of sectional Poisson Voronoi diagrams (see Section 5.7). \mathcal{V}_p has also been used as a microstructural model in simulating fatigue crack propagation (Cox and Morris, 1988) and plastic deformation (Seefeldt and Klimanek, 1997).

A specific example of a polycrystalline microstructure is zinc oxide (ZnO) varistors (multicomponent ceramic devices with highly non-linear current-voltage characteristics widely used as surge arresters), produced by sintering ZnO powder together with small amounts of other oxide additives. Thus varistors consist of semi-conducting ZnO grains surrounded by insulating barriers at the grain boundaries. To model the electrical transport properties of such material, Bartkowiak *et al.* (1996a,b,c) consider the cells of the two-dimensional \mathcal{V}_p to represent the grains of the ceramic and, using prescribed probabilities, randomly assign each Voronoi edge to one of three types; 'good' (high leakage resistance) and 'bad' (lower leakage resistance) electrically non-linear microjunctions, and ohmic (linear with low resistance) microjunctions. In this way, the behaviour of the material in response to changing proportions of microjunctions can be examined.

The same characteristics of \mathcal{V}_p that have made it popular as a microstructural model have also led to it being selected as a basis of a number of models that study the behaviour of time-varying phenomena. For example, Yuan and Edwards (1995) use it as the initial state in simulations of two-dimensional random foams in planar Poiseuille flow, while both Kermode and Weaire (1990) and Neubert and Schreckenberg (1997) adopt it as one of the initial configurations in their simulations of the coarsening of two-dimensional soap froth.

Another example of the direct use of \mathcal{V}_p is provided by Christ *et al.* (1982a,b,c), Friedberg and Ren (1984), Drouffe and Itzykson (1984), Ren (1984) and Itzykson and Drouffe (1989) in the investigation of quantum field theory. Here the traditional concept of a space-time continuum has been replaced by that of a discrete lattice. Initially, regular lattices were used since the links between individual nuclei (points) are clearly defined. However, such lattices are not motion invariant and thus do not possess properties assumed in the traditional concept. As we have seen, the homogeneous Poisson point process, Θ_p , does possess these properties (see Section 1.3.3) and so Christ *et al.* (1982a) propose using a random lattice in which the nuclei are generated by Θ_p and the links between the nuclei correspond to the adjacencies between the Voronoi regions of the Voronoi diagram of nuclei. Such a lattice is equivalent to the Poisson Delaunay tessellation, \mathfrak{D}_p . To distinguish it from other random lattices (see Section 5.12), this particular form is now often referred to as the *Poissonian random lattice* (PRL). Further support for the PRL is provided by the results of Monte Carlo simulations which demonstrate that the PRL displays the same behaviour as a regular lattice for both the Ising model (Espriu *et al.*, 1986; Janke *et al.*, 1993, 1994a,b) and the eight-state Potts model (Janke and Villanova, 1995).

The ability of the PRL to discretize space without introducing any form of anisotropy has led to its adoption in other contexts including modelling the statistical mechanics of membranes (David and Drouffe, 1988) and modelling the growth of sandpiles (Puhl, 1993). Lauritsen *et al.* (1993) have extended the basic concept by creating dynamic random lattices in which thermodynamic energy is distributed over the lattice on the basis of the topological properties of the Voronoi cells of the nuclei. Ostoja-Starzewski and Wang (1989, 1990), Ostoja-Starzewski (1990, 1993), and Ostoja-Starzewski *et al.* (1995) have proposed the two-dimensional PRL as a generic model of the microstructure of discrete granular media such as soils, powders and fibrous materials. In particular, they calculate the effective moduli of such materials by considering each Delaunay vertex as a joint and each Delaunay edge as a two-force member acting as a linear elastic spring of a directly specified length and of a deterministic or random spring constant. They also suggest that for some applications modified, less disordered forms of the PRL created by imposing a minimum edge length condition or by considering the Delaunay tessellation of the centroids of the cells of \mathcal{V}_p (Ostoja-Starzewski and Wang, 1990), may be more appropriate. The approach may also be extended to two-phase media by randomly assigning the vertices

of the PRL to either phase, subject to specified volume fractions (Ostoja-Starzewski *et al.*, 1995). Gasparini *et al.* (1996) use the PRL in a similar way to provide a network of truss or beam elements for use in simulating the behaviour of brittle materials such as concrete or ceramic. In this instance each Delaunay edge is assigned a truss element of the same deterministic axial stiffness and an independently, identically Weibull-distributed tensile strength.

\mathcal{V}_p has also been used in studies of conductivity and percolation in composites consisting of grains and associated pore space (void). When the concern is with movement through the material, the equivalent of the PRL has been proposed as a model of a topologically random network in both \mathbb{R}^2 (Jerauld *et al.*, 1984a) and \mathbb{R}^3 (Jerauld *et al.*, 1984b; Rivier *et al.*, 1985). Once the network is identified, the *bond percolation model* is obtained by choosing each edge to be present independently with a specified probability. The *site percolation model* is produced by choosing each vertex to be present independently with a specified probability and retaining those edges for which both endpoints are present. A third model, the *first-passage percolation (FPP) model*, is defined by independently assigning to each edge a non-negative travel time from a common probability distribution. The first-passage time between two vertices is then defined as the minimum travel time between the vertices over all paths connecting them. Vahidi-Asl and Wierman (1990, 1992) and Howard and Newman (1997) consider different FPP models in which the links are defined by the edges in \mathcal{V}_p or \mathcal{D}_p (see Section 5.6.4).

When the interest is in percolation through the void, the so-called *Swiss cheese model* may be used (Elam *et al.*, 1984; Halperin *et al.*, 1985; Feng *et al.*, 1987; van der Marck, 1996). In this model the pore space is represented by the complement of the union of a set of randomly located, overlapping spheres. Kerstein (1983) showed that when the spheres are of uniform size, the Voronoi diagram of the sphere centres (equivalent to \mathcal{V}_p) is a good representation of the void space since the Voronoi vertices can be considered as the sites (centres, nodes) of the void space and the Voronoi edges contained in the void space define the links over which flows can occur.

DiCenzo and Wertheim (1989) have also used \mathcal{V}_p in modelling the growth of clusters formed by a metal vapour deposited on amorphous substrates. The model is a two-step one in which first nucleation sites are distributed in \mathbb{R}^2 (\mathbb{R}^3) according to Θ_p and then atoms landing on the surface of the substrate are assigned to the nearest nucleation site. The number of atoms in a cluster formed at a nucleation site will be proportional to the area (volume) of the surface closest to the nucleation site which is equal to the area (volume) of the Voronoi cell of the nucleation site. Thus, the distribution of cell areas (volumes) can be used to derive the distribution of cluster sizes. Other studies involving \mathcal{V}_p have also focused on the distribution of cell areas (volumes). For example, it has been used to model the effects of variations in local density on variations in plant size (Miller and Weiner, 1989), the contribution from random noise in an algorithm for source detection in high-energy astrophysics (Ebeling and Wiedenmann, 1993), and particle size

distributions resulting from the abrupt or impulsive application of fracturing forces to a solid body (Grady and Kipp, 1985).

Foss and Zuyev (1996) used \mathcal{V}_p as a model for telecommunications networks. Think of stations as concentration points where cables meet or communications change their routes. They form a Poisson process on \mathbb{R}^2 . Each station serves its zone consisting of those locations that are closer to it than to any other stations, i.e. each station serves its own Voronoi cell. They considered further that subscribers to the telecommunication services form another independent Poisson process on \mathbb{R}^2 . Molchanov and Zuyev (1997) discussed the optimal intensity of stations so that the total connection cost would be minimized. If the connection cost is linearly proportional to the sum of the Euclidean distances between subscribers and stations, the optimal intensity of stations should be proportional to the intensity of subscribers raised to the power 2/3.

\mathcal{V}_p also forms the basis of another frequently used model of structure. This is a specific form of a random mosaic which we label the *Poisson Voronoi Random Mosaic* (PVRM). The creation of a random mosaic involves two steps (Schachter and Ahuja, 1979):

- Step 1: for some bounded region, B , of \mathbb{R}^m , tessellate B ;
- Step 2: independently assign one of k phases to each cell of the tessellation according to a fixed set of probabilities, $p_1, \dots, p_k; \sum_{i=1}^k p_i = 1$.

In this way B is partitioned into subregions, B_1, \dots, B_k , each consisting of the union of all cells of phase k , so that $\bigcup_{i=1}^k B_i = B$. If the tessellation of Step 1 is the Poisson Voronoi diagram, we produce the PVRM. In ecology this model is referred to as the *S-Mosaic* (Pielou, 1977, p. 185).

The simplest PVRM is two-phase. Winterfield *et al.* (1981) have used such a mosaic as a model of a disordered composite in \mathbb{R}^2 which can be used for studying conduction and percolation in continuous media. The two phases are conducting and non-conducting (insulating). Using this approach they are able to study the effects on various conduction and percolation properties of the medium by varying the probabilities associated with each phase. Once established, they also use the two-phase PVRM as a normative model against which other mosaics involving tessellations composed of regular hexagonal and square cells are judged. The two-phase PVRM has also been used to model microemulsions in \mathbb{R}^3 (Talmon and Prager, 1978a,b; Kaler and Prager, 1982; Anderson *et al.*, 1989). Microemulsions are thermodynamically stable three-component systems consisting of an aqueous component, an oil component and a surfactant. The aqueous and oil components are the two phases of the mosaic (with probabilities p_a and p_o , respectively) and the surfactant is distributed over the resulting aqueous-oil interface (the boundaries of the subregions defined by the two phases). Such a model is capable of generating all three classes of microemulsion geometry: oil in water (small values of p_a/p_o), bicontinuous ($p_a/p_o \approx 1$) and water in oil (large values of p_a/p_o). Tipper (1990b) has suggested that the PVRM is also a useful

theoretical model for studying stratigraphic correlation where the phases can represent different lithologies (e.g. sand/shale).

A three-phase PVRM in \mathbb{R}^3 is used by Brumberger and Goodisman (1983) in the interpretation of small angle X-ray scattering observed for heterogeneous catalysts such as porous oxides (e.g. Al_2O_3 , S_iO_2) and oxide supported metals (e.g. $\text{Pt}/\text{Al}_2\text{O}_3$, $\text{Rh}/\text{S}_i\text{O}_2$). Here the three phases are void, support and metal, each of which is considered to contain an internally uniform electron density and whose associated probabilities are equal to the proportion of the total volume of the sample catalyst occupied by that phase.

A variant of the PVRM is described by Ahuja *et al.* (1985) and An *et al.* (1983) who use it in the representation of an image with k colours. A Poisson Voronoi tessellation is superimposed on the image and the individual cells of the tessellation are assigned the colour of the underlying image. In those cases where more than one colour occurs in a cell, the cell is assigned the colour that has the largest representation. The image can then be represented by the set of coordinates of the generators of the individual cells of the tessellation together with their associated colours. They suggest that such a representation is particularly useful for the secure transmission of images since, if the coordinates of the cell generators are produced by a pseudo-random number generator, only the seed for this generator and the colour of each cell need to be transmitted.

On those occasions when we observe a PVRM in a window we may be interested in statistical inference concerning the probabilities of the phases and the intensity of Θ_p . The latter is not straightforward since some of the edges of \mathcal{V}_p disappear as a result of the phase assignment process. Archambault and Moore (1995) provide estimates for the two-phase PVRM.

Although we have illustrated a number of empirical situations where our knowledge of the phenomenon suggests that \mathcal{V}_p may be an appropriate model, there are many other occurrences where such direct use may be unjustified. For instance, we may have little or no information on how a particular tessellation was generated or we may have sufficient information to suggest that it is unlikely that it was created under conditions analogous to those generating \mathcal{V}_p . In the former case our first concern might be to determine if the empirical tessellation differs from \mathcal{V}_p , while in the latter we may be interested in knowing in what ways the tessellation differs from \mathcal{V}_p . In both instances the results of our investigations may provide additional insight into the conditions under which the empirical tessellation was generated. In this way \mathcal{V}_p is used as a normative model against which other tessellations are compared. Such comparisons may be informal in nature or may involve the formal testing of hypotheses concerning the nature of the difference between the empirical tessellation and \mathcal{V}_p (see Section 5.12).

Numerous examples of the use of \mathcal{V}_p in this normative role occur for phenomena in both \mathbb{R}^2 and \mathbb{R}^3 in both the natural and the social sciences. In astronomy \mathcal{V}_p in \mathbb{R}^3 has been used to evaluate phenomena having a basic cellular topology (Pierre, 1990) such as Lyman Alpha absorbers at high redshifts (Pierre *et al.*, 1988) and galaxy distributions in \mathbb{R}^3 (Yoshioka and

Ikeuchi, 1989; Coles, 1990; Zaninetti, 1990, 1992; Ikeuchi and Turner, 1991; van de Weygaert, 1991, 1994; Goldwirth *et al.*, 1995; Doroshkevich *et al.*, 1997). V_p in \mathbb{R}^2 can also be used if the galaxies are considered as either slices of the universe or as projections on the sky (Icke and van der Weygaert, 1987; Zaninetti, 1989). V_p has also been used to evaluate the structure of several monatomic liquids and solids which may be modelled as sphere packings (Rahman, 1966; Finney, 1970a), as well as sections of geological (Crain, 1976) and metallurgical (Schwertel and Stamm, 1996) materials.

In animal ecology tessellations created by territorial units have been compared with V_p in \mathbb{R}^2 (Hamilton, 1971; Hasegawa and Tanemura, 1976; Buckley and Buckley, 1977; Tanemura and Hasegawa, 1980). In geography Boots (1973, 1975a) has used V_p in \mathbb{R}^2 to evaluate service areas associated with public bus services in parts of England and Wales, while Singh and Singh (1978) and Singh (1979) have used them in the evaluation of territories of villages in India.

All the above examples illustrate the use of V_p as a normative model in the examination of empirical tessellations. However, it has also been used extensively as a normative model in the analysis of point patterns. This is because we can compare the characteristics of the Voronoi diagram generated by a given set of points (or, more frequently, the Delaunay tessellation) with those of V_p (or D_p). This provides an indirect way of comparing the empirical point pattern with one generated by Θ_p which provides the generators for V_p . Such endeavours have received considerable attention and as a result are dealt with in more detail in Sections 8.1 and 8.2.

Poisson Voronoi diagrams in the above applications are constructed under the Euclidean distance. Many random *cellular automata* based on the *threshold growth mechanism* can be well approximated by Poisson Voronoi diagrams constructed under different measurements of distances (Gravner and Griffeath, 1997). An example of a cellular automaton is a model for excitable media in which rare 'pacemakers' emit waves that propagate until they encounter waves emanating from other sources (Fisch *et al.*, 1991). The meaning of the threshold growth mechanism can be illustrated in the following *multitype threshold vote automaton* (Durrett and Steif, 1993). Locations of voters are a regular lattice. Initially each voter adopts randomly one of many opinions. According to a deterministic discrete-time update (growth) rule, a voter changes affiliation to agree with the consensus of more than a threshold number of other voters in the voter's neighbourhood, but the voter's opinion remains unchanged in case of ambiguity. If the number of opinions is large, then high location concentrations of agreement have an advantage over their immediate surroundings, and so are able to grow until they encounter a large region controlled by another opinion.

5.4 SIMULATING POISSON VORONOI AND DELAUNAY CELLS

Simulations have been used frequently in studying the characteristics of PVCs, particularly for estimating the distribution of those characteristics. Tables 5.4.1 and 5.4.2 summarize those published studies involving more than 10 000 cells known to the authors, although there are doubtless some others. Although Icke and van de Weygaert (1987) involved only 100 cells, and Ohser and Mücklich (1995) have not reported the method and the number of cells in their simulation study, they are, to the best of our knowledge, the only simulation studies which involve the distances d_1 between a generator and

Table 5.4.1 Simulation studies of Poisson Voronoi cells in \mathbb{R}^2 .

Study	Method	Number of cells	Characteristics
Boots (1987)	R	30 000	L
Boots and Murdoch (1983)	R	50 000	A N P
Crain (1972, 1976)	T	5–11 000	A N P
Crain (1978)	T	25–59 000	A L N P
DiCenzo and Wertheim (1989)	A	~193 500	A
Drouffe and Itzykson (1984)	R	27 000	A N
Hinde and Miles (1980)	T	2 000 000	A N P α
Hutchings and Discombe (1986)	A	42 318	A N P
Icke and van de Weygaert (1987)	A	100	A L N P d_1 d_2 α
Janke <i>et al.</i> (1994a)	A	10 000	N
	A	80 000	N
Kumar and Kurtz (1993)	A	2 000 000	A L P
	A	650 000	N
Le Caër and Ho (1990)	A	600 696	A L N P
	A	1 001 500	A L N P
	A	1 020 800	A L N P
Marthinsen (1996)	A	100 000	A
Moore and Moore (1993)	A	100 000	L N
Moore and Angell (1993)	A	100 000	A N
Quine and Watson (1984)	R	50 000	A N P
Vincent <i>et al.</i> (1976, 1983)	A	10 000	N
Weaire <i>et al.</i> (1986)	A	79 400	A
	A	734 639	A
	A	929 070	A
	A	~96 500	N

Characteristics:

A = area

L = edge length

N = vertices (edges)

P = perimeter

d_1 = distance between a generator and a vertex

d_2 = perpendicular distance between a generator and an edge

α = interior angle

For definitions of methods, see the text.

a vertex and the perpendicular distance d_2 between a generator and an edge, and the maximum breadth (maximum length of the cell's projection onto a line) b_{\max} of a typical cell, respectively. Thus, we also included them in Tables 5.4.1 and 5.4.2.

As noted in Section 1.3.3, the homogeneous Poisson point process Θ_p is ergodic so that limiting distributions of the characteristics of the cells in a single, large Poisson Voronoi diagram V_p will coincide with those obtained from a sequence of individual, typical cells sampled from separate Poisson Voronoi diagrams. Consequently, two main simulation approaches are possible.

The first of these (referred to as method A in Tables 5.4.1 and 5.4.2) involves simply generating a large number of points inside a bounded region B according to Θ_p , constructing V_p and measuring the characteristics of all its cells. There are essentially two complications with this approach. The first is that, no matter how large V_p is, allowance must be made for edge effects introduced by those cells close to the boundary of B . One way to treat such edge effects is to exclude from consideration any cells of V_p in B for which a circle, centred at any vertex v of the cell and passing through the three

Table 5.4.2 Simulation studies of Poisson Voronoi cells in \mathbb{R}^3 .

Study	Method	Number of cells	Characteristics
Jerauld <i>et al.</i> (1984b)	A	10 184	F
Kiang (1966)	A	12 800	V
Kumar <i>et al.</i> (1992)	A	358 000	$B F N S V$
	A	102 000	$A G L P S V$
Kumar and Kurtz (1995)	A	377 000	$A F L N P S V \alpha_1 \alpha_2$
	A	165 000	B
Lorz (1990b, 1991)	R, A	82 870	$A B F L M N P S V$
			$\bar{b} \alpha_1 \alpha_2 \alpha_3$
Lorz and Hahn (1993)	R	1 081 945	$F B S V \bar{b} \alpha_3$
Marthinsen (1996)	A	~25 000	V
Møller (1994)	R	~10 000	V
Moore and Angell (1993)	A	50 000	V
Ohser and Mücklich (1995)	--	—	b_{\max}
Tanemura (1988)	A	100 000	$F M S V$
Thorvaldsen (1992)	R	250 000	$F L M N S V$
Yoshioka and Ikeuchi (1989)	A	64 000	V

Characteristics:

A = area/face	P = edge length/face
B = total edge length/cell	S = surface area/cell
C = full (Gabriel) neighbours	V = volume
F = faces/cell	\bar{b} = mean breadth/cell
G = face area/cell	b_{\max} = maximum breadth/cell
L = edge length	α_1 = face (dihedral) angle at an edge
M = vertices/cell	α_2 = interior angle of a face (bond angle)
N = edges/face	α_3 = face angle of a cell

Note that $M = 2F - 4$.

For definitions of methods, see the text.

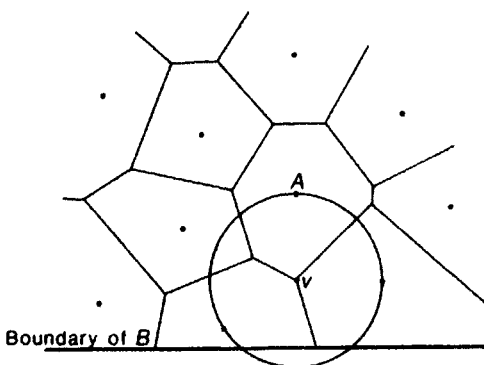


Figure 5.4.1 A procedure for identifying cells subject to edge effects.

points of Θ_p , which are equidistant from v , intersects the boundary of B (Kenkel *et al.*, 1989) (cell A in Figure 5.4.1 is such a cell). If B is a rectangle, an alternative procedure involves creating additional points outside of each edge of B which are translations of points of Θ_p inside the opposite edge of B (the points in the shaded polygons in Figure 5.4.2). The translated points are then used to complete the polygons of those points of \mathcal{V}_p whose polygons intersect the boundary of B . This procedure, which is usually referred to as a periodic boundary condition, is equivalent to converting B into a torus (see Section 3.7.10). The other complication arises because the characteristics of neighbouring cells are not independent (see Section 5.5.3). Thus, the number of cells in the aggregate must be sufficiently large to avoid any bias introduced by this source.

The second simulation approach involves generating a sequence of independent, typical PVCs, measuring the characteristics of each and then aggregating them to obtain the required distributions. The primary advantage of this approach over the previous one is that it avoids problems of edge effects. There are two variants of this approach. The first, method T in Table 5.4.1, involves repeatedly simulating Θ_p within a bounded region B , constructing \mathcal{V}_p and then identifying and measuring only the central cell. This approach involves two considerations: the choice of a single parameter λ (the intensity of Θ_p) and the number of replications n of the procedure. The selection of n is determined primarily by the degree of accuracy at a specified confidence level required of the simulation estimates. The choice of λ represents a compromise between two concerns. If λ is too small the central polygon may intersect the boundary of B or be subject to edge effects (see above), but if it is too large many points will be generated that have no effect on the construction of the central polygon. Estimates of the appropriate value of λ vary considerably even in the case when B is a unit square (for example, Crain, 1978, suggests $\lambda = 35$ is sufficient while Hinde and Miles, 1980, use $\lambda = 100$). Once the values of λ and n have been selected this simulation procedure involves two steps: generating a Poisson distributed variable k with mean $\lambda |B|$ (where $|B|$ is the size of B) and then generating

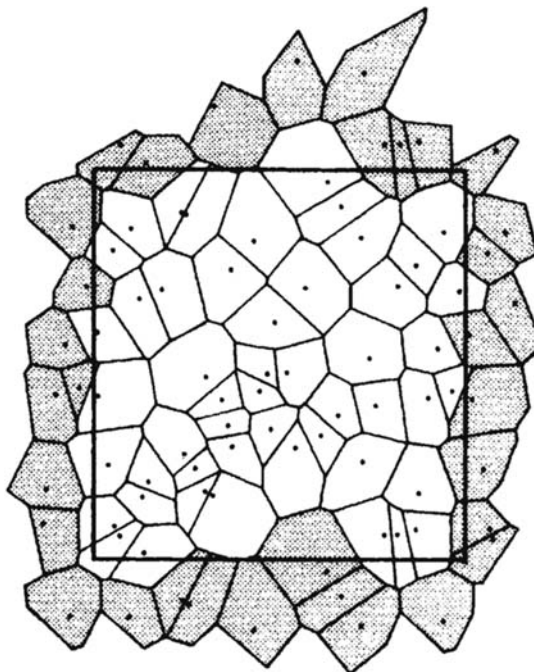


Figure 5.4.2 Periodic boundary condition to avoid edge effects.

k independent uniform random points in B . However, Hinde and Miles (1980) have suggested that, rather than selecting k independently, it is more efficient to choose the values deterministically as the $(i-1/2)/n$ quantiles ($i = 1, \dots, n$) of the Poisson distribution. While they indicate that this approach is superior to selecting the $i/(n+1)$ quantiles ($i = 1, \dots, n$), they make no claims for its optimality.

The second variant of the sequence approach, method R in Tables 5.4.1 and 5.4.2, was proposed by Boots and Murdoch (1983) and Quine and Watson (1984). It exploits the known joint distribution of ordered distances from the origin, o , in Θ_p , since a set of increasing distances with this distribution together with a sequence of random directions gives Θ_p . In two dimensions this simulation process begins by locating the first point, p_0 , at o ; additional points p_i ($i = 1, 2, \dots$) are then generated at random in increasing order of distance from p_0 . As p_i is generated the perpendicular bisector of $\overline{p_0 p_i}$ is drawn. After this step is repeated a number of times p_0 will be surrounded by a convex polygon, P_0 . Additional points are then generated until these points cease to influence the form of P_0 . This occurs when the distance from p_i exceeds the diameter of the smallest circle centred at p_0 containing P_0 . At that time the required characteristics of polygon P_0 are measured and the entire procedure repeated for the next polygon. Unlike method T this procedure is essentially scale invariant and so the choice of λ is no longer a

consideration. Also, since the number of points required to produce the final P_0 is usually about 15 to 20, this procedure is more efficient computationally than method T.

Quine and Watson (1984, p. 551) suggest that a modification of this procedure may be used to gain information about the tails of the distributions of the characteristics of the PVCs. This involves generating the polygon P_1 around p_1 , ignoring p_0 in the construction of P_1 . Thus, P_1 contains p_0 . Since it is known that, in any random tessellation such as \mathcal{V}_p the cell containing the origin is larger on average than other cells (Matheron, 1975, pp. 168–169; Stoyan, 1986; Mecke, 1999), polygons that result from this modified procedure will be larger than those generated by the basic procedure. Thus, knowledge of their characteristics will help to improve the estimates of the tails of the distributions. Drouffe and Itzykson (1984) use a refinement of this approach to ensure that only polygons with a specified number of sides are created.

In \mathbb{R}^3 Quine and Watson (1984) suggest it is easier to work with \mathcal{D}_p rather than \mathcal{V}_p . An initial very large simplex is established with its circumcentre at p_0 . This is subdivided to create a list of Delaunay simplices. As a new point is established this list is updated to include those simplices with the new point as a vertex. This process continues until the distance from p_0 to a new point exceeds twice the maximum circumradius of those simplices with a vertex at p_0 .

Relative to simulating \mathcal{V}_p , less effort has been expended in the simulation of \mathcal{D}_p . In part this is because analytical approaches (particularly the work of Miles, 1970a) have been successful in deriving more thorough knowledge of typical cells than is the case for \mathcal{V}_p . For example, Rathie (1992) derives the exact distribution for the length, area and volume of a typical PDC in \mathbb{R}^m for $m = 1, 2$ and 3 , respectively; Muche (1996b) establishes the distributions for the cell volume, the area and the perimeter of a face, the length of an edge, and an interior angle of a face in the case $m = 3$ (see Section 5.11 for the details). In addition, for $m \leq 3$ the methods of simulating \mathcal{V}_p are also efficient for constructing \mathcal{D}_p . Kumar and Kurtz (1994b) simulate 1.2 million PDCs in \mathbb{R}^3 . However, this is not the case for $m > 3$ and Kendall (1989, 1990) has developed a procedure for simulating individual cells which is particularly efficient in such circumstances. The approach is based on a theorem derived by Miles (1970a) (see equation (5.11.2)) which shows that the size and shape of a PDC are independent if the size is measured in terms of the radius r of its circumsphere and the shape by the angles at its vertices. Furthermore, since the distribution of r is known in terms of the dimensions m (see Section 5.11), the problem of simulation reduces to that of constructing the shape of the PDC. Kendall's approach involves creating a sequence of simplices, each of which consists of $(m+1)$ independent points in \mathbb{R}^m , from a standard normal distribution. For each simplex the values of r (the circumradius), and l , the square root of the sum of the squares of the distances of the $(m+1)$ points from their centroid, are used to create a shape variable, $\rho = r/l$. The j th such simplex in the sequence, with shape measure ρ_j , is retained and its shape recorded if and only if

$$U_j \leq 1 / (\alpha_m \rho_j^{m^2}),$$

where $\alpha_m = (m + 1)^{m^2/2}$ and U_j is the j th of an independent and identically distributed (i.i.d.) sequence of random variables uniformly distributed on the unit interval $[0, 1]$. Kendall (1990) proves that the sequence of recorded shapes will be an i.i.d. sequence of shapes of PDCs. The probability of accepting a simplex in this procedure is known exactly as a function of m (Kendall, 1990, equation (5)). As $m \rightarrow \infty$ this probability tends to zero, thus making the method impracticable for values of $m > 6$. Kendall (1983) has used such an approach to simulate the shapes of 5000 PDCs for $m = 2$ (see Section 5.11).

For larger values of m , Kendall (1988) has developed another simulation method which generates values of two regularity indices for the cells rather than the cells themselves. These indices are F , the volume of a PDC relative to the volume of a regular simplex having the same circumradius, and $\gamma = \log(1/F)$. For $m \geq 3$, Kendall obtains an expression for the expectation of the k th moments of F as the product of $2m$ beta functions. Since each of these beta functions is the $(k/2)$ th moment of a random variable on $[0, 1]$, F can be expressed as the square root of a product of $2m$ independent beta variables. Simulation procedures for such beta variables are available (Ripley, 1987) and so Kendall's method provides a means of simulating an i.i.d. sequence of F values. Initial results suggest that the approach produces useful results for values of m up to at least $m = 10\,000$.

5.5 PROPERTIES OF POISSON VORONOI CELLS

For the Poisson Voronoi diagram \mathcal{V}_p to be used in evaluating empirical tessellations, extensive knowledge of the characteristics of its constituent Poisson Voronoi cells (PVCs) is required. This information includes moments and distributions of individual characteristics of PVCs and correlations between pairs of characteristics.

5.5.1 Moments of the characteristics of Poisson Voronoi cells

Although in principle it should be possible to derive moments analytically, the derivation is notoriously complicated. Møller (1994, Section 4.2, pp. 88–103) demonstrates the complexity and laboriousness of deriving integrals for second-order moments. Several second moments and correlation coefficients of the characteristics of Poisson Voronoi cells in \mathbb{R}^2 and \mathbb{R}^3 have been derived from numerical integration by Gilbert (1962) and Brakke (1986, 1987a,b).

Here we begin by considering first-order moment measures. Many of these can be obtained from general expressions for \mathcal{V}_p in \mathbb{R}^m which can be derived by using either the ergodic theorem (Miles, 1970b, 1974) or the Palm distribution (Møller, 1989, 1994) (see Section 1.3.3).

The expected number of full neighbours of a typical PVC is 2^m (Møller, 1994, equation (4.2.18)), which does not depend on the intensity of the homogeneous Poisson point process. Two cells are full (or Gabriel) neighbours in \mathbb{R}^m if the line joining their generator points intersects their common $(m-1)$ -face (see Section 2.5).

Let λ denote the intensity of the homogeneous Poisson point process Θ_p in \mathbb{R}^m and Θ_{P_s} denote the point process of centroids of the s -faces of the cells of \mathcal{V}_p ($s = 0, \dots, m$) (see Section 5.1). Suppose that the intensity of Θ_{P_s} is λ_s . A main result (Møller, 1989, Theorem 7.2, p. 63) states that the expected value $\lambda_t E_t V_s$ of the total s -dimensional content V_s of the s -faces contained in a typical t -face of \mathcal{V}_p is

$$\lambda_t E_t V_s = \frac{\lambda^{(m-s)/m} 2^{m-s+1} \pi^{(m-s)/2} \Gamma\left(\frac{m^2 - sm + s + 1}{2}\right) \Gamma\left(\frac{m}{2} + 1\right)^{m-s+s/m} \Gamma\left(m - s + \frac{s}{m}\right)}{m (t-s)! (m-t+1)! \Gamma\left(\frac{m^2 - sm + s}{2}\right) \Gamma\left(\frac{m+1}{2}\right)^{m-s} \Gamma\left(\frac{s+1}{2}\right)} \quad (5.5.1)$$

$$(0 \leq s \leq t \leq m),$$

where E_t denotes expectation with respect to the Palm distribution of the random tessellation with respect to the typical t -face (see Møller, 1989, p. 47). That is to say, V_s is the s -dimensional content of the s -faces contained in a t -face which contains the origin o , and the expectation $E_t V_s$ is the expected value of V_s under the condition that the origin o is exactly the centroid of the t -face containing o (see Section 1.3.3 for the details of the Palm distribution). Note that we omit the parameter t from V_s , which can be written as $V_{s,t}$, in equation (5.5.1) because it already appears in E_t . The expected value $E(V_{s,t})$ is also well-defined; it is the average s -dimensional content of s -faces contained in a t -face which contains the origin o , but o is not necessarily the centroid. In general, $E(V_{s,t}) \geq E_t V_s = E_t V_s$ because a larger t -face has a higher chance of containing a fixed point o (size-biased sampling), and an explicit expression for $E(V_{s,t})$ is not yet known.

If we limit our attention to the m -dimensional polytopes of \mathcal{V}_p , $t = m$ and Θ_{P_m} is the set of centroids of the PVCs, so that $\lambda_m = \lambda$ and equation (5.5.1) reduces to

$$E_m V_s = \frac{2^{m-s+1} \pi^{(m-s)/2} \Gamma\left(\frac{m^2 - sm + s + 1}{2}\right) \Gamma\left(\frac{m}{2} + 1\right)^{m-s+s/m} \Gamma\left(m - s + \frac{s}{m}\right)}{\lambda^{s/m} m (m-s)! \Gamma\left(\frac{m^2 - sm + s}{2}\right) \Gamma\left(\frac{m+1}{2}\right)^{m-s} \Gamma\left(\frac{s+1}{2}\right)} \quad (5.5.2)$$

$$(0 \leq s \leq m)$$

(see also Miles, 1970b, 1974, equation (75)). Also for $s = 0$ the total s -dimensional content V_0 of the s -faces contained in a t -face is the number N_0 of o -faces (vertices) contained in the t -face, so that

$$\lambda_i E_i N_0 = \frac{\lambda 2^{m+1} \pi^{(m-1)/2} (m-1)! \Gamma\left(\frac{m^2+1}{2}\right)}{t! (m-t+1)! m \Gamma\left(\frac{m^2}{2}\right)} \left\{ \frac{\Gamma\left(\frac{m}{2}+1\right)}{\Gamma\left(\frac{m+1}{2}\right)} \right\}^m \quad (5.5.3)$$

(see Møller, 1989, p. 66, equation (7.6)). Furthermore, setting $t = 0$ in equation (5.5.3) yields

$$\lambda_0 = \frac{\lambda 2^{m+1} \pi^{(m-1)/2} \Gamma\left(\frac{m^2+1}{2}\right)}{m^2 (m+1) \Gamma\left(\frac{m^2}{2}\right)} \left\{ \frac{\Gamma\left(\frac{m}{2}+1\right)}{\Gamma\left(\frac{m+1}{2}\right)} \right\}^m, \quad (5.5.4)$$

so that using equation (5.1.1) from Section 5.1:

$$\lambda_1 = \frac{\lambda 2^m \pi^{(m-1)/2} (m-1)! \Gamma\left(\frac{m^2+1}{2}\right)}{m^2 \Gamma\left(\frac{m^2}{2}\right)} \left\{ \frac{\Gamma\left(\frac{m}{2}+1\right)}{\Gamma\left(\frac{m+1}{2}\right)} \right\}^m. \quad (5.5.5)$$

In accordance with our concern for empirical applications we present the values of equations (5.5.1)–(5.5.5) for $m = 2$ and $m = 3$ in Tables 5.5.1 and 5.5.2, respectively. To minimize the incidence of subscripts in the text, each of these values, $E_m V_s$, is given a simpler symbol which is identified in Tables 5.5.1 and 5.5.2. Many of these values were first obtained individually by Meijering (1953). Also included in Table 5.5.1 are numerical integration values for second moments of the number of vertices (edges) N , the perimeter P (Brakke, 1986, 1987a), and the cell area A (Gilbert, 1962; Hanson, 1983; Brakke, 1986, 1987a) of a typical cell, and the length L of a typical edge (Brakke, 1986, 1987a) and for the expected values of the products PA , NP and NA (Brakke, 1986, 1987a). The values of the last three second-order moments lead to the following correlation coefficients: $r(P, A) = 0.953$, $r(N, P) = 0.501$ and $r(N, A) = 0.568$. Similarly, Table 5.5.2 includes the second moments for the area A , the perimeter P , the number of vertices/edges N of a typical face, the total edge length B , the number of vertices M , edges E and faces F , the surface area S (Brakke, 1987b) and the volume V (Gilbert, 1962; Brakke, 1987b) of a typical cell of a \mathcal{V}_p in \mathbb{R}^3 and estimates of moments of other characteristics from Monte Carlo simulations by various researchers. Each estimate is taken from the study known to the authors which involves the largest number of cells. Each Voronoi cell satisfies the relation that $M + F - E = 2$ and $M = 2F - 4$. Thus, $M = 2E/3$. Note that the value of $E(N) = 6$ in Table 5.5.1 is a specific instance of a general result

$$E(N) = \frac{2\delta_v}{(\delta_v - 2)}, \quad (5.5.6)$$

where δ_v is the mean number of sides meeting at each vertex of the tessellation (i.e. the mean degree of each node when the tessellation is regarded

Table 5.5.1 The first and/or second-order moments of various characteristics of a Poisson Voronoi diagram in \mathbb{R}^2 .

Moment	Symbol	Exact value	Numerical value
Intensity of cell vertices	λ_0	2λ	
Intensity of mid-points of cell edges	λ_1	3λ	
Intensity of cell centroids	λ_2	λ	
Expected total edge length per unit area	L_A	$2\lambda^{1/2}$	
Expected number of vertices/edges of a typical cell [$E_2 N_0 / E_2 N_1$]	$E(N)$	6	37.781
and its second moment [$E_2(N_0^2)/E_2(N_1^2)$]	$E(N^2)$	4	
Expected number of full neighbours of a typical cell	$E(C)$	λ^{-1}	
Expected area of a typical cell [$E_2(Y_2)$]	$E(A)$	$E(A^2)$	1.280 λ^{-2}
and its second moment [$E_2(Y_2^2)$]	$E(P)$	$4\lambda^{-1/2}$	
Expected perimeter of a typical cell [$E_2(Y_1)$]	$E(P^2)$	$16.945\lambda^{-1}$	
and its second moment [$E_2(Y_1^2)$]	$E(L)$	$2/(3\lambda^{1/2})$	
Expected length of a typical edge [$E_1(V_1)$]	$E(L^2)$	$E(X_1)$	0.630 λ^{-1}
and its second moment [$E_1(V_1^2)$]	$E(X_1^2)$	$2\pi/3$	2.094
Expected value of an angle at a typical vertex	$E(X_1^2)$	$5\pi^2/9 - 5/6$	4.650
and its second moment	$E(PA)$		4.491 $\lambda^{-3/2}$
Expected product of the perimeter and the area of a typical cell [$E_2(Y_1 Y_2)$]	$E(NP)$		24.651 $\lambda^{-1/2}$
Expected product of the number of vertices/edges and the perimeter of a typical cell [$E_2(N_0 V_1)E_2(N_1 V_1)$]	$E(NA)$		6.401 λ^{-1}
Expected product of the number of vertices/edges and the area of a typical cell [$E_2(N_0 V_2)E_2(N_1 V_2)$]			

$\lambda = \text{intensity of } \Theta_P$.

Sources: Meijering (1953), Gilbert (1962), Hanson (1983) and Brakke (1986, 1987a).

as an infinite graph, see Section 1.3.2), which holds for all homogeneous random planar tessellations (Matschinski, 1954). Coefficients of variation and the correlation coefficients derived from numerical integration by Brakke (1987b) or estimated from simulation studies are tabulated in Tables 5.5.3 and 5.5.4. The correlation coefficients will remain unchanged if M is replaced by F or E .

5.5.2 Conditional moments of the characteristics of Poisson Voronoi cells

For $m = 2$, in addition to the unconditional moments reported in Table 5.5.1, Quine and Watson (1984, Tables 1 and 2) also estimate the first four conditional moments for the area A and perimeter P , given the number of vertices (sides) N of a PVC. The conditional moments of A are also estimated by Crain (1978), Drouffe and Itzykson (1984), Le Caer and Ho (1990) and Kumar and Kurtz (1993). Crain (1978) and Kumar and Kurtz (1993) have also estimated the conditional moments of P . The conditional moments of the length of a cell edge L have been studied by Boots (1987) and Kumar and Kurtz (1993). Estimates of the first conditional moments obtained by them are summarized in Table 5.5.5. We also report estimates of the second conditional moments obtained by Kumar and Kurtz (1993) in Table 5.5.6. On the basis of the results for A , Quine and Watson (1984) conjectured that

$$E(A|N) = \frac{2N - 3}{9\lambda}, \quad (5.5.7)$$

where $E(A|N)$ is the conditional expectation of the area A , given that the number of vertices (sides) is N , which is consistent with $E(A) = \lambda^{-1}$, but they are unable to offer a proof. The values for $E(A|N)$ in Table 5.5.5 are also consistent with the so-called *Lewis' law* which describes a linear relationship between $E(A|N)$ and N of the form

$$E(A|N) = \frac{b}{\lambda} (N - 6) + \frac{1}{\lambda}, \quad (5.5.8)$$

where b is a constant. This relationship was originally observed for a variety of biological tessellations (including cucumber epidermis and pigmented epithelium of the retina) (Lewis, 1928, 1930, 1931, 1943, 1944). Rivier and Lissowski (1982) and Rivier (1985a) tried to derive equation (5.5.8) by using the maximum entropy argument, but their argument was shown to be incorrect by Chiu (1995a). Thus, equation (5.5.8) remains an empirical law. See Chiu (1995b) for a review.

Least squares fits of the data in Table 5.5.5 to equation (5.5.8) yield values of $b = 0.199$ (correlation coefficient $r = 0.9906$, Quine and Watson, 1984), 0.219 ($r = 0.9991$, Crain, 1978, assuming that the columns for the conditional average second moment of the perimeter and for the average area have been mistakenly transposed; otherwise $b = 0.178$ and $r = 0.9987$), 0.226 ($r = 0.9997$, Kumar and Kurtz, 1993), 0.228 ($r = 0.9999$, Le Caer and Ho, 1990), 0.257 ($r = 0.9998$, Drouffe and Itzykson, 1984). There is an obvious

Table 5.5.2 The first and/or second-order moments of various characteristics of a Poisson Voronoi diagram in \mathbb{R}^3 .

Moment	Symbol	Exact value	Numerical value	Estimate
Intensity of cell vertices	λ_0	$(24/35) \pi^2 \lambda$	6.768 λ	
Intensity of mid-points of cell edges	λ_1	$(48/35) \pi^2 \lambda$	13.535 λ	
Intensity of centroids of cell faces	λ_2	$(24\pi^2/35 + 1) \lambda$	7.768 λ	
Intensity of cell centroids	λ_3	λ		
Expected total face area per unit volume	S_V	$4(\pi/6)^{1/3} \Gamma(5/3) \lambda^{1/3}$	$2.910\lambda^{1/3}$	
Expected total edge length per unit volume	L_V	$(16/15)(3/4)^{1/3} \pi^{2/3} \Gamma(4/3) \lambda^{2/3}$	$5.832 \lambda^{2/3}$	
Expected number of vertices of a typical cell $[E_3 N_0]$ and its second moment $[E_3(N_0^2)]$	$E(M)$	$(96/35) \pi^2$	27.071	
Expected number of edges of a typical cell $[E_3 N_1]$ and its second moment $[E_3(N_1^2)]$	$E(M^2)$		776.823	
Expected number of faces of a typical cell $[E_3 N_2]$ and its second moment $[E_3(N_2^2)]$	$E(E)$	$(144/35) \pi^2$	40.606	
Expected number of full neighbours of a typical cell and its second moment	$E(F)$	$(48\pi^2/35) + 2$	1747.852	
Expected number of faces of a typical cell $[E_3 N_2]$ and its second moment $[E_3(N_2^2)]$	$E(F^2)$		15.535	
Expected number of full neighbours of a typical cell and its second moment	$E(C)$	8	252.348	
Expected volume of a typical cell $[E_3 V_3]$ and its second moment $[E_3(V_3^2)]$	$E(C^2)$		8	
Expected surface area of a typical cell $[E_3 Y_1]$ and its second moment $[E_3(Y_1^2)]$	$E(V)$	λ^{-1}	68.155 λ^{-1}	
Expected total edge length of a typical cell $[E_3 V_1]$ and its second moment $[E_3(V_1^2)]$	$E(V^2)$		1.180 λ^{-2}	
Expected total face area of a typical cell $[E_3 Y_2]$ and its second moment $[E_3(Y_2^2)]$	$E(S)$	$(256\pi/3)^{1/3} \Gamma(5/3) \lambda^{-2/3}$	5.821 $\lambda^{-2/3}$	
Expected total edge length of a typical cell $[E_3 V_1]$ and its second moment $[E_3(V_1^2)]$	$E(S^2)$		36.070 $\lambda^{-4/3}$	
Expected number of vertices/edges of a typical face $[E_2 N_0 E_2 N_1]$ and its second moment $[E_2(N_0^2)/E_2(N_1^2)]$	$E(B)$	$(4\pi)^{5/3} \Gamma(1/3) / [5(9\lambda)^{1/3}]$	17.496 $\lambda^{-1/3}$	
Expected number of vertices/edges of a typical face $[E_2 N_0 E_2 N_1]$ and its second moment $[E_2(N_0^2)/E_2(N_1^2)]$	$E(B^2)$		319.738 $\lambda^{-2/3}$	
Expected number of vertices/edges of a typical face $[E_2 N_0 E_2 N_1]$ and its second moment $[E_2(N_0^2)/E_2(N_1^2)]$	$E(N)$	$144\pi^2/(24\pi^2 + 35)$	5.228	
Expected number of vertices/edges of a typical face $[E_2 N_0 E_2 N_1]$ and its second moment $[E_2(N_0^2)/E_2(N_1^2)]$	$E(N^2)$		29.825	

Table 5.5.2 continued

Moment	Symbol	Exact value	Numerical value	Estimate
Expected area of a typical face [$E_2 V_1$]	$E(A)$	$35(2)^{8/3} \pi^{1/3} \Gamma(2/3) / [(9\lambda)^{2/3} (24\pi^2 + 35)]$	$0.375\lambda^{-2/3}$	
and its second moment [$E_2(V_2^2)$]	$E(A^2)$		$0.283\lambda^{-4/3}$	
Expected total edge length of a typical face [$E_2 V_1$]	$E(P)$	$7(2)^{10/3} \pi^{5/3} \Gamma(1/3) / [(9\lambda)^{1/3} (24\pi^2 + 35)]$	$2.252\lambda^{-1/3}$	
and its second moment [$E_2(V_2^2)$]	$E(P^2)$		$6.540\lambda^{-2/3}$	
Expected length of a typical edge [$E_1 V_1$]	$E(L)$	$7 \Gamma(1/3) / [9(36\pi\lambda)^{1/3}]$	$0.431\lambda^{-1/3}$	
and its second moment [$E_1(V_1^2)$]	$E(L^2)$		$0.291\lambda^{-2/3}$	
Expected average breadth	$E(b)$	$[(16\pi^2)/243\lambda]^{1/3} [\Gamma(1/3)/5]$	$1.458\lambda^{-1/3}$	
and its second moment	$E(b^2)$		$2.156\lambda^{-2/3}$	
Expected value of a dihedral angle of a typical cell	$E(\alpha_i)$		2.068^\dagger	
and its second moment	$E(\alpha_i^2)$		4.456^\star	
Expected value of an interior angle of a typical face	$E(\alpha_i)$		1.940^\star	
and its second moment	$E(\alpha_i^2)$		4.150^\star	
Expected value of a dihedral angle on a typical edge	$E(\alpha_i)$	$2\pi/3$	2.094	
and its second moment	$E(\alpha_i^2)$	$\pi^2/2 - 3/8$	4.560	
Expected value of an angle at a typical vertex	$E(\gamma)$	$(48\pi^2 - 35)/(72\pi)$	1.940	
and its second moment	$E(\gamma^2)$	$(48\pi^2 - 175)/72$	4.149	

 $\lambda =$ intensity of Θ_P .^d Estimates from Monte Carlo simulation by Lorz and Hahn (1993).^s Estimates from Monte Carlo simulation by Quine and Watson (1984).^{*} Estimates from Monte Carlo simulation by Kumar and Kurtz (1995).

Sources of unmarked values: Gilbert (1962), Miles (1972a), Brakke (1987b) and Möller (1989*, 1994).
^{*} There are typos in the formulae for $E(S)$ [$E_3 V_2$], $E(P)$ [$E_2 V_1$] and $E(L)$ [$E_1 V_1$] in Möller (1989, p. 67).

Table 5.5.3 Coefficients of variation (c.v.) and correlation coefficients for various characteristics of a typical Poisson Voronoi cell in \mathbb{R}^3 .

	<i>V</i>	<i>S</i>	<i>B</i>	<i>M</i>	\bar{b}	α_3
c.v.	0.423*	0.254*	0.211*	0.246*	0.120†	0.204†
<i>V</i>	—	0.982*	0.938*	0.736*	0.945†	0.187†
<i>S</i>	—	—	0.924*	0.712*	0.987†	0.180†
<i>B</i>	—	—	—	0.875*	0.898†	0.222†
<i>M</i>	—	—	—	—	0.671†	0.247†
\bar{b}	—	—	—	—	—	0.170†

Characteristics:

V = volume*F* = number of faces/cell*S* = surface area/cell*M* = number of vertices/cell = $2F - 4 = 2E/3$ *B* = total edge length/cell \bar{b} = mean breadth/cell*E* = number of edges/cell α_3 = face angle of a cell

Sources: * Numerical values from Brakke (1987b) (see also Møller, 1994, Table 4.2.7).

† Estimates from Monte Carlo simulations by Lorz and Hahn (1993).

Table 5.5.4 Coefficients of variation (c.v.) and correlation coefficients for various characteristics of typical faces and edges of a Poisson Voronoi cell in \mathbb{R}^3 .

	<i>N</i>	<i>L</i>	<i>A</i>	<i>P</i>	α_2	α_1
c.v.	0.302*	0.753*	1.007*	0.538*	0.321†	0.199*
<i>N</i>	—	—	0.750*	0.746*	0.577†	—
<i>A</i>	—	—	—	0.928*	0.418†	—
<i>P</i>	—	—	—	—	0.456†	—
<i>L</i>	—	—	—	—	—	-0.000†

Characteristics:

N = number of vertices (edges)/face*P* = total edge length/face*L* = edge length α_2 = interior angle of a face*A* = area/face α_1 = face (dihedral) angle at an edge

Sources: * Numerical values from Brakke (1987b) (see also Møller, 1994, Table 4.2.6).

† Estimate from Monte Carlo simulations by Kumar and Kurtz (1995).

* Exact value = $\sqrt{1/8 - 27/(32\pi^2)}$.

† Estimates from Monte Carlo simulations by Lorz (1990b).

Table 5.5.5 Estimates of the first conditional moments of various characteristics of a typical Poisson Voronoi cell in \mathbb{R}^2 .

N	$\lambda E(A N)$					$\lambda^{1/2}E(P N)$			$\lambda^{1/2}E(L N)$		
	a	b	c	d	e	c	d	e	e	f	
3	0.342	0.342	0.359	0.360	0.342	2.803	2.828	2.747	0.916	0.910	
4	0.560	0.558	0.558	0.567	0.559	3.217	3.260	3.225	0.806	0.805	
5	0.777	0.774	0.778	0.773	0.774	3.650	3.660	3.647	0.729	0.733	
6	0.996	0.996	0.995	0.994	0.996	4.030	4.040	4.032	0.672	0.672	
7	1.228	1.222	1.223	1.214	1.222	4.382	4.396	4.385	0.627	0.625	
8	1.463	1.451	1.447	1.447	1.454	4.701	4.728	4.717	0.590	0.590	
9	1.693	1.688	1.661	1.710	1.688	4.981	5.068	5.029	0.559	0.553	
10	1.930	1.938	1.868	1.850	1.932	5.244	5.240	5.334	0.534	0.519	
11	2.155	2.16	2.063		2.173	5.475		5.625	0.512	0.512	
12	2.400	2.37	1.990		2.371	5.415		5.847	0.488	0.473	
13	2.691	2.6			2.555			6.049	0.465		
14	2.930								0.446		
15	3.200										
16	3.46										
18	4.00										
20	4.53										
25	5.84										
30	7.17										
35	8.42										
40	9.73										
45	11.02										
50	12.28										

λ = intensity of Θ_P .

Characteristics:

A = area of a cell

N = number of vertices (edges)

L = edge length

P = perimeter of a cell

Sources:

a Drouffe and Itzykson (1984, Table 1). Number of cells = 27 000.

b Le Caér and Ho (1990, Table 6). Numbers of cells = 600 696, 1 001 500 and 1 020 800.

c Quine and Watson (1984, Tables 1 and 2). Number of cells = 50 000.

d Crain (1978, Table III). Number of cells = 25 000.

e Kumar and Kurtz (1993, Tables 8, 9 and 10). Number of cells = 2 000 000.

f Boots (1987, Table 1). Number of cells = 30 000.

change in the slope in Drouffe and Itzykson (1984) for $n > 12$; their data for $n \leq 11$ yield $b = 0.228$ and $r = 0.9999$.

Szeto and Tam (1995) found in their study that *Feltham's law*, which states that $E(P|N)$ is linear in N , has a comparable but smaller statistical error than Lewis' law for PVCs. However, the correlation coefficients of $E(P|N)$ and N obtained from other studies (0.9835, Quine and Watson, 1984; 0.9959, Crain, 1978; 0.9941, Kumar and Kurtz, 1993) suggested the opposite, because these values are smaller than the corresponding correlation coefficients

Table 5.5.6 Estimates of the second conditional moments of various characteristics of a typical Poisson Voronoi cell in \mathbb{R}^2 .

N	$\lambda^2 E(A^2 N)$	$\lambda E(P^2 N)$	$\lambda E(L^2 N)$
3	0.161	8.208	0.952
4	0.399	11.064	0.806
5	0.730	13.965	0.710
6	1.168	16.921	0.637
7	1.717	19.899	0.578
8	2.386	22.919	0.530
9	3.172	25.974	0.489
10	4.096	29.125	0.456
11	5.131	32.321	0.428
12	6.007	34.791	0.392
13	6.897	37.068	0.366
14	—	—	0.309

λ = intensity of Θ_p .

Characteristics:

A = area of a cell

N = number of vertices (edges)

L = edge length

P = perimeter of a cell

Sources: Kumar and Kurtz (1993, Tables 8, 9 and 10). Number of cells = 2 000 000.

of $E(A|N)$ and N . Kumar and Kurtz (1993), on the basis of two million simulated PVCs in \mathbb{R}^2 (except for three-sided cells which are based on the simulation of one million cells), suggested empirically that

$$\lambda^{1/2} E(P|N) = 1.4879 N^{0.5519}.$$

Estimations of the correlations $r(A, P|N)$ between A and P , controlling for N , are given by Crain (1978, Table 3). His results show that in general $r(A, P|N)$ increases with N , indicating increasing 'circularity'.

For $m = 3$, the first four conditional moments of the volume V , the surface area S , the total edge length B , the mean breadth \bar{b} , and a randomly selected face (dihedral) angle α_3 of a typical PVC, the number of edges N and an interior angle α_2 of a typical face, and the length L of and the face angle α_1 at a typical edge, given the number of faces F , have been estimated from Monte Carlo simulation by various researchers (see Table 5.5.7). Also, the first two conditional moments of the face area A , the face perimeter P and an interior angle α_2 of a typical face, given the number of edges N , have been estimated. We report only the estimates for the first conditional moments of these characteristics (see Tables 5.5.8 and 5.5.9). Note that

$$E(N|F) = 6 - \frac{12}{F}$$

(see Zallen, 1983).

Table 5.5.7 Simulation studies for the conditional moments of various characteristics of Poisson Voronoi cells in \mathbb{R}^3 .

Study	Number of cells	Characteristics	
		Conditional on F	Conditional on N
Quine and Watson (1984)	2 500	$B S V$	
Lorz (1990b)	82 870	$B S V \bar{b} \alpha_3$	$A P \alpha_2$
Kumar <i>et al.</i> (1992)	358 000	N	
	102 000	$L S V$	$A L$
Kumar and Kurtz (1995)	377 000	$\alpha_1 \alpha_2$	$P \alpha_2$
	165 000	B	

Characteristics:

A = area/face

S = surface area/cell

B = total edge length/cell

V = volume

F = faces/cell

\bar{b} = mean breadth/cell

L = edge length

α_1 = face (dihedral) angle at an edge

N = edges/face

α_2 = interior angle of a face (bond angle)

P = edge length/face

α_3 = face angle of a cell

The values of the mean volume $E(V|F)$ of a typical cell conditional on its number of faces F in Table 5.5.8 show a reasonable fit with the three-dimensional version of Lewis' law (equation (5.5.8)) suggested by Rivier (1982, 1983a,b, 1985a, 1986a) and given by

$$E(V|F) = \frac{b}{\lambda}(F - E(F)) + \frac{1}{\lambda}, \quad (5.5.9)$$

where λ is the intensity of Θ_p and b is a constant. Similar to equation (5.5.8), equation (5.5.9) cannot be derived from the maximum entropy argument (Chiu, 1995a) and remains an empirical law. Values of Kumar *et al.* (1992), Lorz (1990b), and Quine and Watson (1984) in Table 5.5.8 lead to correlation coefficients and least squares estimates of $r = 0.9982$ and $b = 0.0942$, $r = 0.9897$ and $b = 0.095$, and $r = 0.9863$ and $b = 0.084$, respectively, for equation (5.5.9). Kumar *et al.* (1992) and Kumar and Kurtz (1995), based on their simulation studies, suggested empirically that

$$\begin{aligned} E(V|F) &= 0.0942F - 0.4338, \\ E(S|F) &= 0.3102F + 1.002, \\ E(B|F) &= 0.9647F + 2.5078, \\ E(A|N) &= 0.1812N - 0.5725, \\ E(P|N) &= 3.0534 \ln N - 2.7968. \end{aligned}$$

$$\begin{aligned} E(V|F) &= 0.0164F^{1.498}, \\ E(S|F) &= 0.5614F^{0.8526}, \\ E(B|F) &= 1.6552F^{0.8596}, \end{aligned}$$

Such equations are no more than a good empirical approximation and have not been theoretically justified.

Table 5.5.8 Estimates of the first conditional moments of various characteristics of a typical Poisson Voronoi cell in \mathbb{R}^3 .

Table 5.5.8 continued

F	$\lambda E(V F)$			$\lambda^{2/3} E(S F)$			$\lambda^{1/3} E(B F)$			$\lambda^{1/3} E(\bar{b} F)$			$E(\alpha_3 F)$			$\lambda^{1/3} E(L F)$			$E(\alpha_1 F)$		
	a	b	c				d	b				b	d				d'	a			
				a	b	c			d	b	d			b	d	b			a	d'	
26	2.062	1.988	1.885	8.969	8.787	27.653	27.063	1.761	2.321	2.007	0.311	2.307	—	—	—	—	—	—	—	—	—
27	2.154	2.149	—	9.243	9.226	28.206	28.161	1.802	2.312	2.011	0.300	2.322	—	—	—	—	—	—	—	—	—
28	2.247	2.285	—	9.538	9.575	29.500	29.390	1.833	2.366	2.014	0.304	2.333	—	—	—	—	—	—	—	—	—
29	—	2.553	1.878	—	10.150	30.552	30.373	1.876	2.226	2.017	0.296	2.346	—	—	—	—	—	—	—	—	—
30	—	2.106	—	—	9.010	—	29.881	1.773	2.229	2.020	0.309	2.352	—	—	—	—	—	—	—	—	—
31	—	2.838	2.072	—	11.192	—	31.026	1.984	2.378	2.022	0.287	2.375	—	—	—	—	—	—	—	—	—
32	—	—	—	—	—	—	—	—	—	—	—	—	—	—	—	—	—	—	—	—	—

λ = intensity of Θ_p

Characteristics:

B = total edge length/cell

F = number of faces/cell

L = edge length

S = surface area/cell

V = volume

\bar{b} = mean breadth/cell
 α_1 = face (dihedral) angle at an edge
 α_2 = interior angle of a face (bond angle)
 α_3 = face angle of a cell

Sources:

a Kumar *et al.* (1992, Tables VI, VII and IX). Number of cells = 102 000.

b Lorz (1990b). Number of cells = 82 870.

c Quine and Watson (1984, Table 4). Number of cells = 2 500.

d Kumar and Kurtz (1995, Table 7). Number of cells = 165 000.

d' Kumar and Kurtz (1995, Tables 3 and 4). Number of cells = 377 000.

Table 5.5.9 Estimates of the first conditional moments of various characteristics of a typical face of a Poisson Voronoi cell in \mathbb{R}^3 .

N	$\lambda^{2/3} E(A N)$		$\lambda^{1/3} E(P N)$		$\lambda^{1/3} E(L N)$		$E(\alpha_2 N)$	
	a	c	b	c	a	b	c	
3	0.046	0.035	0.752	0.754	0.251	1.047	1.048	
4	0.139	0.136	1.531	1.528	0.382	1.571	1.571	
5	0.304	0.303	2.240	2.237	0.448	1.885	1.884	
6	0.505	0.504	2.833	2.831	0.473	2.095	2.095	
7	0.709	0.709	3.310	3.309	0.473	2.244	2.245	
8	0.907	0.908	3.696	3.699	0.462	2.357	2.358	
9	1.092	1.095	4.018	4.024	0.447	2.444	2.448	
10	1.263	1.260	4.279	4.278	0.429	2.513	2.512	
11	1.433	1.432	4.521	4.530	0.413	2.571	2.573	
12	1.561	1.537	4.721	4.665	0.393	2.618	2.632	
13	1.766	1.724	4.923	4.933	0.384	2.658	2.706	
14	1.839	1.807	5.141	5.152	0.364	2.693	2.639	
15	1.859	2.166	—	5.532	0.335	2.723	2.778	

λ = intensity of \mathcal{V}_p .

Characteristics:

A = area/face

P = total edge length/face

L = individual edge length

α_2 = interior angle of a face (bond angle)

N = number of vertices (edges)/face

Sources:

a Kumar *et al.* (1992, Table VIII). Number of cells = 102 000.

b Kumar and Kurtz (1995, Tables 5 and 6). Number of cells = 377 000.

c Lorz (1990b). Number of cells = 82 870.

5.5.3 Conditional moments of the characteristics of the neighbouring cells of a Poisson Voronoi cell

In some areas of application, particularly materials science and geography, there is considerable interest in how individual cells are arranged within \mathcal{V}_p . Although \mathcal{V}_p is an ergodic tessellation, we know that characteristics of an individual cell cannot be independent of those of contiguous cells. So far these dependences have been explored by examining the relationships between the value of a given characteristic for an individual cell and the mean value of that characteristic for contiguous cells. The most extensively studied characteristic is m_n , the first conditional moment of the number of edges of a randomly selected neighbouring cell of a typical PVC, given that the typical PVC has n edges. Aboav (1970) found empirically that in the cellular structure of a polycrystal,

$$m_n = 5 + \frac{8}{n}.$$

The value of the coefficient of n^{-1} is not always 8 but depends on the structure of the tessellation. Let N denote a random variable having the same

distribution as the random number of edges of a typical cell. Denote $\Pr \{N = n\}$ by p_n . Weaire (1974) showed that

$$\sum m_n n p_n = \text{Var}(N) + 36, \quad (5.5.10)$$

where $\text{Var}(N)$ is the variance of N , and suggested semi-empirically that

$$m_n = 5 + \frac{6 + \text{Var}(N)}{n}. \quad (5.5.11)$$

Later Aboav (1980) proposed

$$m_n = 6 - a + \frac{6a + \text{Var}(N)}{n},$$

where a is a parameter which depends on the structure of the tessellation.

Numerous empirical studies of the relation between m_n and n have been done. See Chiu (1995b) for a review. Most of the studies suggested that $m_n n$ is linear in n with slope 5, where $m_n n$ is the conditional mean of the total number of edges of all neighbouring cells of a typical cell, given that it has n edges. However, deviations do exist. Peshkin *et al.* (1991) used a maximum entropy argument to 'prove' the linearity between $m_n n$ and n . Chiu (1994, 1995a) showed that their argument is incorrect and established the rigorous relation between m_n and n . Denote by $k(n, j)$ the average number of n -edged cells of a typical j -complex. A j -complex is the collection of a j -edged

Table 5.5.10 Estimates of m_n , the first conditional moments of the number of edges of a randomly selected neighbouring cell of a typical Poisson Voronoi cell in \mathbb{R}^2 , given that the typical cell has n edges.

Boots and Murdoch (1983)		Le Caér and Ho (1990)	Kumar and Kurtz (1993)
50 000 cells		1 020 800 cells	650 000 cells
		1 001 500 cells	
		600 696 cells	
n	m_n	m_n	m_n
3	7.013	7.009	7.017
4	6.731	6.718	6.719
5	6.493	6.492	6.485
6	6.312	6.315	6.312
7	6.169	6.171	6.167
8	6.048	6.050	6.044
9	5.932	5.948	5.948
10	5.841	5.859	5.850
11	5.779	5.78	5.774
12	5.655	—	5.703
13	5.615	—	5.615
14	5.5	—	—

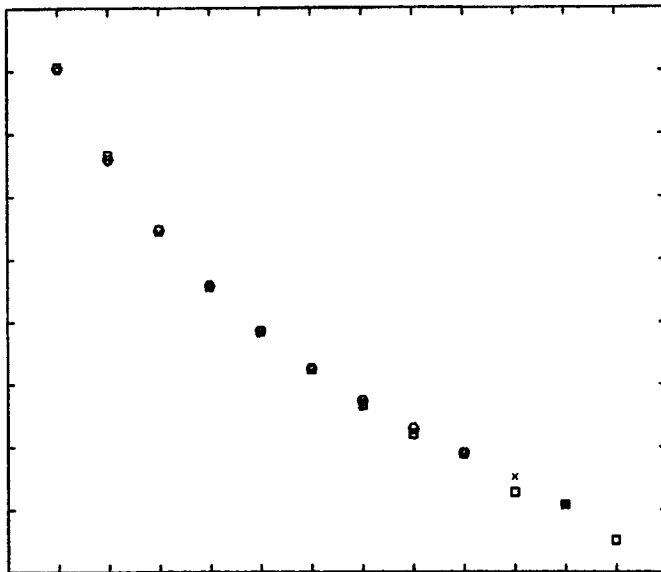


Figure 5.5.1 Values of m_n for Poisson Voronoi cells in \mathbb{R}^2 (values from: \square Boots and Murdoch, 1983; \times Le Caer and Ho, 1990; \circ Kumar and Kurtz, 1993).

cell and all its neighbouring cells. Let c_n denote the covariance between $k(n, N)$ and N . Chiu (1994) has shown that for a stationary regular tessellation in \mathbb{R}^2 ,

$$m_n = 5 + \frac{6 + c_n/p_n}{n}, \quad p_n > 0. \quad (5.5.12)$$

Note that if $p_n = 0$, then m_n is undefined. A general equation similar to equation (5.5.12) for a regular and normal stationary tessellation in \mathbb{R}^m has also been derived. Since in many natural two-dimensional tessellations, $3 \leq n \leq 8$ and both c_n and p_n do not vary too much with n , the ratio c_n/p_n may be well approximated by a constant or a linear function of n . Thus, equation (5.5.12) explains the empirical linearity between m_n , n and n . However, for Poisson Voronoi diagrams, theoretical values of c_n are unknown. Thus, it is desirable to find a good and simple approximation of m_n for \mathcal{V}_p . Table 5.5.10 and Figure 5.5.1 give the simulated values of m_n by Boots and Murdoch (1983), Le Caer and Ho (1990) and Kumar and Kurtz (1993).

Although the data show a reasonably good fit to

$$m_n = B_0 + \frac{B_1}{n}, \quad (5.5.13)$$

for some constants B_0 and B_1 , deviations do exist. Boots and Murdoch (1983) suggested the form

$$m_n = B_0 + \frac{B_1}{n} + \frac{B_2}{n^2}, \quad (5.5.14)$$

whilst Le Caér and Ho (1990) suggested

$$m_n = B_0 + \frac{B_1}{n} + B_3 n, \quad (5.5.15)$$

which means that m_n , n is not a linear but a quadratic function of n . The least squares estimates and the coefficients of determination are summarized in Table 5.5.11. Either equation (5.5.14) or (5.5.15) gives a higher coefficient of determination than equation (5.5.13). Kumar *et al.* (1994) used equation (5.5.29) to argue heuristically that

$$m_n = 4.942 + \frac{7.223}{n} - \frac{6.543}{n^2}, \quad (5.5.16)$$

which has the same form as equation (5.5.14) but the values of the parameters are rather different from those obtained in simulation studies (see Table 5.5.11). Aboav (1987) has also suggested the following equation, which is devoid of any arbitrary constants:

$$m_n = E(N) + \frac{2}{n} + \frac{E(N^{1/2}) - n^{1/2}}{2}, \quad (5.5.17)$$

although he offers no theoretical support for this form. Equation (5.5.17) is not valid for all Voronoi diagrams, since putting equation (5.5.17) into the sum rule given in equation (5.5.10) yields

$$\text{Var}(N) = 2 + \frac{E(6N^{1/2}) - E(N^{3/2})}{2},$$

which is approximately true for Poisson Voronoi diagrams but not for Voronoi diagrams generated by eigenvalues of random matrices (Le Caér and Ho, 1990).

The empirical Aboav's law and all its variations suggest that few-edged cells are more likely to be in contact with many-edged cells and vice versa, which was already observed in planar tessellations seen in epithelia by Lewis (1931). Moreover, the empirical Lewis' law given in equation (5.5.8) suggests that a many-edged cell is more likely to be a large cell. Hence, the area of a given cell and the areas of its neighbouring cells are negatively correlated (see, for example, Seul *et al.*, 1994, Figure 3).

Since the number of edges of a cell is influenced by its neighbouring cells, which in turn are under the influence of their neighbouring cells, *neighbours of higher orders* will also affect the number of edges of a cell. Fortes and Pina (1993) considered such higher order neighbouring relations. Let a typical cell be the zeroth-order neighbour and all its neighbouring cells be the first-order neighbours. The neighbouring cells of a first-order neighbour, excluding the zeroth-order and all other first-order neighbours, are the second-order neighbours. Inductively, the k th-order neighbours can be defined. Let the mean total number of k th-order neighbours of a typical cell, given that this typical cell has n edges, be denoted by $q_n^{(k)}$ and the number of edges of a randomly selected k th-order neighbour by $m_n^{(k)}$. Fortes and Pina (1993) found empirically that $q_n^{(k)}$ and $q_n^{(k)}m_n^{(k)}$ are linear in n for $k = 1, 2, 3$ and 4.

Table 5.5.11 Least squares regressions for various approximations of m_n and the corresponding coefficients of determination R^2 .

m_n	Boots and Murdoch (1983)		Le Caär and Ho (1990)		Kumar and Kurtz (1993)	
	R^2	m_n	R^2	m_n	R^2	
$5.251 + \frac{5.755}{n}$	0.959	$5.399 + \frac{5.012}{n}$	0.977	$5.312 + \frac{5.474}{n}$	0.971	
$4.823 + \frac{11.428}{n} - \frac{14.724}{n^2}$	0.996	$5.010 + \frac{9.615}{n} - \frac{10.901}{n^2}$	1.000	$4.935 + \frac{10.270}{n} - \frac{12.181}{n^2}$	0.998	
$6.165 + \frac{3.164}{n} - 0.063n$	0.999	$6.178 + \frac{3.094}{n} - 0.063n$	1.000	$6.100 + \frac{3.306}{n} - 0.057n$	1.000	

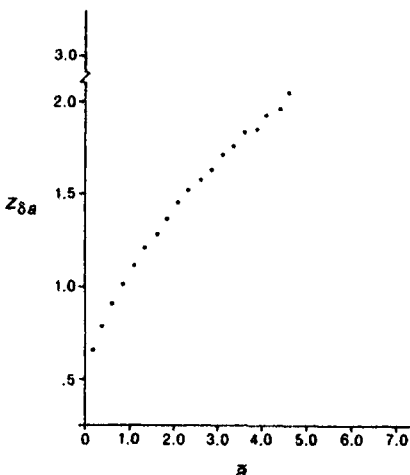


Figure 5.5.2 Values of $z_{\delta a}$ for Poisson Voronoi cells in \mathbb{R}^2 . (Source: Boots and Murdoch, 1983.)

Delannay *et al.* (1992) introduced the *topological correlation function* A_{kn} , which is defined as

$$A_{jn} = \frac{M_j(n)}{p_j},$$

where $M_j(n)$ is the average number of j -edged neighbouring cells of a typical n -edged cell. They used A_{jn} to compare the topological properties of tessellations which show different distributions of number of cell edges. Clearly, A_{jn} satisfies

$$A_{jn} = A_{nj}, \quad A_{jn} \geq 0,$$

$$\sum_j A_{jn} p_j = n, \quad \sum_j j A_{jn} = nm_n.$$

For Voronoi diagrams, since two 3-edged cells cannot share an edge without creating at least one non-convex cell, we have $A_{33} = 0$. Further discussions on A_{jn} can be found in Delannay *et al.* (1993, 1994) and Le Caér and Delannay (1993a,b).

Boots and Murdoch (1983) also estimate the relationships between neighbouring cells for the standardized measures of the area and perimeter of a PVC in \mathbb{R}^2 . Denote by $z_{\delta a}$ the average value of the standardized area λA of the neighbouring cells of a typical PVC, given that the standardized area of the typical PVC is in the interval δa . Values of $z_{\delta a}$ are illustrated in Figure 5.5.2. The relationship may be summarized by

$$z_{\delta a} = b_0 + b_1 \bar{a}^{1/2} + b_2 \bar{a}, \quad (5.5.18)$$

where $b_0 = 0.364$, $b_1 = 0.629$, $b_2 = 0.080$ and \bar{a} is the midpoint of the interval δa . Finally, denote by $r_{\delta p}$ the average value of the standardized perimeter $\lambda^{1/2} P/4$ for the neighbouring cells of a typical PVC, given that the standardized

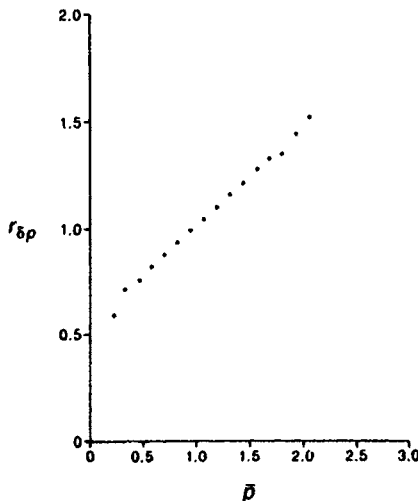


Figure 5.5.3 Values of $r_{\delta p}$ for Poisson Voronoi cells in \mathbb{R}^2 .
 (Source: Boots and Murdoch, 1983.)

perimeter of the typical PVC is in the interval δp . Values of $r_{\delta p}$ are shown in Figure 5.5.3. These values indicate a linear relationship described by

$$r_{\delta p} = b_0 + b_1 \bar{p}, \quad (5.5.19)$$

where $b_0 = 0.564$, $b_1 = 0.456$ and \bar{p} is the midpoint of the interval δp .

Stoyan and Hermann (1986) considered the cell pair of a typical edge. Let \mathcal{A}_1 and \mathcal{A}_2 be the areas of the individual cells of such a cell pair. On the basis of 1290 simulated cells, they obtained the following estimates: $E(\mathcal{A}_1) = 1.06$, $E(\mathcal{A}_1^2) = 1.42$, and $E(\mathcal{A}_1 \mathcal{A}_2) = 1.24$. Thus, the correlation coefficient of \mathcal{A}_1 and \mathcal{A}_2 is 0.39. Moreover, the values of $k_{mm}(r)$, the mean of the product of cell areas corresponding to two generating points of distance r apart, are estimated, which can be approximated by $0.28 + 0.72 [1 - \exp \{-r(0.4 + 1.1 r)\}]$ for $r \geq 0$.

For $m = 3$, relatively few investigations on the conditional moments of the characteristics of the neighbouring cells of a typical PVC have been done. Kumar *et al.* (1992) simulated 3729 PVCs and suggested that

$$m_f^{(3)} = 16.57 - 0.02f,$$

where $m_f^{(3)}$ is the mean number of faces of a randomly selected neighbouring cell of a typical cell in \mathbb{R}^3 , given that the typical cell has f faces. Using the same data set, Fortes (1993) proposed an equation similar to Aboav's law given in equation (5.5.13):

$$m_f^{(3)} = 15.95 + \frac{4.45}{f},$$

with correlation 0.865. Aboav (1991, 1992) found empirically that in a pure aluminium polycrystal, the three-dimensional version of the mean number m_n of edges of a randomly selected neighbouring face of a typical face, given that the typical face has n edges, can be expressed as

$$m_n = E(N) + \frac{\text{Var}(N)}{n},$$

where N has the same distribution as the number of edges of a typical face of a PVC in \mathbb{R}^3 . Chiu (1994) proved that for a regular and a normal stationary tessellation in \mathbb{R}^3

$$m_f^{(3)} = E(F) - 1 + \frac{E(F) + c'_f / p_f}{f},$$

$$m_n = E(N) + \frac{E(N) - n + c_n / p_n}{2n},$$

in which F , N , p_n and c_n are the same as defined above, $p_f = \Pr\{F = f\}$ and c'_f is the covariance of $k^{(3)}(f, F)$ and F , where $k^{(3)}(f, j)$ is the number of f -faced neighbouring cells of a typical three-dimensional j -complex. A three-dimensional j -complex is the collection of a j -faced cell and all its neighbouring cells.

5.5.4 Distributional properties

Since many of the moments and correlations of the characteristics for the PVCs given in Tables 5.5.1–5.5.6 and 5.5.8–5.5.9 may not differ greatly from the corresponding values for cells in tessellations where the generating set is located in \mathbb{R}^m according to point processes other than Θ_p (Hermann *et al.*, 1989), for empirical applications it is desirable to know the nature of the distributions of the PVC characteristics. Analytical expressions for the distributions of the length of a typical edge L (Brakke, 1987a,b; Muche, 1996a; Schlather 1999) and various angles (Miles, 1970a; Muche, 1996a, 1998) are known. The spherical and linear contact distributions have been obtained by Muche and Stoyan (1992). Simulation has been used to study the distributions of other characteristics. In particular most attention has been focused on the distributions of N and A in \mathbb{R}^2 and L and V in \mathbb{R}^3 , since the first of these is easy to measure manually and the second can be simply determined by image processing systems.

Mecke and Muche (1995) proved that the distribution of the length L of a typical edge of \mathcal{V}_p in \mathbb{R}^m has the same distribution as the length of an edge at a typical vertex. Using this result, Muche (1996a) showed that the distribution function F_L of L in \mathbb{R}^m is given by

$$F_L(l) = \int_0^\infty \int_0^\pi \left\{ 1 - \exp[-\lambda v_m(r, r_{l,\beta}, l)] \right\} f_\beta(\beta) f_R(r) d\beta dr, \quad (5.5.20)$$

where

$$r_{l,\beta} = \sqrt{r^2 + l^2 - 2lr \cos \beta}, \quad (5.5.21)$$

and $v_m(r, r_{l,\beta}, l)$ is the difference between the volume of an m -dimensional ball with radius $r_{l,\beta}$ and the volume of the intersection of this ball and another m -dimensional ball with radius r where the distance between the two centres is l . The explicit expressions for $v_m(r, r_{l,\beta}, l)$ are given in Muche (1996a,

equations (3.3) and (3.4)) (cf. equation (5.5.26)). The function f_R is the probability density function (pdf) of the distance from an arbitrary vertex to either one of its $m + 1$ nearest neighbouring generators, which is the generalized gamma distribution (Miles, 1970b, 1974):

$$f_R(r) = \frac{m(\lambda\omega_m)^m}{(m-1)!} r^{m^2-1} \exp(-\lambda\omega_m r^m), \quad r \geq 0, \quad (5.5.22)$$

where $\omega_m = \pi^{m/2}/\Gamma(m/2 + 1)$ is the volume of an m -dimensional sphere of unit radius. The function f_β is the pdf of the angle spanned by an edge emanating from a typical vertex and the line joining the typical vertex and the generator of a cell containing this edge. The result in Mecke and Muche (1995, equation (4.3)) implies that this density is the same as that given in equation (5.11.12) in the case $m = 2$:

$$f_\beta(\beta) = \frac{4}{3\pi} [(\pi - \beta) \cos \beta + \sin \beta] \sin \beta, \quad 0 \leq \beta < \pi. \quad (5.5.23)$$

Muche (1996a) gave explicitly the analytical expression of f_β for $m = 3, 4$ and 5 :

$$\begin{aligned} m=3, \quad f_\beta(\beta) &= \frac{105}{128} (1 + \cos \beta)^2 \sin^5 \beta, & 0 \leq \beta < \pi, \\ m=4, \quad f_\beta(\beta) &= \frac{2^{12}}{2145\pi} [3 \sin \beta - \sin^3 \beta + 3(\pi - \beta) \cos \beta] \sin^{11} \beta, & 0 \leq \beta < \pi, \\ m=5, \quad f_\beta(\beta) &= \frac{3380195}{3 \cdot 2^{21}} (3 - \cos \beta) (1 + \cos \beta)^3 \sin^{19} \beta, & 0 \leq \beta < \pi. \end{aligned} \quad (5.5.24)$$

The densities are shown in Figure 5.5.4. Schlather (1999) gave a more complete general expression of F_L for \mathcal{V}_p in \mathbb{R}^m :

$$\begin{aligned} F_L(l) &= 1 - \frac{\frac{m^2 \Gamma\left(\frac{m^2}{2}\right)}{2} \pi^{(m^2-1)/2}}{2\Gamma\left(\frac{m^2+1}{2}\right) \Gamma(m-1)} \left[\frac{\lambda}{\Gamma\left(\frac{m+2}{2}\right)} \right]^m \\ &\quad \times \int_0^\infty \int_0^\pi r^{m^2-1} \exp[-\lambda U_m(r, r_{l,\beta}, l)] \sin^{m^2-m-1} \beta \\ &\quad \times \left(m \cos \beta \int_\beta^\pi \sin^m \varphi d\varphi + \sin^{m+1} \beta \right) d\beta dr, \quad l \geq 0, \end{aligned} \quad (5.5.25)$$

where $r_{l,\beta}$ is given in equation (5.5.21) and $U_m(r, r_{l,\beta}, l)$ denotes the volume of the union of two m -dimensional balls with radii r and $r_{l,\beta}$ and the distance between their centres is l :

$$U_m(r, r_{l,\beta}, l) = \omega_{m-1} \left[r^m I_m(\beta) + r_{l,\beta}^m I_m \left(\cos^{-1} \frac{l - r \cos \beta}{r_{l,\beta}} \right) \right], \quad (5.5.26)$$

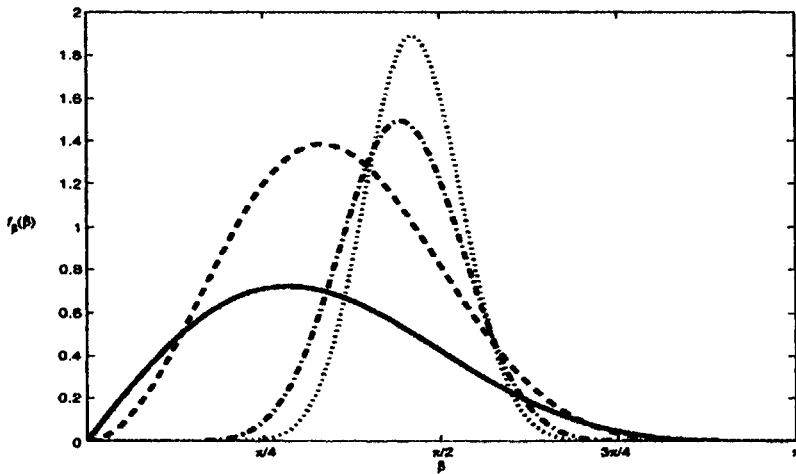


Figure 5.5.4 Probability density functions of the angle β spanned by an edge emanating from a typical vertex and the line joining the typical vertex and the generator of a cell containing this edge: — $m = 2$; - - $m = 3$; · - $m = 4$; ··· $m = 5$.

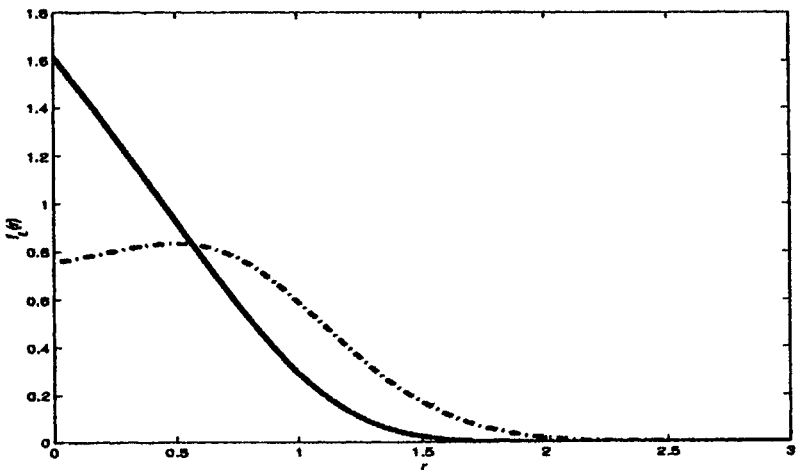


Figure 5.5.5 Probability density function of the length L of a typical edge in an m -dimensional Poisson Voronoi diagram with intensity $\lambda = 1$: — $m = 3$; · - $m = 2$ (values from Brakke, 1987a, b) (see also Muche, 1996a, Figure 1).

Table 5.5.12 Probability density functions for the length L of a typical edge in an m -dimensional Poisson Voronoi diagram with intensity $\lambda = 1$.

r	$f_L(r)$		r	$f_L(r)$	
	$m = 2$	$m = 3$		$m = 2$	$m = 3$
0.00	0.7545	1.6169	1.55	0.1413	0.0167
0.05	0.7636	1.5509	1.60	0.1171	0.0113
0.10	0.7732	1.4841	1.65	0.0962	0.0075
0.15	0.7831	1.4165	1.70	0.0782	0.0049
0.20	0.7933	1.3482	1.75	0.0631	0.0031
0.25	0.8035	1.2793	1.80	0.0504	0.0019
0.30	0.8133	1.2098	1.85	0.0399	0.0012
0.35	0.8222	1.1399	1.90	0.0312	0.0007
0.40	0.8295	1.0695	1.95	0.0243	0.0004
0.45	0.8344	0.9990	2.00	0.0187	0.0002
0.50	0.8361	0.9284	2.05	0.0143	0.0001
0.55	0.8340	0.8581	2.10	0.0108	0.0001
0.60	0.8274	0.7882	2.15	0.0081	0.0000
0.65	0.8156	0.7192	2.20	0.0060	0.0000
0.70	0.7985	0.6513	2.25	0.0044	0.0000
0.75	0.7758	0.5850	2.30	0.0032	0.0000
0.80	0.7478	0.5207	2.35	0.0023	0.0000
0.85	0.7147	0.4590	2.40	0.0017	0.0000
0.90	0.6770	0.4003	2.45	0.0012	0.0000
0.95	0.6356	0.3450	2.50	0.0008	0.0000
1.00	0.5911	0.2937	2.55	0.0006	0.0000
1.05	0.5446	0.2467	2.60	0.0004	0.0000
1.10	0.4970	0.2042	2.65	0.0003	0.0000
1.15	0.4492	0.1665	2.70	0.0002	0.0000
1.20	0.4021	0.1335	2.75	0.0001	0.0000
1.25	0.3564	0.1053	2.80	0.0001	0.0000
1.30	0.3129	0.0815	2.85	0.0001	0.0000
1.35	0.2721	0.0619	2.90	0.0000	0.0000
1.40	0.2343	0.0460	2.95	0.0000	0.0000
1.45	0.1998	0.0335	3.00	0.0000	0.0000
1.50	0.1688	0.0239	3.05	0.0000	0.0000

Source: Brakke (1987a, b).

with

$$I_m(x) = \int_x^\pi \sin^m \phi \, d\phi. \quad (5.5.27)$$

Brakke (1987a,b) has given equivalent expressions for the pdf of L in the case $m = 2$ and $m = 3$ and the values obtained from numerical integration are given in Table 5.5.12 and Figure 5.5.5.

The simulation studies by Le Caer and Ho (1990) and Moore and Moore (1993) suggested that in the case $m = 2$ the distribution of the standardized

length of a typical edge of a PVC ($3\lambda^{1/2}L/2$) is well approximated by a folded normal distribution, i.e. the distribution of the absolute value of a Gaussian variable with mean μ and variance σ^2 , with $\mu = 0.9144$ and $\sigma = 0.7623$. This result is consistent with that from the simulations of Boots (1987).

Denote by E^1 a typical edge. Let β_1 and β_2 be the angles spanned by E^1 and the lines joining one of the neighbouring generators and an endpoint of E^1 . These two angles are identically distributed. Denote by E^0 an edge emanating from a typical vertex. Mecke and Muche (1995, equation (4.3)) showed that β_1 and β_2 have the same joint distribution as the two angles spanned by E^0 and the lines passing one of the neighbouring generators and an endpoint of E^0 . Thus, β_1 and β_2 have the same marginal distribution f_β and is given in equations (5.5.23) and (5.5.24) when $m = 2, 3, 4$ and 5. Muche (1996a) derived the joint pdf of β_1 and β_2 for $m = 2$:

$$f_{\beta_1, \beta_2}(\beta_1, \beta_2) = \frac{16\pi}{3} \frac{[(\pi - \beta_1) \cos \beta_1 + \sin \beta_1][(\pi - \beta_2) \cos \beta_2 + \sin \beta_2] \sin^3 \beta_1 \sin^3 \beta_2}{[(\pi - \beta_1) \sin^2 \beta_2 + (\pi - \beta_2) \sin^2 \beta_1 + \sin \beta_1 \sin \beta_2 \sin(\beta_1 + \beta_2)]^3},$$

$$\beta_1 \geq 0, \beta_2 \geq 0, \beta_1 + \beta_2 < \pi,$$

and for $m = 3$:

$$f_{\beta_1, \beta_2}(\beta_1, \beta_2) = \frac{945}{2} \frac{(1 + \cos \beta_1)^2 (1 + \cos \beta_2)^2 \sin^8 \beta_1 \sin^8 \beta_2}{[(2 + (2 + \sin^2 \beta_2) \cos \beta_2) \sin^3 \beta_1 + [2 + (2 + \sin^2 \beta_1) \cos \beta_1] \sin^3 \beta_2]^4},$$

$$\beta_1 \geq 0, \beta_2 \geq 0, \beta_1 + \beta_2 < \pi.$$

Schlather (1999) gave the general expression of the joint pdf of β_1 and β_2 for \mathcal{V}_P in \mathbb{R}^m :

$$f_{\beta_1, \beta_2}(\beta_1, \beta_2) = \frac{2m\Gamma\left(\frac{m^2+2}{2}\right)\pi^{(m-1)/2}}{m(m+1)\Gamma\left(\frac{m^2-1}{2}\right)} \left(\frac{\Gamma\left(\frac{m+1}{2}\right)}{\Gamma\left(\frac{m+2}{2}\right)}\right)^m$$

$$\times \frac{(mI_m(\beta_1) \cos \beta_1 + \sin^{m+1} \beta_1)(mI_m(\beta_2) \cos \beta_2 + \sin^{m+1} \beta_2) \sin^{m^2-1} \beta_1 \sin^{m^2-1} \beta_2}{(I_m(\beta_1) \sin^m \beta_2 + I_m(\beta_2) \sin^m \beta_1)^{m+1}},$$

where I_m is given in equation (5.5.27).

In \mathbb{R}^2 , there are exactly three edges meeting at a typical vertex. The joint distribution of two randomly selected angles X_1 and X_2 spanned by these three edges is

$$f_{X_1, X_2}(x_1, x_2) = -\frac{8}{3\pi} \sin x_1 \sin x_2 \sin(x_1 + x_2), \quad \pi - x_1 \leq x_2 \leq \pi, \quad (5.5.28)$$

$$0 \leq x_1 \leq \pi,$$

whilst the marginal density is

$$f_{X_1}(x) = \frac{4}{3\pi} (\sin x - x \cos x) \sin x, \quad 0 \leq x \leq \pi, \quad (5.5.29)$$

which gives $E(X_1) = 2\pi/3$ and $E(X_1^2) = (5\pi^2/9 - 5/6)$. The mode of the density given in equation (5.5.29) is at $x = 2.2467$ radians ($128^\circ 43' 36''$). In addition, $\Pr(X_1 < \pi/2) = 1/6$. The density f_{X_1} is shown in Figure 5.5.6. Hinde and Miles (1980, Figure 5) have also estimated the conditional density of X_1 , given the number of edges of the typical cell.

There is a complementarity in π between the interior angles X_1 and X_2 of the polygons at a typical vertex in an ordinary Voronoi diagram \mathcal{V} and the angles of a Delaunay triangle whose circumcentre is that vertex. Thus, equations (5.5.28) and (5.5.29) can be derived from equations (5.11.11) and (5.11.12), respectively. The joint distribution given in equation (5.5.28) also governs the distribution of the third angle X_3 , since $X_1 + X_2 + X_3 = 2\pi$. Let $X_{(1)} \leq X_{(2)} \leq X_{(3)}$ denote the order statistics of X_1, X_2 and X_3 . The marginal pdfs of them are:

$$f_{X_{(1)}}(x) = \begin{cases} \frac{4}{\pi} (\sin x - x \cos x) \sin x, & 0 \leq x < \frac{\pi}{2}, \\ \frac{4}{\pi} [-\sin 3x - (2\pi - 3x) \cos x] \sin x, & \frac{\pi}{2} \leq x < \frac{2\pi}{3}, \\ \frac{8}{\pi} [2 \sin^3 x - \sin x - (\pi - x) \cos x] \sin x, & \frac{2\pi}{3} \leq x < \pi \end{cases}$$

$$f_{X_{(2)}}(x) = \begin{cases} \frac{4}{\pi} (\pi - 2x + \sin 2x) \sin 2x, & \frac{\pi}{2} \leq x < \frac{2\pi}{3}, \\ \frac{8}{\pi} [2 \sin^3 x - \sin x - (\pi - x) \cos x] \sin x, & \frac{2\pi}{3} \leq x < \pi \end{cases}$$

$$f_{X_{(3)}}(x) = \frac{4}{\pi} [(2\pi - 3x) \cos x + \sin 3x] \sin x \quad \frac{2\pi}{3} \leq x < \pi$$

(cf. equations (5.11.13) to (5.11.15)). These densities are illustrated in Figure 5.5.6. The details of deriving these densities from Miles' formula (5.11.2) can be found in Muche (1998), who also successfully simplified Miles' formula for the case $m = 3$ and obtained the following densities. Let E^0 denote an edge emanating from a typical vertex and E^1 denote a typical edge. A result from Mecke and Muche (1995, equation (4.3)) implies that the distributional properties associated with E^0 are the same as those associated with E^1 . Suppose p_1, p_2 and p_3 are the three generators of the neighbouring cells of E^0 (or E^1) and p is the projection of p_1 onto E^0 (or E^1). Let Y_1 and Y_2 be the angles $\angle p_1 p p_2$ and $\angle p_2 p p_3$, respectively. The joint pdf of Y_1 and Y_2 is

$$f_{Y_1, Y_2}(y_1, y_2) = \frac{16}{3\pi^2} \left(\sin \frac{y_1}{2} \sin \frac{y_2}{2} \sin \frac{y_1 + y_2}{2} \right)^2, \quad (5.5.30)$$

$$0 \leq y_2 < 2\pi - y_1, \quad 0 \leq y_1 < 2\pi,$$

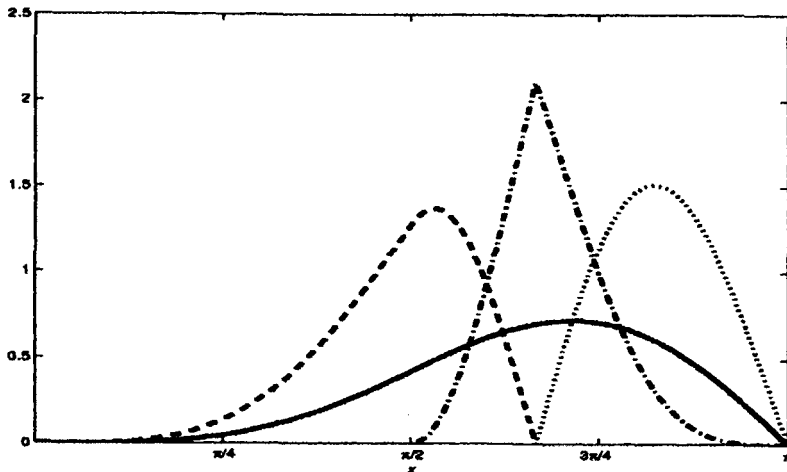


Figure 5.5.6 Probability density functions of angles at a typical vertex of a Poisson Voronoi diagram in \mathbb{R}^2 : — randomly selected angle X_1 ; - - - minimum $X_{(1)}$; · - middle $X_{(2)}$; . . . maximum $X_{(3)}$ of the three angles at a typical vertex (see also Muche, 1998, Figure 1).

and the marginal density is

$$f_{Y_1}(y) = \frac{[(2\pi - y)(2 + \cos y) + 3 \sin y](1 - \cos y)}{3\pi^2}, \quad 0 \leq y < 2\pi.$$

In \mathbb{R}^3 there are three faces meeting at an edge. Denote by X_1 , X_2 and X_3 the three face angles at a typical edge. These face angles, without loss of generality, can be expressed as $X_1 = \pi - Y_1/2$, $X_2 = \pi - Y_2/2$ and $X_1 + X_2 + X_3 = 2\pi$. Using these relationships, Muche (1998) derived from equation (5.5.30) the joint pdf of the face angles and the marginal pdfs of X_1 and their order statistics $X_{(1)} \leq X_{(2)} \leq X_{(3)}$:

$$f_{X_1, X_2}(x_1, x_2) = \frac{64}{3\pi^2} [\sin x_1 \sin x_2 \sin(x_1 + x_2)]^2, \quad \pi - x_1 \leq x_2 < \pi, \quad 0 \leq x_1 < \pi,$$

$$f_{X_1}(x) = \frac{8}{3\pi^2} [x(3 - 2 \sin^2 x) - 3 \sin x \cos x] \sin^2 x, \quad 0 \leq x < \pi,$$

$$f_{X_{(1)}}(x) = \begin{cases} \frac{8}{\pi^2} [x(3 - 2 \sin^2 x) - 3 \sin x \cos x] \sin^2 x, & x < \frac{\pi}{2}, \\ \frac{8}{\pi^2} [(2\pi - 3x)(3 - 2 \sin^2 x) + (9 - 16 \sin^4 x) \sin x \cos x] \sin^2 x, & \frac{\pi}{2} \leq x < \frac{2\pi}{3} \end{cases}$$

$$f_{X_{(2)}}(x) = \begin{cases} \frac{16}{\pi^2} [(2x - \pi)(3 - 2 \sin^2 x) + 2(4 \sin^4 x - 3) \sin x \cos x] \sin^2 x, & \frac{\pi}{2} \leq x < \frac{2\pi}{3}, \\ \frac{16}{\pi^2} [(\pi - x)(3 - 2 \sin^2 x) + (3 - 8 \sin^4 x) \sin x \cos x] \sin^2 x, & \frac{2\pi}{3} \leq x < \pi, \end{cases}$$

$$f_{X_{(3)}}(x) = \frac{8}{\pi^2} [(3x - 2\pi)(3 - 2 \sin^2 x) + (16 \sin^4 x - 9) \sin x \cos x] \sin^2 x, \quad \frac{2\pi}{3} \leq x < \pi.$$

These densities are illustrated in Figure 5.5.7. Let β denote the angle between E^0 (or E^1) and the line joining the typical vertex (or an endpoint of E^1) and a neighbouring generator. The pdf of β is given by the first density in equation (5.5.24) and

$$E(\cos^k \beta) = \begin{cases} \frac{105}{4} \frac{k+4}{(k+1)(k+3)(k+5)(k+7)} & \text{for even } k, \\ \frac{105}{4} \frac{1}{(k+2)(k+4)(k+6)} & \text{for odd } k. \end{cases}$$

Denote by γ the angle between two randomly chosen edges from a typical vertex. The pdf of it is:

$$f_\gamma(\gamma) = \frac{35}{16\pi^3} \int_{-1}^1 \int_{-(1-y_1^2)^{1/2}}^{(1-y_1^2)^{1/2}} \sqrt{1-y_1^2-y_2^2} \times \left\{ [(1-y_1^2-y_2^2) + 3(y_1 \sin \gamma + y_2 \cos \gamma)^2] \left[\frac{\pi}{2} - \tan^{-1} \frac{y_2}{\sqrt{1-y_1^2-y_2^2}} \right] \right. \\ - 3y_2 \sqrt{1-y_1^2-y_2^2} \left\{ 3(y_1 \sin \gamma + y_2 \cos \gamma) \sqrt{1-y_1^2-y_2^2} \right. \\ \left. + [(1-y_1^2-y_2^2) + 3(y_1 \sin \gamma + y_2 \cos \gamma)^2] \right\} \\ \times \left[\frac{\pi}{2} + \tan^{-1} \frac{y_1 \sin \gamma + y_2 \cos \gamma}{\sqrt{1-y_1^2-y_2^2}} \right] \left. \right\} \sin \gamma dy_2 dy_1, \quad 0 \leq \gamma \leq \pi$$

(see Figure 5.5.8) and the first two moments are

$$E(\gamma) = \frac{48\pi^2 - 35}{72\pi},$$

$$E(\gamma^2) = \frac{48\pi^2 - 175}{72}.$$

The density of the angle ζ between the lines from a typical vertex to two neighbouring generators chosen at random is

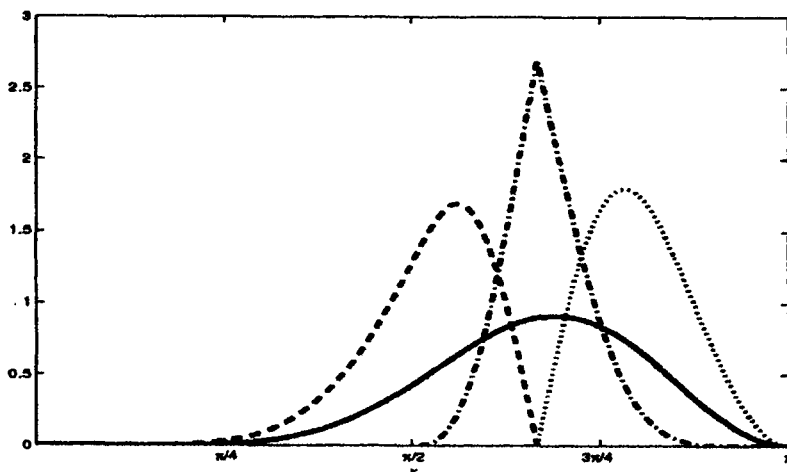


Figure 5.5.7 Probability density functions of face angles at a typical edge of a Poisson Voronoi diagram in \mathbb{R}^3 : — randomly selected angle X_1 ; - - minimum $X_{(1)}$; · — middle $X_{(2)}$; ··· maximum $X_{(3)}$ of the three face angles at a typical edge (see also Muche, 1998, Figure 2).

$$f_\zeta(\zeta) = \frac{35}{256} \left(8 + 8 \cos^2 \frac{\zeta}{2} - \cos^4 \frac{\zeta}{2} \right) \sin^2 \frac{\zeta}{2} \cos \frac{\zeta}{2}, \quad 0 \leq \zeta < \pi$$

(see Figure 5.5.8) and the first two moments are

$$E(\zeta) = \pi - \frac{4829}{3360},$$

$$E(\zeta^2) = \pi^2 - \frac{72598}{11025}.$$

Some other angular properties which are related to the Poisson Delaunay tessellation are discussed in Section 5.11.

A typical cell of V_p , using the definition of the Palm distribution approach, is the cell containing the origin o , which is also the generator of the cell. However, in general the cell P_o which contains the origin is not typical, since a larger cell has a higher chance of containing the origin (size-biased sampling). Mecke (1999) showed that all moments of the volume of a typical cell of a stationary tessellation in \mathbb{R}^m do not exceed the corresponding moments of the volume of P_o . Gilbert (1962) studied the distributions of the length of the longest line segment from the origin to the boundary of P_o in \mathbb{R}^m , which is known as the linear contact distribution function:

$$H_1(r) = 1 - A_m \lambda \int_0^\infty \int_0^\pi y^{m-1} \sin^{m-2} \beta \exp(-\lambda U_m(y, r_{y,\beta}, r)) d\beta dy, \quad r \geq 0, \quad (5.5.31)$$

where A_m is a normalizing constant, and $r_{y,\beta}$ and $U_m(y, r_{y,\beta}, r)$ have been defined in equations (5.5.21) and (5.5.26), respectively. Muche and Stoyan

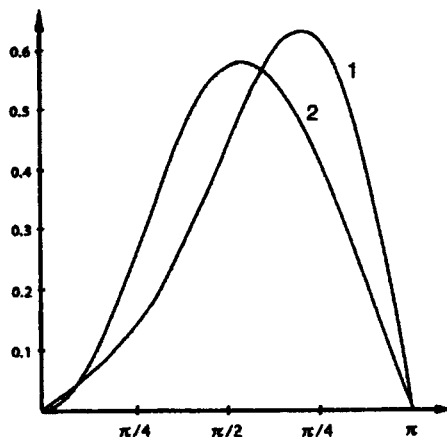


Figure 5.5.8 Probability density functions for (1) the angle γ spanned by two edges emanating from a typical vertex and (2) the angle ζ between the lines from a typical vertex to two neighbouring generators. (Source: Muche, 1998, Figure 3.)

(1992) derived the spherical contact distribution function in \mathbb{R}^2 and \mathbb{R}^3 , i.e. the distribution of the radius of the maximal ball lying completely within P_o and centred at the origin. For $m = 2$ the function is given by

$$H_s(r) = 1 - \frac{1}{2} \exp(-4\pi\lambda r^2) + \frac{1}{2} \exp(-6\pi\lambda r^2) \\ - 2\pi\lambda \int_r^\infty y \exp \left\{ -\lambda \left[(4r^2 + 2y^2) \left(\pi - \cos^{-1} \frac{r}{y} \right) + 6r \sqrt{y^2 - r^2} \right] \right\} dy, \quad r \geq 0,$$

whilst for $m = 3$:

$$H_s(r) = 1 - 4\pi\lambda \int_0^r y^2 \exp \left[\frac{32\pi\lambda}{3} r(r^2 + y^2) \right] dy \\ - 4\pi\lambda \int_r^\infty y^2 \exp \left[\frac{4\pi\lambda}{3y} (r+y)^4 \right] dy, \quad r \geq 0.$$

They also used the linear contact distribution to derive a numerically tractable expression for the chord length distribution (see Section 5.7).

Although Miles and Maillardet (1982, p. 108) have been able to derive an expression for the probability p_n that a PVC has n vertices (edges), this is computationally complex. Table 5.5.13 (see also Figure 5.5.9) gives the estimated values of p_n obtained by Hinde and Miles (1980), Drouffe and Itzykson (1984), Le Caer and Ho (1990) and Kumar and Kurtz (1993). Note that the largest value of n encountered amongst the two million polygons generated by Hinde and Miles is 14. On the basis of their estimates, Itzykson and Drouffe (1989, p. 745) suggested that asymptotically $p_n \sim n^{-\kappa n}$, where κ lies between 1 and 2.

Table 5.5.13 Estimates, \hat{p}_n , of the probability p_n that a typical Poisson Voronoi cell in \mathbb{R}^2 has n edges.

<i>n</i>	a		b		c		d
	\hat{p}_n	$\hat{\sigma}_n$	\hat{p}_n	$\hat{\sigma}_n$	\hat{p}_n	$\hat{\sigma}_n$	\hat{p}_n
3	0.01131	0.00007	0.01127	0.00894	0.0113	0.0002	0.011
4	0.1071	0.00022	0.1077	0.03316	0.1068	0.0002	0.107
5	0.2591	0.00031	0.258	0.04472	0.2595	0.0005	0.260
6	0.2944	0.00032	0.294	0.05477	0.2946	0.0003	0.294
7	0.1991	0.00028	0.198	0.05477	0.1986	0.0001	0.199
8	0.0902	0.00020	0.090	0.14142	0.0905	0.0003	0.090
9	0.0295	0.00012	0.0288	0.02646	0.0295	0.0003	0.030
10	0.00743	0.00006	0.00695	0.01414	0.0074	0.0001	0.007
11	0.00149	0.00003	0.00153	0.00949	0.00144	0.00003	0.0015
12	0.00025	0.00001	0.00024	0.00548			0.00023
13	0.000034	0.000004	0.000029	0.00224			0.00004
14	0.000005	0.0000016	0.0000028	0.00063			
15			2.6×10^{-7}	2.2×10^{-4}			
16			2.3×10^{-8}	5×10^{-5}			
18			1.3×10^{-10}	7.1×10^{-6}			
20			1.5×10^{-13}	2.8×10^{-7}			
25			9.6×10^{-21}	7.7×10^{-11}			
30			1.3×10^{-29}	3.3×10^{-15}			
35			3.6×10^{-40}				
40			2.4×10^{-50}				
45			2.0×10^{-63}				
50			1.5×10^{-75}				

$\hat{\sigma}_n$ = standard deviation of \hat{p}_n .

Sources:

- a Hinde and Miles (1980, Table III). Number of cells = 2 000 000.
- b Drouffe and Itzykson (1984, Table 1). Number of cells = 27 000.
- c Le Caér and Ho (1990, Table I). Number of cells = 600 696, 1 001 500, 1 020 800.
- d Kumar and Kurtz (1993, Table 3). Number of cells = 650 000.

Consider a three-parameter gamma probability density function of the form

$$f_3(x) = \frac{rb^{q/r} x^{q-1} \exp(-bx')}{\Gamma\left(\frac{q}{r}\right)}, \quad r > 0, b > 0, q > 0. \quad (5.5.32)$$

Hinde and Miles (1980) suggested a discretized three-parameter gamma distribution $\int_{n-1/2}^{n+1/2} f_3(x) dx$ with $r = 1.0186$, $b = 3.130$ and $q = 19.784$ to approximate p_n . Kumar and Kurtz (1993) used a discretized (two-parameter) gamma distribution. The general form of the pdf of a gamma distribution is that of equation (5.5.32) with $r = 1$:

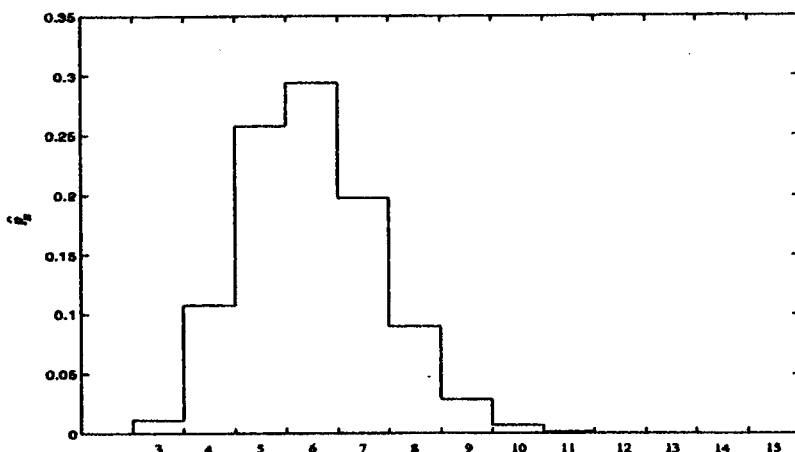


Figure 5.5.9 Normalized histogram of the number of edges N of a typical Poisson Voronoi cell in \mathbb{R}^2 (values from Drouffe and Itzykson, 1984).

$$f_2(x) = \frac{b^q x^{q-1} \exp(-bx)}{\Gamma(q)}, \quad b > 0, q > 0. \quad (5.5.33)$$

They suggested that $q = 21.199$ and $1/b = 0.283$, but the fit is rejected by the Kolmogorov-Smirnov test at the 0.01 significance level. Kumar and Kurtz (1993) also found that if the sample size is less than 50 000, a discretized lognormal distribution can be used to approximate the distribution of the number of edges. The reason has been given by Vaz and Fortes (1988): the difference between a gamma and a lognormal distribution with suitably chosen parameters is very small. Solomon and Stephens (1980) suggested using $(cw)^k$ to approximate the number of edges of a typical PVC, where $c = 4.457$, $k = 0.485$ and w has a χ^2 -distribution with 3.429 degrees of freedom. A χ^2 -distribution with p degrees of freedom is the gamma distribution given in equation (5.5.33) with $q = p/2$ and $b = 1/2$.

Turning to \mathbb{R}^3 , Hanson (1983), Quine and Watson (1984), Lorz (1990b, 1991) and Kumar *et al.* (1992) have estimated the distributions of the number of faces F per cell and the number of vertices (edges) N per face. Their estimates are reported in Tables 5.5.14 and 5.5.15 and illustrated in Figures 5.5.10 and 5.5.11, respectively. Kumar *et al.* (1992) suggested that the gamma distribution given in equation (5.5.33) with $q = 21.6296$ and $1/b = 0.7199$ can be used to describe the distribution of F , but again it is rejected by the Kolmogorov-Smirnov test at the 0.01 significance level.

Numerous researchers, including Kiang (1966), Crain (1972, 1978), Hinde and Miles (1980), Weaire *et al.* (1986), Icke and van de Weygaert (1987), DiCenzo and Wertheim (1989), Hermann *et al.* (1989), Kumar and Kurtz (1993), Quine and Watson (1984), Vaz and Fortes (1988), Zaninetti (1992), Moore and Angell (1993) and Marthinsen (1996), have produced estimates

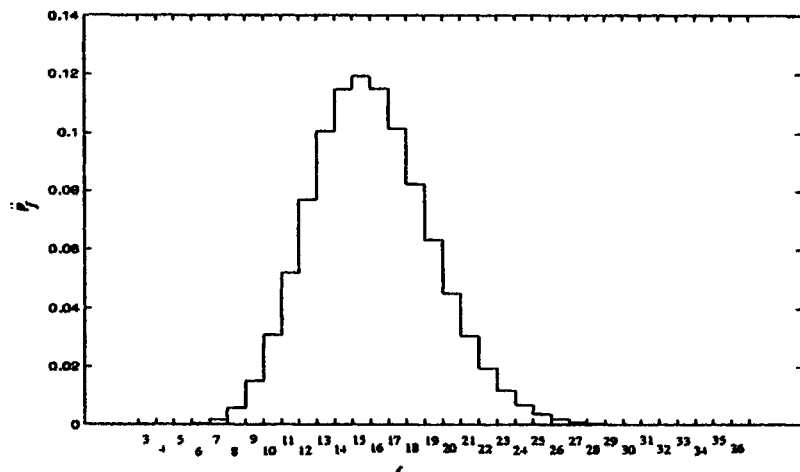


Figure 5.5.10 Normalized histogram of the number of faces F of a typical Poisson Voronoi cell in \mathbb{R}^3 (values from Kumar *et al.*, 1992).

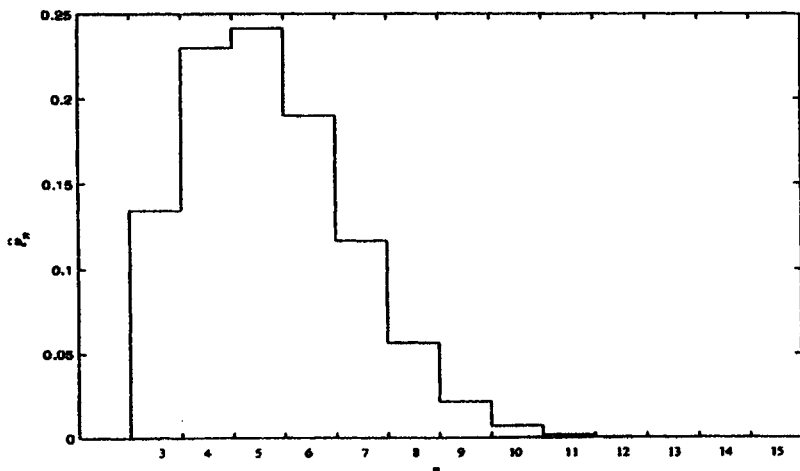


Figure 5.5.11 Normalized histogram of the number of edges (vertices) N of a randomly selected face of a typical Poisson Voronoi cell in \mathbb{R}^3 (values from Kumar *et al.*, 1992).

Table 5.5.14 Estimates, \hat{p}_f , of the probability p_f that a typical Poisson Voronoi cell in \mathbb{R}^3 has f faces.

f	\hat{p}_f		f	\hat{p}_f	
	a	b		a	b
4	0.0000055866	—	21	0.030620	0.02993
5	0.000027933	0.00006	22	0.019349	0.01895
6	0.00032682	0.00019	23	0.011640	0.01144
7	0.0015922	0.00193	24	0.0067207	0.00691
8	0.0058101	0.00578	25	0.0038156	0.00373
9	0.014936	0.01496	26	0.0018575	0.00215
10	0.030885	0.03102	27	0.00097486	0.00091
11	0.052115	0.05164	28	0.00050000	0.00042
12	0.076950	0.07806	29	0.00019832	0.00017
13	0.10041	0.09865	30	0.000061453	0.000048
14	0.11465	0.11492	31	0.000039106	0.000024
15	0.11927	0.12088	32	0.000013966	0.000012
16	0.11485	0.11418	33	0.0000027933	—
17	0.10144	0.10297	34	0.0000055866	—
18	0.082444	0.08219	35	0.0000027933	0.000012
19	0.063249	0.06287	36	0.0000027933	—
20	0.045232	0.04500			

*Sources:*a Kumar *et al.* (1992, Table III). Number of cells = 358 000.

b Lorz (1991). Number of cells = 82 870.

Table 5.5.15 Estimates, \hat{p}_n , of the probability p_n that a face of a typical Poisson Voronoi cell in \mathbb{R}^3 has n edges (vertices).

n	\hat{p}_n		n	\hat{p}_n	
	a	b		a	b
3	0.13448	0.1355	10	0.0068203	0.0068
4	0.23013	0.2301	11	0.0017689	0.0017
5	0.24161	0.2404	12	0.00038117	0.00038
6	0.19021	0.1900	13	0.000068471	0.000066
7	0.11646	0.1162	14	0.000010064	0.0000047
8	0.056384	0.0569	15	0.0000025160	0.0000039
9	0.021680	0.0220			

*Sources:*a Kumar *et al.* (1992, Table III). Number of cells = 358 000.

b Lorz (1991). Number of cells = 82 870.

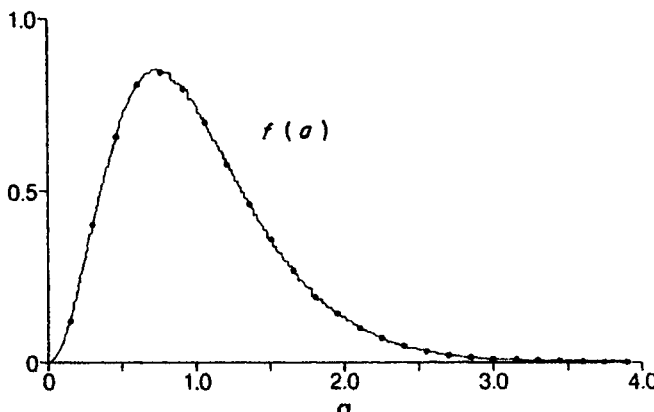


Figure 5.5.12 Normalized histogram of the standardized area λA of a typical Poisson Voronoi cell in \mathbb{R}^2 showing point values of the generalized gamma fit (5.5.32). (Source: Hinde and Miles, 1980 Figure 4.)

of the distribution f_A of the area of a typical PVC in \mathbb{R}^2 . The last five papers, as well as Hanson (1983), Andrade and Fortes (1988), Lorz (1990b, 1991), Kumar *et al.* (1992), Thorvaldsen (1992) and van de Weygaert (1994), also estimate the pdf f_V of the volume V of a typical PVC in \mathbb{R}^3 . Quine and Watson (1984) and Kumar and Kurtz (1993) have also examined the distribution of A conditioned by the number of edges N . Figure 5.5.12 shows the distribution of the standardized area λA (Hinde and Miles, 1980, Figure 4).

There has been considerable conjecture on the theoretical form of f_A . Hinde and Miles (1980, p. 219) fit a three-parameter generalized gamma function. Values obtained from equation (5.5.32) with $r = 1.0787$, $b = 3.0328\lambda'$ and $q = 3.3095$ are plotted in Figure 5.5.12. Visually this provides a good fit, although it is rejected by a χ^2 test. Tanemura (1988) follows Hinde and Miles and fits equation (5.5.32) to the volume of a typical cell in \mathbb{R}^3 . His estimates of the parameters are $r = 1.409$, $b = 2.813\lambda'$ and $q = 4.120$. He found that a three-parameter gamma distribution fits better than a two-parameter gamma. Solomon and Stephens (1980) used $(cw)^k$, where $c = 0.723$, $k = 0.445$ and w has a χ^2 -distribution with 1.855 degrees of freedom, to approximate A . Hermann *et al.* (1989, p. 194) claimed that Maxwell, lognormal and gamma distributions fit equally well the values of A derived from their simulations. Vaz and Fortes (1988) found that although lognormal and gamma distributions are very close, the description of the cell area or volume by a lognormal distribution is in general not as adequate as by a gamma distribution. On the basis of his simulations, Kiang (1966) suggests that the cell size (area if $m = 2$ and cell volume if $m = 3$) follows the gamma distribution given in equation (5.5.33) with $q = 2m$ and $b = 2m\lambda$. Both Rivier (1986b) and Weaire *et al.* (1986) offer some limited analytical support for A having a gamma distribution but the latter authors suggest values of $q = 3.61$ and $b = 3.61\lambda$.

Since the k th moments obtained from the gamma pdf given in equation (5.5.33) are $[\Gamma(q+k)\Gamma(q)]b^{-k}$, these values yield $E(A^2) = 1.277$, which is not consistent with Gilbert's value reported in Table 5.5.1. However, the fit to their observed values is excellent (Weaire *et al.*, 1986, p. L104). Other researchers also report an excellent fit of A to equation (5.5.33) with $q = 3.61$ and $b = 3.57\lambda$ (DiCenzo and Wertheim, 1989), $q = 3.61$ and $b = 3.61\lambda$ (Marthinsen, 1996), $q = 3.571$ and $b = 3.571\lambda$ (Vaz and Fortes, 1988), $q = 3.37$ and $b = 3.37\lambda$ (Zaninetti, 1992) and V to equation (5.5.33) with $q = 5.56$ and $b = 5.56\lambda$ (Andrade and Fortes, 1988; Vaz and Fortes, 1988; Thorvaldsen, 1992; Marthinsen, 1996), $q = 5.38$ and $b = 5.38\lambda$ (Zaninetti, 1992). Kumar and Kurtz (1993) and Kumar *et al.* (1992) estimated $q = 3.718$ and $b = 3.718\lambda$ for A and $q = 5.7869$ and $b = 5.7869\lambda$ for V , respectively, but each fit is rejected by the Kolmogorov-Smirnov test at the 0.01 significance level. Note that except for DiCenzo and Wertheim (1989), all these estimates fulfilled the condition that $E(A) = q/b = \lambda^{-1}$. A review of Kiang's conjecture and related simulation studies can be found in Moore and Angell (1993). Furthermore, Miles and Maillardet (1982, p. 101) considered that the conditional distribution of A , given that the number of edges is N . They suggested that if N is large, this conditional distribution can be approximated by the gamma distribution given in equation (5.5.33) with $q = N$ and $b = 4\lambda$. Quine and Watson (1984) estimated the conditional area of a typical cell with N edges in \mathbb{R}^2 and the conditional volume of a typical cell with F faces in \mathbb{R}^3 . Kumar and Kurtz (1993, Table 8) and Kumar *et al.* (1992, Table VI) also found that gamma distributions with suitably chosen parameters can be used to describe such conditional area and conditional volume distributions, respectively. Unlike the conditional perimeter discussed below, none of their fits has been rejected by the Kolmogorov-Smirnov test at the 0.05 significance level. Mulheran (1992) used a heuristic argument to derive an approximation of the distribution of the conditional area of a typical cell V_p in \mathbb{R}^2 , given that it has N edges, but simulation results are not well fitted by his approximation. For V_p in \mathbb{R}^m , Zuyev (1992, 1993) defined the *fundamental region* of a typical PVC to be the union of the m -dimensional spheres with centres at the vertices of the cell and containing the generator of the cell on their boundaries. He showed that given the number of $(m-1)$ -faces of a typical cell is $N (\geq m+1)$, the volume of its fundamental region has a gamma distribution with $q = N$ and $b = \lambda$ (see also Møller and Zuyev, 1996). Since the volume of a cell does not exceed $1/2^m$ of the volume of its fundamental region, a rough upper bound on the conditional distribution of the volume of a typical cell V , given that the number of $(m-1)$ -faces on its boundary is N , has been obtained:

$$\Pr(V > x | N) \leq \sum_{k=1}^N \frac{(2^m \lambda x)^k}{k!} e^{-2^m \lambda x},$$

for all $x > 0$.

Hinde and Miles (1980, Figure 3) have estimated the distribution of the standardized perimeter $(\sqrt{\lambda}/4)P$ of a typical cell (see Figure 5.5.13). They

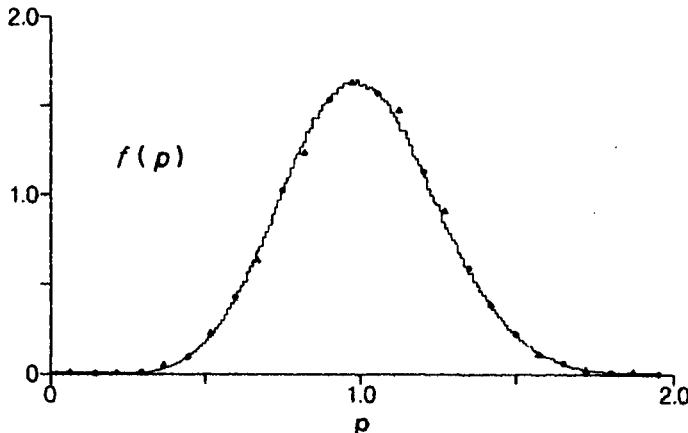


Figure 5.5.13 Normalized histogram of the standardized perimeter $\lambda^{1/2}P/4$ of a typical Poisson Voronoi cell in \mathbb{R}^2 showing point values for two fits: ● generalized gamma fit (5.5.32); ▲ normal fit. (Source: Hinde and Miles, 1980 Figure 3.)

again fit equation (5.5.32) to their data with $r = 2.3389$, $b = 2.9563$ and $q = 7.5579$. This fit is shown in Figure 5.5.13. As with the standardized cell area, while the visual impression is one of a good fit, it is rejected by a χ^2 test at the 0.05 significance level. They also note that, since their estimates of the coefficients of skewness and kurtosis of the standardized cell perimeter $(\sqrt{\lambda}/4)P$ are 0.193 and 2.983, respectively, $(\sqrt{\lambda}/4)P$ is approximately normally distributed with mean 1 and variance 0.0592. Values for this normal distribution are also plotted in Figure 5.5.13. Quine and Watson (1984, Figure 3) and Kumar and Kurtz (1993, Table 9) have studied the distribution of P conditioned on the number of edges N . The values can be described by gamma distributions with suitable parameters, although most of the fits are rejected by the Kolmogorov–Smirnov test at the 0.05 significance level.

The conditional number of edges of a randomly selected neighbouring cell of a typical cell with N edges can also be well described by gamma distributions and a lognormal distribution (Kumar and Kurtz, 1993, Table 6). In general, the lognormal distribution fits for this conditional number, as well as for the cell area A and perimeter P , are not as good as the gamma distribution fits (see Vaz and Fortes, 1988).

Quine and Watson (1984), Lorz (1990b) and Kumar *et al.* (1992) have estimated the distribution of the surface area S of a typical PVC in \mathbb{R}^3 . The last fits S to equation (5.5.33) and yields $q = 15.4847$ and $1/b = 0.3778 \lambda^{-2/3}$ and $q = 16.1576$ and $1/b = 0.3603 \lambda^{-2/3}$. The former is a better fit but the latter ensures $E(S) = 5.821 \lambda^{-2/3}$. Nevertheless, both fits are rejected by the Kolmogorov–Smirnov test at the 0.01 significance level. The conditional surface area, given that the typical cell has F faces, can also be well described by gamma distributions with suitably chosen parameters (Kumar *et al.*, 1992,

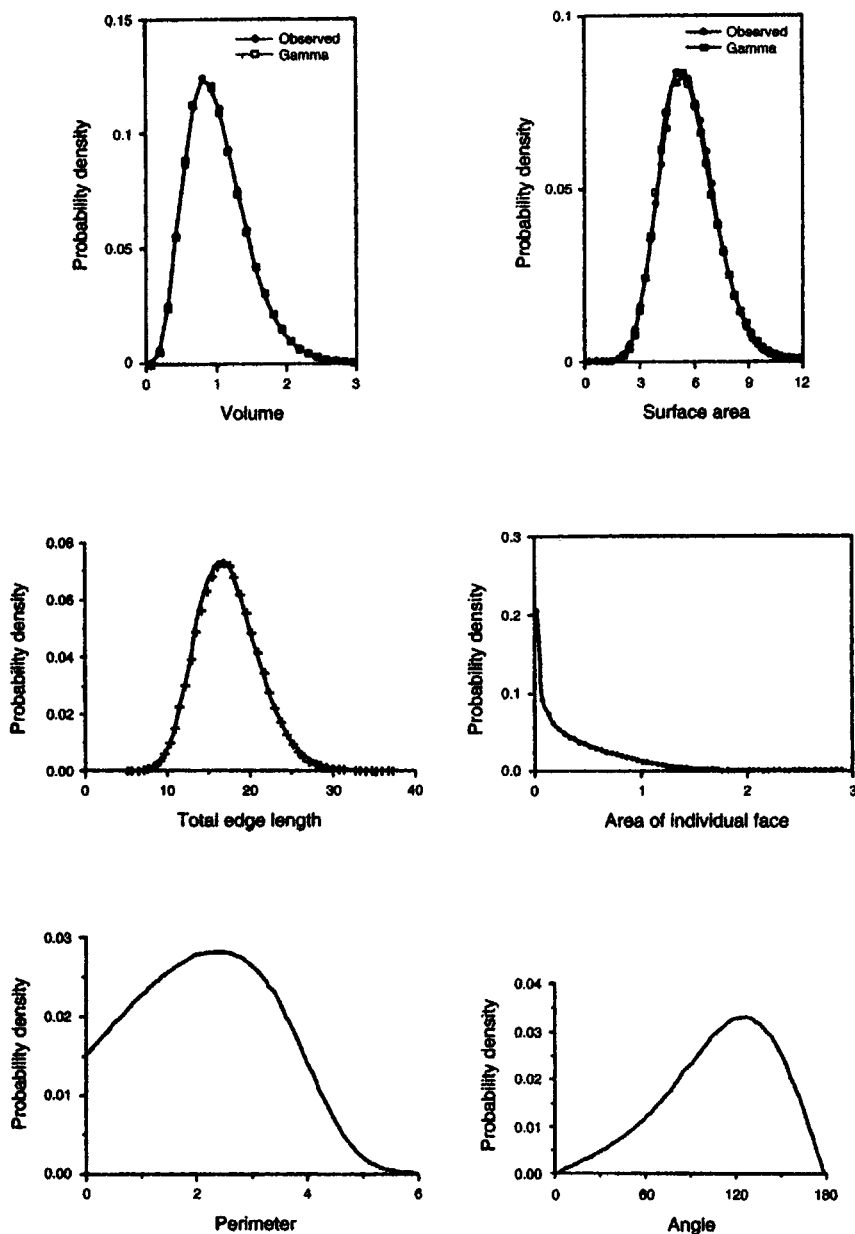


Figure 5.5.14 Normalized histograms of the volume V , surface area S and total edge length B of a typical Poisson Voronoi cell (with the best fit gamma distributions) and the area A , perimeter P and interior angle α_2 of a typical face of a Poisson Voronoi cell in \mathbb{R}^3 . (Sources: Kumar *et al.*, 1992, and Kumar and Kurtz, 1995.)

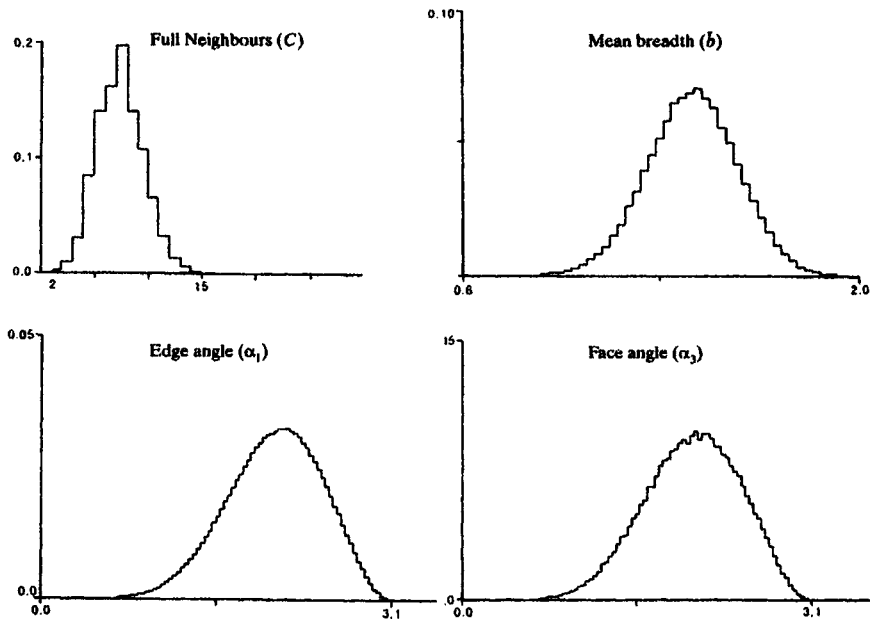


Figure 5.5.15 Normalized histograms of the number of full neighbours C , mean breadth \bar{b} , and face angle α_3 of a typical Poisson Voronoi cell and the face angle α_1 at a typical edge in \mathbb{R}^3 . (Sources: Quine and Watson, 1984, and Lorz, 1990b.)

Table VII) and all of them pass the Kolmogorov-Smirnov test at the 0.05 significance level.

Quine and Watson (1984), Lorz (1990b), Kumar *et al.* (1992) and Kumar and Kurtz (1995) also estimated the distributions of various characteristics of a PVC in \mathbb{R}^3 . The estimates are given in Figures 5.5.14 and 5.5.15. Kumar *et al.* (1992, Figures 12 and 13) also have estimated the conditional distribution of the area of a face of a typical PVC in \mathbb{R}^3 , given that the typical cell has F faces or that the face has N edges.

Avrami and Bertsimas (1993) have established central limit theorems for the total edge length of \mathcal{V}_P in $[0, 1]^2$ and \mathcal{D}_P in $[0, 1]^m$, as the intensity λ of the Poisson process tends to infinity. Let L_λ denote the total edge of \mathcal{V}_P in $[0, 1]^2$ or \mathcal{D}_P in $[0, 1]^m$. They showed that

$$\left| \Pr\left\{ \frac{L_\lambda - E(L_\lambda)}{\sqrt{\text{Var}(L_\lambda)}} \leq x \right\} - \int_0^x \frac{1}{\sqrt{2\pi}} e^{-z^2/2} dz \right| = O\left(\frac{(\log \lambda)^{1+3/(2m)}}{\lambda^{1/4}} \right),$$

where $m = 2$ for \mathcal{V}_P and $m \geq 2$ for \mathcal{D}_P . Heinrich (1994) provided a tool to show the asymptotic normality of the total length of \mathcal{V}_P in a very large m -dimensional cube.

5.6 STOCHASTIC PROCESSES INDUCED BY POISSON VORONOI DIAGRAMS

In addition to the point processes of centroids of faces mentioned in Section 5.1, there are also other stochastic processes induced by Poisson Voronoi diagrams. In this section we study the properties of some of these processes.

5.6.1 Point processes of centroids of faces

As indicated in Section 5.1 it is possible to generate other point processes from \mathcal{V}_P that share properties of the Poisson point process Θ_P , which generated \mathcal{V}_P . One such process with motion invariance is that of the centroids of s -faces of \mathcal{V}_P ($s = 0, \dots, m$), which is denoted by Θ_{P_s} . Suppose the intensity of Θ_{P_s} is λ_s . The relation between λ_s and λ is given by equations (5.1.1) and (5.5.4). Let $\lambda_0 = \kappa_m \lambda$. By equation (5.5.4),

$$\kappa_m = \frac{2^{m+1} \pi^{(m-1)/2} \Gamma\left(\frac{m^2 + 1}{2}\right)}{m^2(m+1) \Gamma\left(\frac{m^2}{2}\right)} \left\{ \frac{\Gamma\left(\frac{m}{2} + 1\right)}{\Gamma\left(\frac{m+1}{2}\right)} \right\}^m.$$

In particular, $\kappa_1 = 1$, $\kappa_2 = 2$ and $\kappa_3 = 24\pi^2/35$.

Consider a stationary point process Θ with intensity μ . The probability that an infinitesimally small disc of area dA_1 contains a point of Θ is μdA_1 . For two infinitesimally small discs of area dA_1 and dA_2 , with a distance r between their centres, the probability that both discs contain a point of Θ depends only on the distance r , because the point process Θ is stationary. Denote this probability by

$$\rho^{(2)}(r) dA_1 dA_2, \quad r \geq 0,$$

where $\rho^{(2)}$ is known as the *second-order product density*. This density is equal to λ^2 for a stationary Poisson point process of intensity λ . It is natural to divide $\rho^{(2)}$ by the square of the intensity of the point process as a normalization, which gives

$$g(r) = \frac{\rho^{(2)}(r)}{\mu^2}, \quad r \geq 0.$$

This is called the *pair correlation function* (see, for example, Stoyan and Stoyan, 1994, pp. 248–249). For Θ_P , $g(r) = 1$.

The pair correlation function for Θ_{P_0} , the point process of vertices of \mathcal{V}_P , is of particular interest. One reason is that Θ_{P_0} is also the point process of cell centroids of \mathcal{D}_P . For Θ_{P_0} of \mathcal{V}_P in \mathbb{R} :

$$g(r) = 1 + (2\lambda r - 1) e^{-2\lambda r}, \quad r \geq 0.$$

Heinrich and Muche (1994) have derived the general form of g for the point process of vertices Θ_{P0} of a Poisson Voronoi diagram \mathcal{V}_P in \mathbb{R}^m for $m \geq 2$:

$$g(r) = \frac{g_{0,m}^*(r)}{[(m+1)!]^2} + \sum_{j=0}^m \frac{g_{j,m}(r)}{j! [(m-j+1)!]^2}, \quad r \geq 0,$$

where

$$\begin{aligned} g_{0,m}^*(r) &= m^4 (m+1)^2 \int_0^{(\lambda\omega_m)^{1/m}} \int_0^{r_1 - r(\lambda\omega_m)^{1/m}} \exp\{-(r_1^m + r_2^m)\} \\ &\quad \times r_1^{m^2-1} r_2^{m^2-1} dr_2 dr_1, \\ &= m^2 (m+1)^2 (m-1)! \int_0^{\lambda\omega_m r^m} f\left(\{r[\lambda\omega_m]^{1/m} - r_1^{1/m}\}^m\right) \\ &\quad \times e^{-r_1} r_1^{m-1} dr_1, \quad r \geq 0, \end{aligned} \tag{5.6.1}$$

with $\omega_m = \pi^{m/2}/\Gamma(1+m/2)$ being the volume of an m -dimensional sphere of unit radius, and

$$f(x) = \frac{1}{(m-1)!} \int_0^x y^{m-1} e^{-y} dy = 1 - e^{-x} \left\{ 1 + x + \dots + \frac{x^{m-1}}{(m-1)!} \right\}, \quad x \geq 0.$$

Explicit expressions for $g_{j,m}$ are known but messy. We state only the pair correlation function of Θ_{P0} in \mathbb{R}^m for $m = 2$ and $m = 3$.

For $m = 2$,

$$g(r) = \frac{g_{0,2}^*(r)}{36} + \frac{g_{0,2}(r)}{36} + \frac{g_{1,2}(r)}{4} + \frac{g_{2,2}(r)}{2}, \quad r \geq 0, \tag{5.6.2}$$

where $g_{0,2}^*$ can be obtained from equation (5.6.1):

$$\begin{aligned} g_{0,2}^*(r) &= 36 \int_0^{\lambda\pi r^2} \left\{ 1 - \left[1 + (r\sqrt{\lambda\pi} - \sqrt{y})^2 \right] \right. \\ &\quad \times \left. \exp[-(r\sqrt{\lambda\pi} - \sqrt{y})^2] \right\} y \exp(-y) dy, \end{aligned}$$

and

$$g_{2,2}(r) = \frac{\lambda^2 r^4}{2} \int_1^\infty \int_0^1 \exp\{-\lambda r^2 v_2(y_1, y_2)\} F_2(y_1, y_2) F_2(-y_1, y_2) dy_1 dy_2,$$

$$g_{1,2}(r) = \frac{\lambda^3 r^6}{4} \int_1^\infty \int_0^1 \frac{\exp\{-\lambda r^2 v_2(y_1, y_2)\}}{\sqrt{(1-y_1^2)(y_2^2-1)}} F_1(y_1, y_2) F_1(-y_1, y_2) dy_1 dy_2,$$

$$g_{0,2}(r) = \frac{9\lambda^4 r^8}{4} \int_1^\infty \int_0^1 \exp\{-\lambda r^2 v_2(y_1, y_2)\} F_0(y_1, y_2) F_0(-y_1, y_2) dy_1 dy_2.$$

The functions F_2 , F_1 , F_0 and v_2 are given by:

$$F_2(y_1, y_2) = (y_1 + y_2) \left[(1 + y_1 y_2) \left(\pi - \cos^{-1} \frac{1 + y_1 y_2}{y_1 + y_2} \right) \right. \\ \left. + \sqrt{(1 - y_1^2)(y_2^2 - 1)} \right],$$

$$F_1(y_1, y_2) = (y_1 + y_2) \left\{ \left[(y_1 + y_2)^2 + 2(1 + y_1 y_2)^2 \right] \left(\pi - \cos^{-1} \frac{1 + y_1 y_2}{y_1 + y_2} \right) \right. \\ \left. + 3(1 + y_1 y_2) \sqrt{(1 - y_1^2)(y_2^2 - 1)} \right\},$$

$$F_0(y_1, y_2) = (y_1 + y_2) \left[(y_1 + y_2)^2 \left(\pi - \cos^{-1} \frac{1 + y_1 y_2}{y_1 + y_2} \right)^2 - 2(1 - y_1^2)(y_2^2 - 1) \right. \\ \left. - (1 + y_1 y_2) \sqrt{(1 - y_1^2)(y_2^2 - 1)} \left(\pi - \cos^{-1} \frac{1 + y_1 y_2}{y_1 + y_2} \right) \right],$$

$$v_2(y_1, y_2) = \frac{1}{2} \sqrt{(1 - y_1^2)(y_2^2 - 1)} + \frac{\pi}{2} (y_1^2 + y_2^2) \\ - \left(\frac{y_1 + y_2}{2} \right)^2 \cos^{-1} \frac{1 + y_1 y_2}{y_1 + y_2} - \left(\frac{y_2 - y_1}{2} \right)^2 \cos^{-1} \frac{1 - y_1 y_2}{y_2 - y_1}.$$

Table 5.6.1 Values of the pair correlation function g for the point process of vertices of \mathcal{V}_P in \mathbb{R}^2 .

r	$g(r)$	r	$g(r)$	r	$g(r)$
0.05	3.8263	1.05	1.0055	2.05	1.0190
0.10	2.0372	1.10	1.0289	2.10	1.0153
0.15	1.4503	1.15	1.0487	2.15	1.0121
0.20	1.1651	1.20	1.0648	2.20	1.0095
0.25	1.0017	1.25	1.0769	2.25	1.0074
0.30	0.9003	1.30	1.0854	2.30	1.0057
0.35	0.8356	1.35	1.0902	2.35	1.0043
0.40	0.7948	1.40	1.0920	2.40	1.0032
0.45	0.7712	1.45	1.0910	2.45	1.0024
0.50	0.7607	1.50	1.0877	2.50	1.0018
0.55	0.7606	1.55	1.0828	2.55	1.0013
0.60	0.7690	1.60	1.0766	2.60	1.0009
0.65	0.7844	1.65	1.0696	2.65	1.0007
0.70	0.8054	1.70	1.0622	2.70	1.0005
0.75	0.8307	1.75	1.0547	2.75	1.0003
0.80	0.8590	1.80	1.0474	2.80	1.0002
0.85	0.8892	1.85	1.0405	2.85	1.0001
0.90	0.9200	1.90	1.0342	2.90	1.0001
0.95	0.9503	1.95	1.0285	2.95	1.0001
1.00	0.9791	2.00	1.0234	≥ 3.00	1.0000

Source: Muche (1999).

Numerical values of $g(r)$ are given in Table 5.6.1 and Figure 5.6.1.

For $m = 3$,

$$g(r) = \frac{g_{0,3}^*(r)}{576} + \frac{g_{0,3}(r)}{576} + \frac{g_{1,3}(r)}{36} + \frac{g_{2,3}(r)}{8} + \frac{g_{3,3}(r)}{6}, \quad r \geq 0, \quad (5.6.2)$$

where $g_{0,3}^*$ can be obtained from equation (5.6.1):

$$\begin{aligned} g_{0,3}^*(r) = & 288 \int_0^{\frac{4\pi}{3}\lambda r^3} \left\{ 1 - \left[1 + \left(r \left(\frac{4\pi}{3} \right)^{1/3} - y^{1/3} \right)^3 + \frac{1}{2} \left(r \left(\frac{4\pi}{3} \right)^{1/3} - y^{1/3} \right)^6 \right] \right. \\ & \times \exp \left[- \left(r \left(\frac{4\pi}{3} \right)^{1/3} - y^{1/3} \right)^3 \right] \left. \right\} y^2 \exp(-y) dy, \end{aligned}$$

and for $j = 0, 1, 2$ and 3 ,

$$\begin{aligned} g_{j,3} = & \left(\frac{35}{96\pi^2} \right)^2 \left(\frac{r^3}{4} \right)^{6-j} \int_1^\infty \int_0^1 \exp \left\{ - \frac{\pi r^3}{12} [2y_2(3y_1^2 + y_2^2) + 3(y_1^2 + y_2^2 + y_1^2 y_2^2) - 1] \right\} \\ & \times (y_2^2 - y_1^2)^{8-j} \Delta_j(y_1, y_2) dy_1 dy_2. \end{aligned}$$

The functions Δ_j are given by

$$\begin{aligned} \Delta_0 = & J_0 \left(\cos^{-1} \frac{1 + y_1 y_2}{y_2 + y_1} \right) J_0 \left(\cos^{-1} \frac{1 - y_1 y_2}{y_2 - y_1} \right), \\ \Delta_j = & \int_{[-\pi, \pi]^j} J_j \left(\cos^{-1} \frac{1 + y_1 y_2}{y_2 + y_1}, \psi_1, \dots, \psi_j \right) J_j \left(\cos^{-1} \frac{1 - y_1 y_2}{y_2 - y_1}, \psi_1, \dots, \psi_j \right) d(\psi_1, \dots, \psi_j), \end{aligned}$$

where

$$\begin{aligned} J_3(\alpha, \psi_1, \psi_2, \psi_3) = & \int_{[-\pi, \pi]} \int_{[\alpha, \pi]} \left| \det \begin{pmatrix} 1 & \sin \phi_1 \sin \varphi_1 & \cos \phi_1 \sin \varphi_1 & \cos \varphi_1 \\ 1 & \sin \psi_1 \sin \alpha & \cos \psi_1 \sin \alpha & \cos \alpha \\ 1 & \sin \psi_2 \sin \alpha & \cos \psi_2 \sin \alpha & \cos \alpha \\ 1 & \sin \psi_3 \sin \alpha & \cos \psi_3 \sin \alpha & \cos \alpha \end{pmatrix} \right| \\ & \times \sin \phi_1 d\phi_1 d\varphi_1, \end{aligned}$$

$$\begin{aligned} J_2(\alpha, \psi_1, \psi_2) = & \int_{[-\pi, \pi]^2} \int_{[\alpha, \pi]^2} \left| \det \begin{pmatrix} 1 & \sin \phi_1 \sin \varphi_1 & \cos \phi_1 \sin \varphi_1 & \cos \varphi_1 \\ 1 & \sin \phi_2 \sin \varphi_2 & \cos \phi_2 \sin \varphi_2 & \cos \varphi_2 \\ 1 & \sin \psi_1 \sin \alpha & \cos \psi_1 \sin \alpha & \cos \alpha \\ 1 & \sin \psi_2 \sin \alpha & \cos \psi_2 \sin \alpha & \cos \alpha \end{pmatrix} \right| \\ & \times \sin \phi_1 \sin \varphi_2 d(\phi_1, \varphi_2) d(\phi_1, \varphi_2), \end{aligned}$$

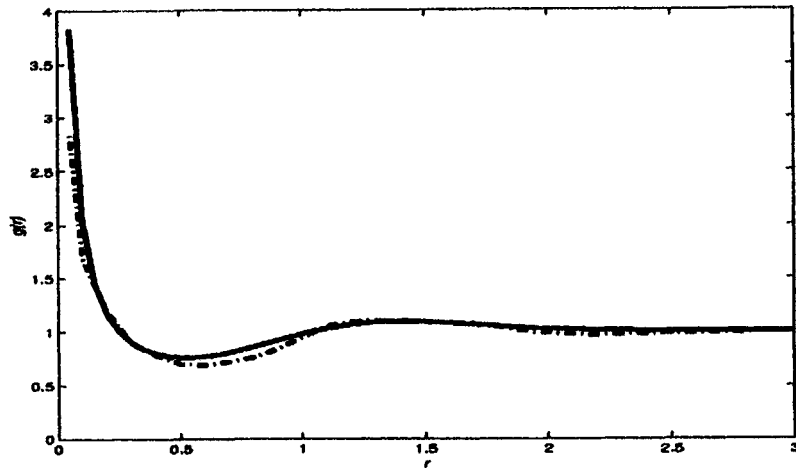


Figure 5.6.1 Pair correlation function g for the point process of vertices of \mathcal{V}_P in \mathbb{R}^2 (— numerical values from Muche, 1999; - - estimates from Stoyan and Stoyan, 1990).

$$\begin{aligned}
 J_1(\alpha, \psi_1) &= \int_{[-\pi, \pi]^3} \int_{[\alpha, \pi]^3} \left| \det \begin{pmatrix} 1 & \sin \phi_1 \sin \varphi_1 & \cos \phi_1 \sin \varphi_1 & \cos \varphi_1 \\ 1 & \sin \phi_2 \sin \varphi_2 & \cos \phi_2 \sin \varphi_2 & \cos \varphi_2 \\ 1 & \sin \phi_3 \sin \varphi_3 & \cos \phi_3 \sin \varphi_3 & \cos \varphi_3 \\ 1 & \sin \psi_1 \sin \alpha & \cos \psi_1 \sin \alpha & \cos \alpha \end{pmatrix} \right| \\
 &\quad \times \sin \phi_1 \sin \varphi_2 \sin \varphi_3 d(\phi_1, \phi_2, \phi_3) d(\psi_1, \phi_2, \phi_3), \\
 J_0(\alpha) &= 2\pi \int_0^\pi \int_0^\pi \int_0^{\pi/2} |\cos \psi - \cos \tau| T(\alpha, \varphi, \tau) U(\alpha, \varphi, \psi) \\
 &\quad \times \sin^5 \tau \sin \varphi \sin \psi d\tau d\varphi d\psi
 \end{aligned}$$

with

	$0 \leq b + c \leq a$ or $a + b + c \geq 2\pi$	$ b - c \geq a$	Otherwise
$T(a, b, c)$	0	$12\pi^3$	$S\left(\cos^{-1} \frac{\cos b \cos c - \cos a}{\sin b \sin c}\right)$
$U(a, b, c)$	0	2π	$2 \cos^{-1} \frac{\cos b \cos c - \cos a}{\sin b \sin c}$

Table 5.6.2 Values of the pair correlation function g for the point process of vertices of \mathcal{V}_P in \mathbb{R}^3 .

r	$g(r)$	r	$g(r)$	r	$g(r)$
0.01	764.2665	0.65	0.8984	1.65	1.0678
0.02	200.9408	0.70	0.8725	1.70	1.0614
0.03	91.7755	0.75	0.8562	1.75	1.0532
0.04	52.9836	0.80	0.8478	1.80	1.0443
0.05	34.8224	0.85	0.8462	1.85	1.0354
0.06	24.8332	0.90	0.8505	1.90	1.0272
0.07	18.7338	0.95	0.8599	1.95	1.0201
0.08	14.7256	1.00	0.8739	2.00	1.0143
0.09	11.9437	1.05	0.8917	2.05	1.0098
0.10	9.9299	1.10	0.9125	2.10	1.0064
0.15	5.0193	1.15	0.9355	2.15	1.0040
0.20	3.2034	1.20	0.9596	2.20	1.0025
0.25	2.3217	1.25	0.9838	2.25	1.0014
0.30	1.8230	1.30	1.0069	2.30	1.0008
0.35	1.5125	1.35	1.0277	2.35	1.0004
0.40	1.3065	1.40	1.0451	2.40	1.0002
0.45	1.1639	1.45	1.0584	2.45	1.0001
0.50	1.0623	1.50	1.0673	2.50	1.0001
0.55	0.9891	1.55	1.0715	2.55	1.0000
0.60	0.9361	1.60	1.0714	≥ 2.60	1.0000

Source: Heinrich *et al.* (1998, Table 9).

and $S(a) = 12a^3 - 3a \sin^2 2a - 24a \sin^2 a + 12 \sin 2a \sin^2 a$. The computation of $g_{j,3}$ is laborious and numerical values of $g_{0,3}^*(r)$ and $g_{j,3}(r)$ are presented in Heinrich *et al.* (1998, Tables 3–7, Figures 3–7). Numerical values of $g(r)$ is given in Table 5.6.2 (see Heinrich *et al.*, 1998, Tables 8–9, Figures 8–9) and Figure 5.6.2.

Heinrich and Muche (1994) showed that $\lim_{r \rightarrow 0} r^{m-1} g(r)$ exists and is non-zero. For example, if $m = 2$, $\lim_{r \rightarrow 0} r g(r) = 16/(9\pi^2\sqrt{\lambda})$. Therefore, g possesses a pole of order $m-1$ at $r = 0$.

The asymptotic behaviour of g for large r is governed by the following exponential bounds:

$$1 - \frac{g_{0,m}^*(r)}{[(m+1)!]^2} \leq 2 \exp\left(\frac{\lambda \omega_m r^m}{2^m}\right)^{m-1} e^{-\lambda \omega_m r^m / 2^m}, \quad r \geq 2(\omega_m \lambda)^{-1/m^2},$$

$$g_{j,m}(r) \leq c_m (\lambda r^m)^{2m-j-1} e^{-\lambda \omega_m r^m / 2^m}, \quad r \geq 2(\omega_m \lambda)^{-1/m}, \\ j = 0, 1, \dots, m,$$

for some positive constant c_m . These bounds guarantee the existence of the integral $\int_0^\infty r^{m-1} [g(r) - 1] dr$, which is closely related to the variance of the following estimator of λ_0 .

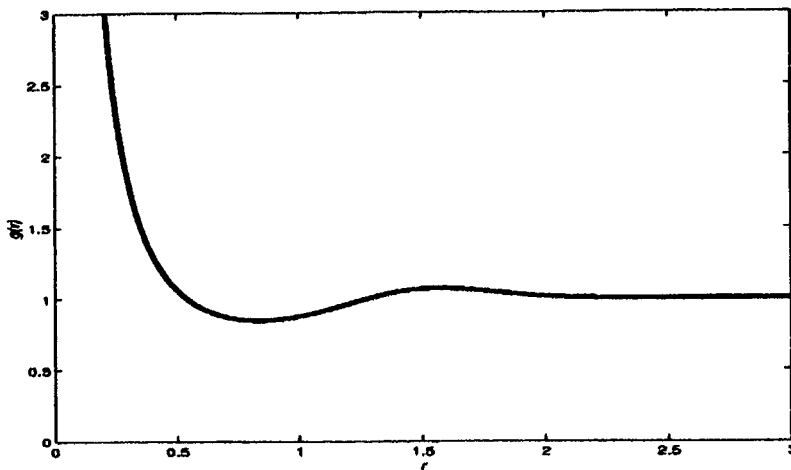


Figure 5.6.2 Pair correlation function g for the point process of vertices of \mathcal{V}_P in \mathbb{R}^3 (values from Heinrich *et al.*, 1998).

A natural unbiased estimator $\hat{\lambda}_{0,L}$ of λ_0 from point patterns observed within a cube $[0, L]^m$ in \mathbb{R}^m is

$$\hat{\lambda}_{0,L} = \frac{\Theta_{P_0} \cap [0, L]^m}{L^m},$$

where $\Theta_{P_0} \cap [0, L]^m$ is the number of points of Θ_{P_0} within $[0, L]^m$. A central limit theorem for $\Theta_{P_0} \cap [0, L]^m$ can be deduced from Heinrich (1994, Corollary of Theorem 2.3):

$$\frac{\hat{\lambda}_{0,L} L^m - \kappa_m \lambda L^m}{\sqrt{\lambda \kappa_m (1 + \kappa_m \sigma_m^2) L^m}} \longrightarrow Z \text{ in distribution as } L \rightarrow \infty,$$

where Z denotes a standard normal random variable and

$$\sigma_m^2 = m \omega_m \int_0^\infty r^{m-1} [g(r \lambda^{-1/m}) - 1] dr$$

is a constant depending only on m (Heinrich and Muche, 1994). In particular, $\sigma_2 = 0.744$ and $\sigma_3 = 2.255$ (Heinrich *et al.*, 1998). Central limit theorems for the fibre process of edges and other point processes associated with Poisson Voronoi diagrams and Voronoi diagrams satisfying a β -mixing (absolute regularity) condition (see Section 1.3.3) have also been established in Heinrich (1994).

Stoyan and Stoyan (1990) provide methods for estimating g and $\rho^{(2)}$ from point patterns observed within a bounded region in \mathbb{R}^2 . Using Monte Carlo simulation, they estimate g for Θ_{P_0} and Θ_{P_1} of \mathcal{V}_P in \mathbb{R}^2 . These functions are shown in Figures 5.6.1 and 5.6.3. The estimated pair correlation function for

the point process of a vertex is quite close to the theoretical form given in equation (5.6.2).

This approach may be developed further by considering marked point processes in which one or more values (or marks) are associated with each of the points. Stoyan and Stoyan (1990) considered the situation where each edge centre c_i is marked by the angle, $\alpha(c_i)$ between the line through the end points of the edge and a given fixed line ($0 \leq \alpha(c_i) \leq 2\pi$). They defined an angle correlation function g_α by

$$g_\alpha(r) = \frac{\rho_\alpha^{(2)}(r)}{\rho^{(2)}(r)}, \quad r \geq 0,$$

where $\rho_\alpha^{(2)}(r)$ is a product density defined as follows. Again consider two infinitesimally small discs of area dA_1 and dA_2 with distance r between their centres and suppose that $\rho^{(2)}(r) dA_1 dA_2$ is the probability that there is an edge centre in each of the discs. Define

$$f(u, v) = \min \{ |u - v|, 2\pi - |u - v| \}$$

as the minimum angle between the two lines, of directions u and v , containing the edge centres. Then $\rho_\alpha^{(2)}(r) = f(u, v) dA_1 dA_2$ and $g_\alpha(r)$ can be interpreted as the conditional mean of the angles between the two edges. Stoyan and Stoyan (1990) estimated g_α for the edge centres of \mathcal{V}_p and this is illustrated in Figure 5.6.4. Stoyan and Hermann (1986) considered marking c_i using the areas, A_1 and A_2 of the two cells on each side of the edge containing c_i , where A_1 is the area of the cell lying in the upper half of \mathbb{R}^2 defined by a line through the end points of the edge. Thus, A_1 and A_2 have the same distribution. Possible marks for c_i include $A_1 \cdot A_2$ and $(A_1 + A_2)$. They calculated the means and variances for these marks for \mathcal{V}_p .

It is also possible to mark the original generator points of \mathcal{V}_p . Stoyan and Hermann (1986) did this in terms of the area of the cell associated with the generator to define an area correlation function g_A analogous to g_α defined above, where $g_A(r)$ may be interpreted as the mean of the product of the areas of two cells with generators a distance r apart. They estimated g_A for \mathcal{V}_p using a Monte Carlo simulation approach.

5.6.2 Voronoi growth models

Voronoi diagrams can be regarded as the resultant structure of a growth process. Each generator starts generating a cell at the same time by growing radially in all directions in \mathbb{R}^m with the same non-zero speed. When two growing cells meet each other, they stop growing at the contact surface so that the cell associated with a point is fully grown when growth ceases in all directions. At the end of such a growth process the whole space is occupied by cells and the resultant structure is a Voronoi diagram. Such a Voronoi growth model is also known as the *cell model* (Meijering, 1953) or the *site saturation model* (Saetre *et al.*, 1986). Further discussion on growth models

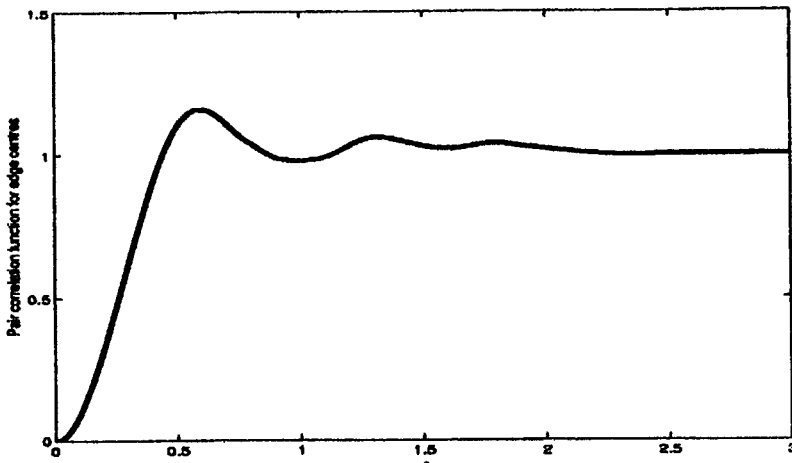


Figure 5.6.3 Pair correlation function for the edge centres of the Poisson Voronoi diagram in \mathbb{R}^2 (estimates from Stoyan and Stoyan, 1990).

can be found in Section 7.2. In Section 5.8 we will discuss a generalization of such a growth process in which generators do not start at the same time.

Chiu (1995c) studied the distribution of the *time of complete tessellation* T_L until a very large cube $[0, L]^m$ is completely occupied by cells of such a growth process, the generators of which form a Poisson point process of intensity λ . Assume that the growth starts at time 0 and suppose that the growth rate at time τ is v_τ . Chiu (1995c, Theorem 3) states that for each real number u ,

$$\Pr \left\{ \lambda \omega_m \left(\int_0^{T_L} v_\tau d\tau \right)^m - \log [\lambda L^m (\log \lambda L^m)^{m-1}] \leq u \right\} \rightarrow \exp(-\psi_m e^{-u})$$

as $L \rightarrow \infty$,

where $\omega_m = \pi^{m/2}/\Gamma(m/2 + 1)$ is the volume of an m -dimensional sphere of unit radius and

$$\psi_m = \frac{1}{m! \left\{ 2\Gamma\left(\frac{m+1}{2}\right) / m\sqrt{\pi} \Gamma\left(\frac{m}{2}\right) \right\}^{m-1}}. \quad (5.6.3)$$

Furthermore,

$$\frac{\lambda \omega_m \left(\int_0^{T_L} v_\tau d\tau \right)^m}{\log [\lambda L^m (\log \lambda L^m)^{m-1}]} \rightarrow 1 \text{ in probability as } L \rightarrow \infty.$$

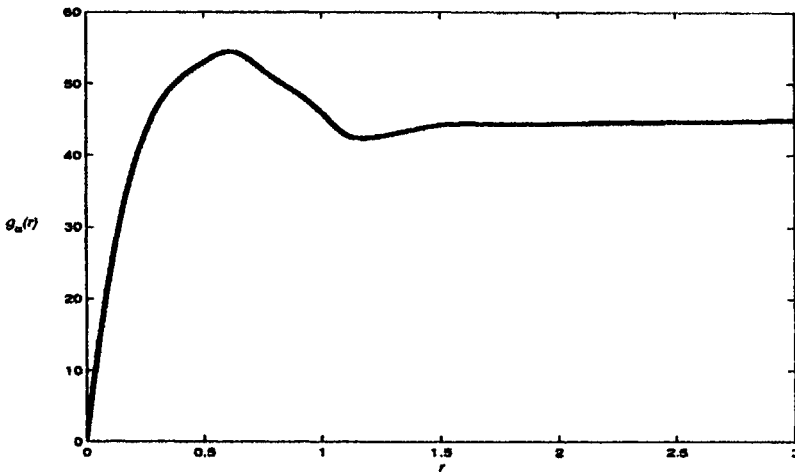


Figure 5.6.4 Angle correlation function g_a of the Poisson Voronoi diagram in \mathbb{R}^2 (estimates from Stoyan and Stoyan, 1990).

In particular, if v_t is equal to a constant v , then

$$T_L \simeq \left\{ \frac{\log [\lambda L^m (\log \lambda L^m)^{m-1}]}{\lambda \omega_m v^m} \right\}^{1/m} \quad \text{for large } L.$$

At any finite time t the space \mathbb{R}^m is not yet filled by cells and so we do not have a tessellation of the space. The union of all cells at time $t < \infty$ is called an *incomplete Voronoi diagram* (Muche, 1993). It is in fact a Boolean model (see, for example, Stoyan *et al.*, 1995, Chapter 3) with equal radius balls as grains. Muche (1993) has obtained the intensities $L_A(t)$ and $S_V(t)$ of the fibre process and the surface process of boundaries of cells at time t in \mathbb{R}^2 and in \mathbb{R}^3 , respectively:

$$\begin{aligned} L_A(t) &= 4\lambda \int_0^t \exp(-\lambda \pi x^2) dx + (2\pi - 4)\lambda t \exp(-\lambda \pi t^2), \\ S_V(t) &= \frac{16\pi\lambda}{3} \int_0^t x \exp\left(-\frac{4}{3}\pi\lambda x^3\right) dx + \frac{4}{3}\pi\lambda t^2 \exp\left(-\frac{4}{3}\pi\lambda t^3\right). \end{aligned}$$

The linear and spherical contact distribution function (see Section 5.5.4) and the mean chord length (see Section 5.7) have also been derived.

Schulze *et al.* (1993) studied the normalized Euler characteristics of an incomplete Voronoi diagram at time t . The normalized Euler characteristic $\chi(t)$ is the mean of the difference of the number of connected components of the region occupied by cells in a square of area $1/\lambda$ and the number of connected components of the unoccupied region in the same square. Suppose the growth rate is a constant v , then

$$\chi(t) = (1 - \pi v^2 t^2) \exp(-\pi v^2 t^2).$$

Chiu (1995c) showed that as $t \rightarrow \infty$ in such a way that

$$\lambda L^m (\log \lambda L^m)^{m-1} e^{-\lambda \omega_m v^m t^m} \rightarrow e^{-u} \text{ as } L \rightarrow \infty,$$

for some real number u , then the number of connected components of the unoccupied region within $[0, L]^m$ follows a Poisson distribution with mean $\psi_m e^{-u}$ (see equation (5.6.3)), and such a component, after suitable normalization, converges essentially in distribution to a typical Poisson polyhedron formed by a stationary Poisson hyperplane process in \mathbb{R}^m (see Section 1.3.3) with intensity 1 (see also Hall, 1985).

5.6.3 The Stienen model

Stienen (1982) considered the maximal ball which can be inscribed in a Poisson Voronoi cell and centred at the generator of the cell. The union of these balls is now known as the *Stienen model*. It can also be regarded as the result of the following growth process: each generator starts growing radially in all directions. When two growing cells meet, these two cells stop growing. Thus, the Stienen model Ξ is the union of non-overlapping balls. The diameter of a typical sphere has the same distribution function D as the nearest neighbour distance of the Poisson point process, which is

$$D(r) = 1 - e^{-\lambda \omega_m r^m}, \quad r \geq 0.$$

This leads to the mean volume $1/(2^m \lambda)$. The covariance $C(r)$ is defined as $\Pr(o \in \Xi, r \in \Xi)$, where o is the origin and r a point at distance r from o . An analytical expression for $C(r)$ can be determined but the formula is very complicated except in the case when $m = 1$ (Schlather and Stoyan, 1997), which is given by

$$C(r) = \frac{1}{4} + 2e^{-3\lambda r/2} + \frac{e^{-2\lambda r}}{2} - \frac{2e^{-3\lambda r}}{5} + \left(\frac{\lambda r}{4} - \frac{21}{10}\right)e^{-4\lambda r/3} + \left(\frac{\lambda r}{12} + \frac{1}{4}\right)e^{-4\lambda r}$$

for $r \geq 0$. Wiencek and Stoyan (1993) have studied $C(r)$ for \mathcal{V}_P in \mathbb{R}^2 by simulation.

Another second-order statistic is $D_r(x, y)$, the probability that the diameter of a sphere at o is greater than x and the diameter of a sphere at r is greater than y , under the condition that there are sphere centres at o and r . In what follows we consider the Stienen model in \mathbb{R}^3 only. Stoyan (1990) showed that

$$D_r(x, y) = e^{-\lambda V(x, y, r)}, \quad r \geq 0,$$

where

$$V(x, y, r) = \begin{cases} \infty, & x \geq r \text{ or } y \geq r, \\ \frac{\pi}{3} [4x^3 + 4y^3 - (x-t)^2(2x+t) + (y+t-r)^2(2y-t+r)], & x+y > r, x < r \text{ and } y < r, \\ \frac{4}{3}\pi(x^3 + y^3), & x+y \leq r \end{cases}$$

and $t = (x^2 - y^2 + r^2)/(2r)$. A moment characteristic related to D_r is $k_{dd}(r)$, the mean of the product of the diameters of the spheres centred at o and r , where

$$k_{dd}(r) = \int_0^r \int_0^r e^{-\lambda V(x, y, r)} dx dy, \quad r \geq 0.$$

Note that $k_{dd}(0) = 0$ and $k_{dd}(\infty)$ is the square of the mean diameter of a typical sphere. The mean diameter is $[3/(4\pi)]^{1/3} \Gamma(4/3) \lambda^{-1/3} \approx 0.554 \lambda^{-1/3}$. Stoyan (1990) evaluated k_{dd} numerically. The values are reported in Table 5.6.3. The function k_{dd} is monotonic and $k_{dd}(2)$ is already very close to $k_{dd}(\infty)$. This indicates a short-range correlation.

5.6.4 Percolation on Poisson Voronoi diagrams and Poisson Delaunay tessellations

A *bond percolation model* is constructed from an infinite random lattice graph with periodic structure. Each edge will be assigned a value of 1 independently from the others with probability p and 0 with probability $1-p$. An edge assigned 0 will be deleted, whilst an edge assigned 1 will remain present. If instead of each edge we assign each vertex a value of 1 independently with probability p and 0 otherwise and retain those edges for which both endpoints have a value of 1, then a *site percolation model* is obtained. An important quantity in a percolation model is the critical or threshold probability p_c . If $p < p_c$, the expected cluster size is finite, and if $p > p_c$, there exists an infinite cluster with positive probability. The threshold probabilities for the bond and site percolation models on Poisson Voronoi diagrams and Poisson Delaunay tessellations in \mathbb{R}^2 and \mathbb{R}^3 are given in Table 5.6.4.

Table 5.6.3 Numerical values of the mean of the product of the diameters of two spheres whose centres are a distance r apart for the Stienen model in \mathbb{R}^3 .

r	0.1	0.2	0.3	0.4	0.5	0.6
$\lambda^{2/3} k_{dd}(r)$	0.010	0.039	0.085	0.141	0.196	0.243
r	0.7	0.8	0.9	1.0	2.0	
$\lambda^{2/3} k_{dd}(r)$	0.276	0.294	0.303	0.306	0.307	

Source: Stoyan (1990).

Table 5.6.4 The threshold probabilities for the bond and site percolation models on Poisson Voronoi diagrams and Poisson Delaunay tessellations in \mathbb{R}^m .

		Site	Bond
$m = 2$	Delaunay	0.5	0.347 [†]
	Voronoi	0.5	0.332*
$m = 3$	Voronoi	0.1453*	0.0822*

[†] Exact value = $2 \sin(\pi/18)$.

* Estimate.

Source: Jerauld *et al.* (1984a,b).

A *first-passage percolation*, originally suggested to model fluid flow in a random porous medium (Hammersly and Welsh, 1965), is a generalization of the bond percolation model in which each edge is independently assigned a non-negative random travel time from the same distribution, say F . The first-passage time between two vertices is the minimum travel time between the vertices over all paths connecting the vertices.

First-passage percolations on \mathcal{V}_p and \mathcal{D}_p in \mathbb{R}^2 were first suggested by Vahidi-Asl and Wierman (1990). They defined the first-passage time $t(u, v)$ in \mathcal{V}_p (\mathcal{D}_p) between two points u and v to be the minimum travel time between the vertices $p(u)$ and $p(v)$ which are the (almost surely unique) nearest vertices of u and v in \mathcal{V}_p (\mathcal{D}_p), respectively. Consider the first-passage time from the origin o to a point x . The limit $\lim_{\|x\| \rightarrow \infty} t(o, x)/\|x\| = \tau$ exists if and only if $\int_0^\infty [1 - F(t)]^3 dt < \infty$. Vahidi-Asl and Wierman (1992) established a shape theorem concerning the set $\mathcal{A}_t = \{x \in \mathbb{R}^2 : t(o, x) \leq t\}$ for $t > 0$. For all $\epsilon > 0$, the set \mathcal{A}_t contains a disc of radius $\tau^{-1}t(1 - \epsilon)$ and is contained in a disc of radius $\tau^{-1}t(1 + \epsilon)$ almost surely for all sufficiently large t if and only if $\int_0^\infty t[1 - F(t)]^3 dt < \infty$. Vahidi-Asl and Wierman (1993) studied the almost sure existence of the optimal path and the upper and lower bounds for the route length divided by the geometrical distance.

Howard and Newman (1997) suggested another first-passage percolation model on \mathcal{V}_p in \mathbb{R}^m . The distance between the two generators at locations x_1 and x_2 is defined to be $\|x_1 - x_2\|^\alpha$ for $\alpha \geq 0$. A route from a point u to v is the sequence (x_1, \dots, x_k) , where x_1 and x_k are the locations of the nearest generators of u and v , respectively; the length of this route is $\sum_{i=1}^{k-1} \|x_i - x_{i+1}\|^\alpha$ if $k \geq 2$ and zero otherwise. The first-passage time $t(u, v)$ from u to v is the length of the shortest route from u to v . Similar to Vahidi-Asl and Wierman (1990, 1992), they showed that the limit $\lim_{\|x\| \rightarrow \infty} t(o, x)/\|x\| = \tau_1$ exists and established a shape theorem for the set $\mathcal{B}_t = \{x \in \mathbb{R}^m : t(o, x) \leq t\}$ for $t > 0$. If $\alpha > 1$, then for each $\epsilon \in (0, \tau_1^{-1})$ the set \mathcal{B}_t contains an m -dimensional sphere of radius $\tau_1^{-1}t(1 - \epsilon)$ and is contained in an m -dimensional sphere of radius $\tau_1^{-1}t(1 + \epsilon)$ almost surely for all sufficiently large t .

5.7 SECTIONAL VORONOI DIAGRAMS

In many empirical situations involving tessellations in \mathbb{R}^3 it is not possible to observe the constituent cells directly. Instead the cells are examined by means of linear probes or planar sections. Indeed, the prevalence of such occurrences led to the development of the subject of stereology, which is concerned with drawing inferences about the geometric properties of three-dimensional material on the basis of observed, lower dimensional information.

We label the structure produced by the intersection between an s -dimensional hyperplane H_s ($1 \leq s \leq m$) and a Voronoi diagram \mathcal{V}_Θ generated by point process Θ in \mathbb{R}^m as the s -dimensional sectional Voronoi diagram denoted by $\mathcal{V}_\Theta(s, m)$. In particular, if Θ is the stationary Poisson point process, then the corresponding sectional diagram is called the *s-dimensional sectional Poisson Voronoi diagram* and is denoted by $\mathcal{V}_P(s, m)$. Thus, \mathcal{V}_P in \mathbb{R}^3 is equivalent to $\mathcal{V}_P(3, 3)$. Also, the intersection of H_t with $\mathcal{V}_P(s, m)$ is equal to $\mathcal{V}_P(t, m)$, $t < s$ (Miles, 1986a, p. 153). Figure 5.7.1 shows a portion of $\mathcal{V}_P(2, 3)$. Since \mathcal{V}_P in \mathbb{R}^3 is homogeneous, isotropic and ergodic, $\mathcal{V}_P(s, m)$ has the same properties. Similarly, since \mathcal{V}_P is normal, so too is $\mathcal{V}_P(s, m)$. Nevertheless, a planar section of \mathcal{V}_P in \mathbb{R}^2 is not equivalent to a *Poisson Voronoi diagram* in \mathbb{R}^2 , because the mean values for the characteristics of $\mathcal{V}_P(2, 3)$ clearly deviate from the corresponding mean values of \mathcal{V}_P in \mathbb{R}^2 (Mecke, 1984). However,

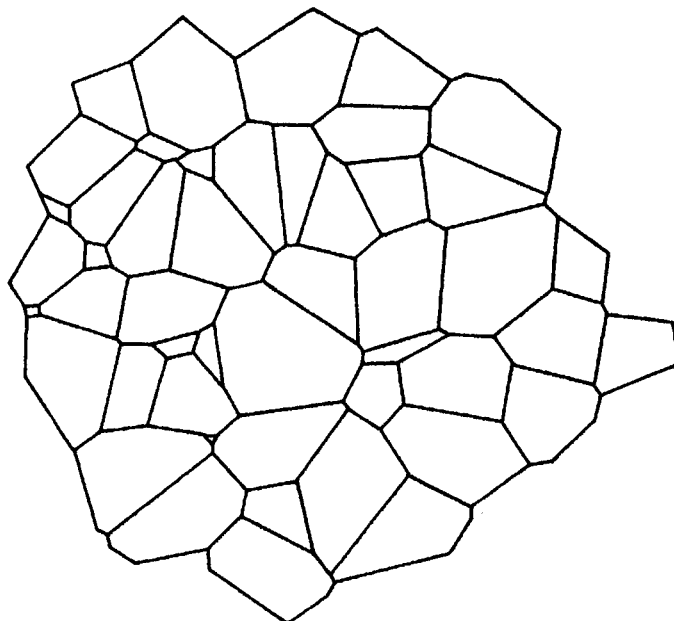


Figure 5.7.1 Portion of a two-dimensional sectional Poisson Voronoi diagram $\mathcal{V}_P(2, 3)$. (Source: Lorz, 1991.)

whether $\mathcal{V}_p(2, 3)$ is a Voronoi diagram generated by a *non-Poisson* point process cannot be answered by inspecting mean value formulae only. Chiu *et al.* (1996) proved that $\mathcal{V}_p(s, m)$ ($1 < s < m$) is *not* a Voronoi diagram, i.e. there does not exist any point process in \mathbb{R}^s ($1 < s < m$) the Voronoi diagram of which is the same as $\mathcal{V}_p(s, m)$. Moreover, almost surely each cell of $\mathcal{V}_p(s, m)$ is a *non-Voronoi cell*, i.e. a cell, together with all its neighbouring cells, is not possible to be present in a Voronoi diagram.

Only limited information about the characteristics of the individual cells of $\mathcal{V}_e(s, m)$ and $\mathcal{V}_p(s, m)$ has been obtained analytically and researchers have again resorted to Monte Carlo simulations as a source of supplementary information. General expressions paralleling those given in Table 5.1.1 for \mathcal{V}_e and equations (5.5.1)–(5.5.5) for \mathcal{V}_p may be derived by either the ergodic theorem (Miles, 1972a, 1984, 1986a) or the Palm distribution (Møller, 1989) (see Section 1.3.3). We use the same symbols employed in Section 5.5, and in addition use the superscript (s) to refer to the dimensionality of the hyperplane. Table 5.7.1 gives formulae for isotropic $\mathcal{V}_e(s, m)$, where $1 \leq s < m$ and $m = 2, 3$. The first moments given are only in terms of the intensities λ of the point process Θ , λ_0 of the point process of vertices, L_A and L_V of the fibre process of edges of \mathcal{V}_e for $m = 2$ and 3, respectively, and S_V of the surface process of cell faces of \mathcal{V}_e for $m = 3$. Since all these intensities for \mathcal{V}_p are known, explicit expressions for $\mathcal{V}_p(s, m)$, where $1 \leq s < m$ and $m = 2, 3$, can be derived (see Table 5.7.2). For an arbitrary m , Møller (1989) shows that the intensities of the vertices $\lambda_0^{(s)}$ and the midpoints of the edges of the cells $\lambda_1^{(s)}$ in $\mathcal{V}_p(s, m)$ are given by

$$\lambda_0^{(s)} = \frac{2}{s+1} \lambda_1^{(s)}, \quad (5.7.1)$$

$$\lambda_1^{(s)} = \frac{\lambda^{s/m} \pi^{s/2} \Gamma\left(\frac{ms+m-s+1}{2}\right) \Gamma\left(\frac{m}{2}+1\right)^{s+1-s/m} \Gamma\left(s+1-\frac{s}{m}\right)}{m \Gamma\left(\frac{s}{2}+1\right) \Gamma\left(\frac{ms+m-s}{2}\right) \Gamma\left(\frac{m+1}{2}\right)^{s+1}}. \quad (5.7.2)$$

Denote by $E_t^{(s)}$ the expectation with respect to the Palm distribution with respect to the typical t -faces of $\mathcal{V}_p(s, m)$ and by $E_t^{(s)} V_k$ the expected k -dimensional content of a k -face contained in a typical t -face of $\mathcal{V}_p(s, m)$. The expected length of a typical edge $E_1^{(s)} V_1$ in $\mathcal{V}_p(s, m)$ is

$$E_1^{(s)} V_1 = \frac{\Gamma\left(\frac{ms-s}{2}+1\right) \Gamma\left(\frac{ms+m-s}{2}\right) \Gamma\left(\frac{m+1}{2}\right) \Gamma\left(s-\frac{s-1}{m}\right)}{\lambda^{1/m} \Gamma\left(\frac{ms-s+1}{2}\right) \Gamma\left(\frac{ms+m-s+1}{2}\right) \Gamma\left(s-\frac{s}{m}+1\right) \Gamma\left(\frac{m}{2}+1\right)^{1-1/m}}. \quad (5.7.3)$$

For $s = 1$ and $m \geq 2$,

$$\lambda_0^{(1)} = \lambda_1^{(1)} = (\mathbf{E}_1^{(1)} V_1)^{-1} = \frac{2\lambda^{1/m} (m-1)! \Gamma\left(\frac{m}{2} + 1\right)^{2-1/m} \Gamma\left(2 - \frac{1}{m}\right)}{m \Gamma\left(m - \frac{1}{2}\right) \Gamma\left(\frac{m+1}{2}\right)^2}. \quad (5.7.4)$$

For $s = 2$ and $m \geq 3$,

$$\lambda_1^{(2)} = \frac{\lambda^{2/m} \pi \Gamma\left(\frac{3m-1}{2}\right) \Gamma\left(\frac{m}{2} + 1\right)^{3-2/m} \Gamma\left(3 - \frac{2}{m}\right)}{m \Gamma\left(\frac{3m}{2} - 1\right) \Gamma\left(\frac{m+1}{2}\right)^3},$$

$$\lambda_0^{(2)} = \frac{2}{3} \lambda_1^{(2)},$$

$$\lambda_2^{(2)} = \frac{1}{3} \lambda_1^{(2)},$$

$$\mathbf{E}_2^{(2)} V_0 = \mathbf{E}_2^{(2)} N_0 = \mathbf{E}_2^{(2)} N_1 = 6,$$

$$\mathbf{E}_2^{(2)} V_1 = \frac{6(m-1)! \Gamma\left(2 - \frac{1}{m}\right) \Gamma\left(\frac{3m}{2} - 1\right) \Gamma\left(\frac{m+1}{2}\right)}{\lambda^{1/m} \Gamma\left(\frac{m}{2} + 1\right)^{1-1/m} \Gamma\left(\frac{3m-1}{2}\right) \Gamma\left(m - \frac{1}{2}\right) \Gamma\left(3 - \frac{2}{m}\right)},$$

$$\mathbf{E}_1^{(2)} V_1 = \frac{(m-1)! \Gamma\left(\frac{3m}{2} - 1\right) \Gamma\left(\frac{m+1}{2}\right) \Gamma\left(2 - \frac{1}{m}\right)}{\lambda^{1/m} \Gamma\left(m - \frac{1}{2}\right) \Gamma\left(\frac{3m-1}{2}\right) \Gamma\left(3 - \frac{2}{m}\right) \Gamma\left(\frac{m}{2} + 1\right)^{1-1/m}},$$

$$\mathbf{E}_0^{(2)} V_1 = 3\mathbf{E}_1^{(2)} V_1.$$

Since our primary concern is with applications, the values of the above expressions for $s = 1, 2$ and $m = 2, 3$ are given in Table 5.7.2. As in Section 5.5, in order to avoid excessive use of subscripts, these values are given simpler symbols which are identified in the table. This table also includes a value for $\mathbf{E}^{(1)}(L_{1,2}^2)$ derived by numerical integration (Gilbert, 1962) and other moments estimated by Lorz (1990b, 1991) using Monte Carlo simulations. Lorz (1990b) has also estimated moments and correlation coefficients for the area, perimeter and a randomly chosen interior angle conditional on the number of edges for a typical cell of $\mathcal{V}_p(2, 3)$.

In addition to the exact mean sectional values given in Table 5.7.2, Miles (1972a, 1984) has derived asymptotic values as $m \rightarrow \infty$. These are reported in Table 5.7.3. Note that these mean values do not depend on the intensity

of the generators. Recall that the values for $\mathcal{V}_P(1, m)$ and $\mathcal{V}_P(2, m)$ are equivalent to the line sections of both $\mathcal{V}_P(3, m)$ and $\mathcal{V}_P(2, m)$ and the plane section of $\mathcal{V}_P(3, m)$, respectively.

A lemma due to Miles (1972a, p. 260) shows that an s -dimensional section of \mathcal{V}_P is stochastically equivalent to an s -dimensional section of a corresponding inhomogeneous $(s+1)$ -dimensional structure. In particular, let Θ_P^* be an inhomogeneous Poisson point process in \mathbb{R}^m with intensity $\lambda_m = \lambda_m(x_4, \dots, x_m)$ and \mathcal{V}_P^* be its associated Voronoi diagram. If ${}^0[3]$ is the three-dimensional subspace of \mathbb{R}^m defined by $x_4 = \dots = x_m = 0$, then since λ_m is functionally independent of (x_1, x_2, x_3) , the three-dimensional section of \mathcal{V}_P^* by ${}^0[3]$ is a homogeneous normal tessellation, denoted by $\mathcal{V}^*(3, m)$. Thus, $\mathcal{V}_P(3, m)$ is stochastically equivalent to $\mathcal{V}^*(3, 4)$ with respect to

$$\lambda_4(x_4) = \lambda x_4^{m-4} \left\{ \frac{2\pi^{(m-3)/2}}{\Gamma\left(\frac{m-3}{2}\right)} \right\} \quad (5.7.5)$$

(Miles, 1972a, pp. 260–261). This lemma extends from three-dimensional sections to general s -dimensional sections and Miles (1984) exploits it to derive a four-fold integral expression for the distribution of line segments when $s = 1$ but this is hardly tractable. However, Muche and Stoyan (1992) have derived numerically tractable double integral formulae for the chord length ($s = 1$) distribution functions, $F_{L_{1,2}}$ and $F_{L_{1,3}}$, in \mathbb{R}^2 and \mathbb{R}^3 , respectively. These distributions are derived from the linear contact distribution function $H_1(r)$ given in equation (5.5.31) (Gilbert, 1962) which gives the probabilities that a fixed line segment of length r , $r \geq 0$, with one end point in the origin, lies completely in the cell P_o containing the origin. The distribution of the chord length $L_{1,m}$ in $\mathcal{V}_P(1, m)$ and the linear contact distribution are linked by

$$H_1(r) = \frac{1}{E(L_{1,m})} \int_0^r [1 - F_{L_{1,m}}(x)] dx, \quad r \geq 0.$$

The mean chord length has been obtained by Gilbert (1962):

$$E(L_{1,m}) = \frac{\lambda^{-1/m} m \Gamma\left(\frac{m+1}{2}\right)^2 \Gamma\left(m - \frac{1}{2}\right)}{2(m-1)! \Gamma\left(2 - \frac{1}{m}\right) \Gamma\left(\frac{m}{2} + 1\right)^{(2m-1)/m}}.$$

The cumulative distributions of $L_{1,2}$ and $L_{1,3}$ as derived by Muche and Stoyan (1992) using numerical integration are given in Table 5.7.4. Explicit expressions for the pdf are given in equations (5.7.7) and (5.7.8), with $s = 1$. The densities for $2 \leq m \leq 7$ are illustrated in Figure 5.7.2.

The chord length distribution for $\mathcal{V}_P(1, m)$ is given in Schlather (1999), in which the distribution of the length $L_{s,m}$ of a typical edge in $\mathcal{V}_P(s, m)$ ($1 \leq s \leq m$) has also been given (cf. Muche, 1996a, p. 280):

Table 5.7.1 Moments of various characteristics of an s -dimensional homogeneous sectional Voronoi diagram $\mathcal{V}_\Theta(s, m)$.

Moment	Symbol	Exact value
$s = 1, m = 2$		
Intensity of vertices	$\lambda_0^{(1)}$	$2L_A/\pi$
Intensity of mid-points of line segments	$\lambda_1^{(1)}$	$2L_A/\pi$
Expected length of a typical line segment $[E_1^{(1)}V_1]$ and its third moment $E_1^{(1)}(V_1^3)$	$E^{(1)}(L_{1,2})$ $E^{(1)}(L_{1,2}^3)$	$\pi/(2L_A)$ $3\lambda E_2(V_2^2)/(2L_A)$
$s = 1, m = 3$		
Intensity of vertices	$\lambda_0^{(1)}$	$S_V/2$
Intensity of mid-points of line segments	$\lambda_1^{(1)}$	$S_V/2$
Expected length of a typical line segment $[E_1^{(1)}V_1]$, its third moment $[E_1^{(1)}(V_1^3)]$ and its fourth moment $[E_1^{(1)}(V_1^4)]$	$E^{(1)}(L_{1,3})$ $E^{(1)}(L_{1,3}^3)$ $E^{(1)}(L_{1,3}^4)$	$2/S_V$ $3L_V E^{(2)}(A^2)/(2\pi S_V)$ $6\lambda E_3(V_3^2)/(\pi S_V)$
$s = 2, m = 3$		
Intensity of vertices	$\lambda_0^{(2)}$	$L_V/2$
Intensity of mid-points of cell edges	$\lambda_1^{(2)}$	$3L_V/4$
Intensity of cell centroids	$\lambda_2^{(2)}$	$L_V/4$
Expected number of vertices of a typical cell $[E_2^{(2)}N_0]$ (edges of a typical cell $[E_2^{(2)}N_1]$)	$E^{(2)}(N)$	6
Expected area of a typical cell $[E_2^{(2)}V_2]$	$E^{(2)}(A)$	$4/L_V$
Expected perimeter of a typical cell $[E_2^{(2)}V_1]$	$E^{(2)}(P)$	$2\pi S_V/L_V$
Expected length of a typical edge $[E_2^{(2)}V_1]$ and its third moment $[E_1^{(2)}(V_1^3)]$	$E^{(2)}(L_{2,3})$ $E^{(2)}(L_{2,3}^3)$	$(\pi/3)(S_V/L_V)$ $(\lambda + \lambda_0) E_2(V_2^2)/L_V$

L_A = intensity of the fibre process of edges of \mathcal{V}_Θ in \mathbb{R}^2 .

L_V = intensity of the fibre process of edges of \mathcal{V}_Θ in \mathbb{R}^3 .

S_V = intensity of the surface process of faces of \mathcal{V}_Θ in \mathbb{R}^3 .

λ_0 = intensity of the point process of vertices of \mathcal{V}_Θ .

λ = intensity of Θ .

V_2 = area of a typical cell of \mathcal{V}_Θ in \mathbb{R}^2 /a typical face of \mathcal{V}_Θ in \mathbb{R}^3 .

V_3 = volume of a typical cell of \mathcal{V}_Θ in \mathbb{R}^3 .

Source: Møller (1994, Propositions 3.4.4 and 3.4.5).

Table 5.7.2 The first and/or second-order moments of various characteristics of an s -dimensional sectional Poisson Voronoi diagram.

Moment	Symbol	Exact value	Numerical value	Estimate*
$s = 1, m = 2$				
Intensity of vertices	$\lambda_0^{(1)}$	$4\lambda^{1/2}/\pi$	$1.273\lambda^{1/2}$	
Intensity of mid-points of line segments	$\lambda_{\text{mid}}^{(1)}$	$4\lambda^{1/2}/\pi$	$1.273\lambda^{1/2}$	
Expected length of a typical line segment $[E_1^{(1)}V_1]$ and its second moment $E_1^{(1)}(V_1^2)$	$E_1^{(1)}(L_{1,2}^{(1)})$	$\pi/(4\lambda^{1/2})$	$0.785\lambda^{-1/2}$	$0.804\lambda^{-1}$
$s = 1, m = 3$				
Intensity of vertices	$\lambda_0^{(1)}$	$\Gamma(2/3)(32\pi\lambda/81)^{1/3}$	$1.455\lambda^{1/3}$	
Intensity of mid-points of line segments	$\lambda_{\text{mid}}^{(1)}$	$\Gamma(2/3)(32\pi\lambda/81)^{1/3}$	$1.455\lambda^{1/3}$	
Expected length of a typical line segment $[E_1^{(1)}V_1]$ and its second moment $E_1^{(1)}(V_1^2)$	$E_1^{(1)}(L_{1,3}^{(1)})$	$(32\pi\lambda/81)^{-1/3}\Gamma(2/3)^{-1}$	$0.687\lambda^{-1/3}$	$0.632\lambda^{-2/3}$
$s = 2, m = 3$				
Intensity of vertices	$\lambda_0^{(2)}$	$2\Gamma(1/3)(16\pi^2\lambda^2/27)^{1/3}/15$	$2.916\lambda^{2/3}$	
Intensity of mid-points of cell edges	$\lambda_{\text{mid}}^{(2)}$	$\Gamma(1/3)(16\pi^2\lambda^2/27)^{1/3}/5$	$4.374\lambda^{2/3}$	
Intensity of cell centroids	$\lambda_{\text{cent}}^{(2)}$	$\Gamma(1/3)(16\pi^2\lambda^2/27)^{1/3}/15$	$1.458\lambda^{2/3}$	
Expected number of vertices of a typical cell $[E_2^{(2)}N_3]$ (edges of a typical cell $[E_2^{(2)}N_1]$ and its second moment $[E_2^{(2)}(N_0^2)E_2^{(2)}(N_1^2)]$)	$E_2^{(2)}(N)$	6	6	
Expected area of a typical cell $[E_2^{(2)}V_2]$ and its second moment $[E_2^{(2)}(V_1^2)]$	$E_2^{(2)}(A)$	$15[\Gamma(1/3)(16\pi^2\lambda^2/27)^{1/3}]$	$0.686\lambda^{-2/3}$	38.827
Expected perimeter of a typical cell $[E_2^{(2)}V_1]$ and its second moment $[E_2^{(2)}(V_1^2)]$	$E_2^{(2)}(P)$	$5(6\pi)^{1/3}\Gamma(2/3)\lambda^{-1/3}/\Gamma(1/3)$	$0.699\lambda^{-4/3}$	
Expected length of a typical edge $[E_1^{(2)}V_1]$ and its second moment $[E_1^{(2)}(V_1^2)]$	$E_1^{(2)}(P')$	$5\Gamma(2/3)(36\pi\lambda)^{-1/3}/\Gamma(1/3)$	$3.136\lambda^{-1/3}$	$11.308\lambda^{-2/3}$
Expected value of an interior angle of a typical cell and its second moment	$E_2^{(2)}(L_{2,3}^{(2)})$		$0.523\lambda^{-1/3}$	
Expected value of an angle at a typical vertex and its second moment	$E_2^{(2)}(\alpha_2)$	$0.404\lambda^{-2/3}$	$0.404\lambda^{-2/3}$	2.000
	$E_2^{(2)}(\alpha_1)$	$2\pi/3$	2.094	4.349
	$E_2^{(2)}(\alpha_1^2)$			4.689

λ = intensity of the m -dimensional Poisson point process Θ_p .

* Estimates from Monte Carlo simulation by Lorz (1990b, 1991).

Table 5.7.3 Asymptotic moments of various characteristics of an s -dimensional sectional Poisson Voronoi diagram $\gamma_p(s, m)$, as $m \rightarrow \infty$.

Symbol	Characteristic		Simpler symbol	Exact value	Numerical value
$s = 1$					
$E_1^{(1)} V_1$	Length of a typical line segment		$E^{(1)}(L_{1,\infty})$	$(2e)^{-1/2}$	0.429
$s = 2$					
$E_2^{(2)} N_6$ $(E_2^{(2)} N_1)$	Number of vertices of a typical cell (edges of a typical cell)	$E^{(2)}(N)$	6	6	6
$E_2^{(2)} V_2$	Area of a typical cell	$E^{(2)}(A)$	$3^{1/2}/(\pi e)$	0.203	
$E_2^{(2)} V_1$	Perimeter of a typical cell	$E^{(2)}(P)$	$(6/e)^{1/2}$	1.486	
$s = 3$					
$E_3^{(3)} N_6$	Number of vertices of a typical cell	$E^{(3)}(M)$	$1/\phi$	22.795	
$E_3^{(3)} N_1$	Number of edges of a typical cell	$E^{(3)}(E)$	$3/(2\phi)$	34.192	
$E_3^{(3)} N_2$	Number of faces of a typical cell	$E^{(3)}(F)$	$2 + 1/(2\phi)$	13.397	
$E_3^{(3)} N_6$	Number of vertices of a typical face (edges of a typical face)	$E^{(3)}(N)$	$6/(4\phi + 1)$	5.104	
$(E_3^{(3)} N_1)$	Volume of a typical cell	$E^{(3)}(V)$	$1/(16\pi e^{3/2}\phi)$	0.101	
$E_3^{(3)} V_3$	Surface area of a typical cell	$E^{(3)}(S)$	$1/(2^{3/2}\pi\phi)$	0.944	
$E_3^{(3)} V_2$	Total edge length of a typical cell	$E^{(3)}(B)$	$3/[4(3e)^{1/2}\phi]$	5.987	
$E_3^{(3)} V_1$	Area of a typical face	$E^{(3)}(A)$	$1/[2^{1/2}ne(4\phi + 1)]$	0.070	
$E_2^{(3)} V_2$	Total edge length of a typical face	$E^{(3)}(P)$	$(3e)^{1/2}/(4\phi + 1)$	0.894	
$E_2^{(3)} V_1$	Length of a typical edge	$E^{(3)}(L_{3,\infty})$	$1/[2(3e)^{1/2}]$	0.175	

$$\phi = 1/8 - [3/(4\pi)] \sin^{-1}(1/3).$$

Source: Miles (1972a, 1984).

Table 5.7.4 Chord length distributions for line segments $L_{1,2}$ for $\mathcal{V}_P(1, 2)$ and $L_{1,3}$ for $\mathcal{V}_P(1, 3)$.

r	$F_{L_{1,m}}(r)$		r	$F_{L_{1,m}}(r)$	
	$m = 2$	$m = 3$		$m = 2$	$m = 3$
0.00	0.000000	0.000000	1.65	0.969415	0.993309
0.05	0.021818	0.032205	1.70	0.975859	0.995651
0.10	0.044602	0.065057	1.75	0.981105	0.997247
0.15	0.068508	0.098591	1.80	0.985335	0.998305
0.20	0.093721	0.132843	1.85	0.988714	0.998985
0.25	0.120442	0.167850	1.90	0.991387	0.999410
0.30	0.148868	0.203651	1.95	0.993481	0.999667
0.35	0.179170	0.240286	2.00	0.995108	0.999818
0.40	0.211472	0.277787	2.05	0.996359	0.999903
0.45	0.245824	0.316178	2.10	0.997312	0.999950
0.50	0.282201	0.355461	2.15	0.998033	0.999975
0.55	0.320481	0.395611	2.20	0.998572	0.999988
0.60	0.360450	0.436560	2.25	0.998972	0.999995
0.65	0.401805	0.478188	2.30	0.999266	0.999998
0.70	0.444167	0.520312	2.35	0.999480	0.999999
0.75	0.487098	0.562677	2.40	0.999635	1.000000
0.80	0.530122	0.604958	2.45	0.999746	1.000000
0.85	0.572744	0.646764	2.50	0.999824	1.000000
0.90	0.614478	0.687650	2.55	0.999880	1.000000
0.95	0.654865	0.727139	2.60	0.999918	1.000000
1.00	0.693491	0.764751	2.65	0.999945	1.000000
1.05	0.730005	0.800029	2.70	0.999963	1.000000
1.10	0.764122	0.832570	2.75	0.999976	1.000000
1.15	0.795637	0.862056	2.80	0.999984	1.000000
1.20	0.824420	0.888273	2.85	0.999989	1.000000
1.25	0.850416	0.911122	2.90	0.999993	1.000000
1.30	0.873636	0.930625	2.95	0.999996	1.000000
1.35	0.894154	0.946912	3.00	0.999997	1.000000
1.40	0.912091	0.960209	3.05	0.999998	1.000000
1.45	0.927606	0.970813	3.10	0.999999	1.000000
1.50	0.940887	0.979067	3.15	0.999999	1.000000
1.55	0.952140	0.985333	3.20	1.000000	1.000000
1.60	0.961578	0.989969	3.25	1.000000	1.000000

Source: Muche and Stoyan (1990) and Muche (1999).

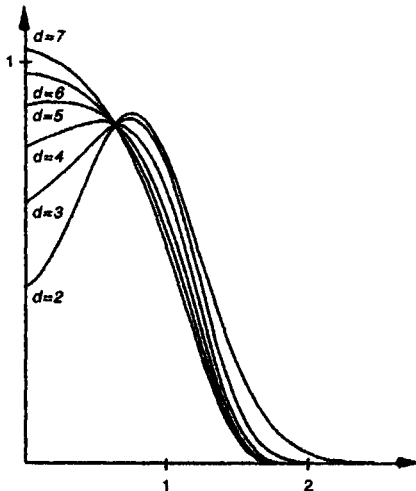


Figure 5.7.2 Probability density functions for the chord length $L_{1,m}$ in $\mathcal{V}_P(1, m)$ for $2 \leq m \leq 7$ ($\lambda = 1$). It should be noted that the six curves do not intersect at a common point. (Source: Muche and Stoyan, 1992, Figure 2.)

$$F_{L_{s,m}}(l) = 1 - \frac{m^2 \Gamma\left(\frac{ms-s+m}{2}\right) \pi^{(m-1)(s+1)/2}}{2\Gamma\left(\frac{ms+m-s+1}{2}\right) \Gamma\left(\frac{s(m-1)}{m}\right)} \left[\frac{\lambda}{\Gamma\left(\frac{m+2}{2}\right)} \right]^{(ms-s+m)/m} \\ \times \int_0^\infty \int_0^\pi r^{(m-1)(s+1)} \exp[-\lambda U_m(r, r_{l,\beta}, l)] \sin^{ms-s-1} \beta \\ \times \left(m \cos \beta \int_\beta^\pi \sin^m \varphi \, d\varphi + \sin^{m+1} \beta \right) d\beta \, dr, \quad l \geq 0, \quad (5.7.6)$$

where $r_{l,\beta}$ is given in equation (5.5.21) and $U_m(r, r_{l,\beta}, l)$ in equation (5.5.26), which denotes the volume of the union of two m -dimensional balls with radii r and $r_{l,\beta}$ and the distance between their centres is l . In particular, $F_{L_{s,m}}$ is the chord length distribution when $s = 1$ and the distribution of the length of a typical edge in \mathcal{V}_P given in equation (5.5.25) when $s = m$. Muche (1999) gave equivalent expressions of the pdf $f_{L_{s,m}}$ of $L_{s,m}$ for $1 \leq s \leq m \leq 3$:

$$f_{L_{s,2}}(l) = \frac{2s\lambda^{3/2}(\lambda\pi)^{(s+1)/2}}{\Gamma\left(\frac{s+3}{2}\right)} l^{s+3} \int_0^\pi \int_0^{\pi-\beta_1} \frac{\sin^{s+1} \beta_1 \sin^{s+1} \beta_2 [\sin \beta_1 + (\pi - \beta_1) \cos \beta_1]}{\sin^{s+4}(\beta_1 + \beta_2)} \\ \times [\sin \beta_2 + (\pi - \beta_2) \cos \beta_2] \exp\left(-\lambda l^2 \frac{\sin \beta_1 \sin \beta_2 \sin(\beta_1 + \beta_2)}{\sin^2(\beta_1 + \beta_2)}\right) \\ \times \exp\left(-\lambda l^2 \frac{(\pi - \beta_1) \sin^2 \beta_2 + (\pi - \beta_2) \sin^2 \beta_1}{\sin^2(\beta_1 + \beta_2)}\right) d\beta_2 \, d\beta_1, \quad l \geq 0, \quad (5.7.7)$$

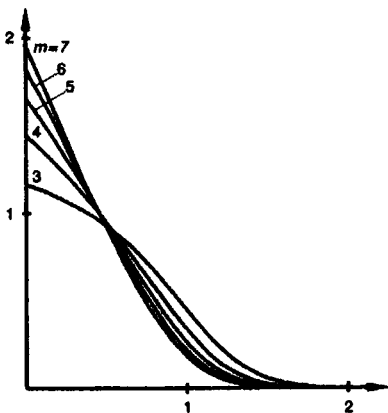


Figure 5.7.3 Probability density functions for the length $L_{2,m}$ of a typical edge in $V_p(2, m)$ for $3 \leq m \leq 7$ ($\lambda = 1$). (Source: Muche, 1996a, Figure 2.)

Table 5.7.5 Simulation studies of sectional Poisson Voronoi diagrams $V_p(2,3)$ and $V_p(1,3)$.

Study	Number of cells	Characteristics
Hahn and Lorz (1994)	400 000	m_n
Kumar and Kurtz (1993)	120 000	$N A_n m_n$
Lorz (1990b, 1991)	1 050 036	$A L_{2,3} N P \alpha_2 \alpha_1$
Lorz and Hahn (1993)	5 421 886	$A N P \alpha_2$
Mahin <i>et al.</i> (1980)	1 241	$A N L_{1,3}$
Marthinsen (1996)	25 000 – 100 000	$A L_{2,3} L_{1,3}$
van de Weygaert (1994)	–*	$A L_{2,3} N P \alpha_2 L_{1,3}$

* 20 planar sections of 1000 three-dimensional Poisson Voronoi cells.

Characteristics in $V_p(2,3)$:

A = area of a typical cell.

$L_{2,3}$ = edge length of a typical edge.

N = number of vertices (edges) of a typical cell.

P = perimeter of a typical cell.

α_2 = randomly selected interior angle of a typical sectional cell.

α_1 = angle of an edge at a typical vertex.

A_n = conditional area of a typical cell, given that it has n edges.

m_n = number of edges of a neighbouring cell of a typical cell, given that the typical cell has n edges.

Characteristics in $V_p(1,3)$:

$L_{1,3}$ = length of a line segment.

Table 5.7.6 Estimates, \hat{p}_n , of the probability that a typical polygon in a two-dimensional section of a Poisson Voronoi diagram in \mathbb{R}^3 has n edges (vertices).

n	\hat{p}_n	n	\hat{p}_n
3	0.0631	10	0.0178
4	0.1358	11	0.0051
5	0.2047	12	0.0012
6	0.2273	13	0.000263
7	0.1837	14	0.000042
8	0.1104	15	0.0000048
9	0.0506	16	0.00000095

Source: Lorz (1990b, 1991).

Table 5.7.7 Coefficients of variation (c.v.) and correlation coefficients for various characteristics of typical cells and edges in a two-dimensional section of a Poisson Voronoi diagram in \mathbb{R}^3 .

	N	A	P	$L_{2,3}$	α_2	α_1
c.v.	0.282*	0.695*	0.388*	0.691*	0.296†	—
N	—	0.753*	0.727*	-0.000*	0.566†	—
A	—	—	0.941*	0.221*	0.434†	—
P	—	—	—	0.264*	0.459†	—
$L_{2,3}$	—	—	—	—	—	-0.201‡

Characteristics:

A = area of a typical cell.

$L_{2,3}$ = edge length of a typical edge.

N = number of vertices (edges) of a typical cell.

P = perimeter of a typical cell.

α_2 = randomly selected interior angle of a typical sectional cell.

α_1 = angle of an edge at a typical vertex.

Sources: * Exact values from numerical integration by Brakke (1987b).

† Estimate from Monte Carlo simulations by Lorz and Hahn (1993).

‡ Estimate from Monte Carlo simulations by Lorz (1990b, 1991).

$$f_{L_{2,3}}(l) = \frac{27\Gamma\left(s + \frac{3}{2}\right)}{8\sqrt{\pi}\Gamma\left(\frac{2s}{3}\right)\Gamma(s+2)} \left(\frac{4\pi\lambda}{3}\right)^{2+2s/3} l^{2s+5} \int_0^\pi \int_0^{\pi-\beta_1} \frac{\sin^{2s+2}\beta_1 \sin^{2s+2}\beta_2}{\sin^{2s+6}(\beta_1 + \beta_2)} \\ \times (1 + \cos\beta_1)^2 (1 + \cos\beta_2)^2 \exp\left(-\frac{\lambda\pi l^3 [2 + (2 + \sin^2\beta_2) \cos\beta_2] \sin^3\beta_1}{3 \sin^3(\beta_1 + \beta_2)}\right) \\ \times \exp\left(-\frac{\lambda\pi l^3 [2 + (2 + \sin^2\beta_1) \cos\beta_1] \sin^3\beta_2}{3 \sin^3(\beta_1 + \beta_2)}\right) d\beta_2 d\beta_1, \quad l \geq 0. \quad (5.7.8)$$

The densities for $L_{2,m}$ for $3 \leq m \leq 7$ are illustrated in Figure 5.7.3.

As with \mathcal{V}_P , knowledge of such distributions is valuable in empirical work because existing evidence indicates that moment measures of many characteristics of individual cells of $\mathcal{V}_P(s, m)$ vary little from those cells in sectional tessellations where the set of generator points is not a realization of Θ_P (Lorz, 1990a). However, other distributions are all estimated from Monte Carlo simulations, and there have been far fewer reported simulation studies of $\mathcal{V}_P(s, m)$ than \mathcal{V}_P , all of which emphasize $\mathcal{V}_P(2, 3)$ (Mahin *et al.*, 1976, 1980; Lorz, 1990a,b, 1991; Lorz and Hahn, 1993; Kumar and Kurtz, 1993; Hahn and Lorz, 1994; van de Weygaert, 1994; Marthinsen, 1996). Of these the most extensive are Lorz (1990b, 1991) and Lorz and Hahn (1993) whose studies involved 1 050 036 and 5 421 886 cells, respectively. Table 5.7.5 summarizes these simulation studies. The distributions of characteristics in $\mathcal{V}_P(2, 3)$ are illustrated in Figure 5.7.4. The distribution of N for $\mathcal{V}_P(2, 3)$ is also reported in Table 5.7.6. Comparing Table 5.7.6 with Table 5.5.1 clearly reinforces the observation that $\mathcal{V}_P(2, 3)$ is not the same as \mathcal{V}_P in \mathbb{R}^2 . Table 5.7.7 gives the coefficients of variation and correlation of these characteristics obtained from numerical integration by Brakke (1987b) or from Monte Carlo simulations by Lorz and Hahn (1993) and Lorz (1990b, 1991). Conditional distributions of area, perimeter and interior angle, given the number of cell vertices (edges), have also been estimated by Lorz (1990b).

Kumar and Kurtz (1993) suggested the following empirical Aboav's law and Lewis' law in $\mathcal{V}_P(2, 3)$:

$$m_n = 5.09 + \frac{8.13}{n},$$

$$A_n = 0.2677n - 0.6064,$$

where m_n is the mean number of edges of a randomly selected neighbouring cell of a typical cell, under the condition that the typical cell has n edges, and A_n is the mean area of a typical cell, given that it has n edges.

Hahn and Lorz (1994) discussed how to use the statistics of a two-dimensional sectional diagram to estimate the parameters of the original three-dimensional tessellation and to test whether the original three-dimensional structure is a Poisson Voronoi diagram or not (see also Section 5.12).

5.8 ADDITIVELY WEIGHTED POISSON VORONOI DIAGRAMS: THE JOHNSON-MEHL MODEL

In Section 5.3 we discussed a variety of circumstances in which the Poisson Voronoi model could be used in a normative way in the examination of empirical tessellations. There are, however, other empirical tessellations for which it is not an appropriate model. One group of such tessellations consists of those in which the members of the generator set P are not

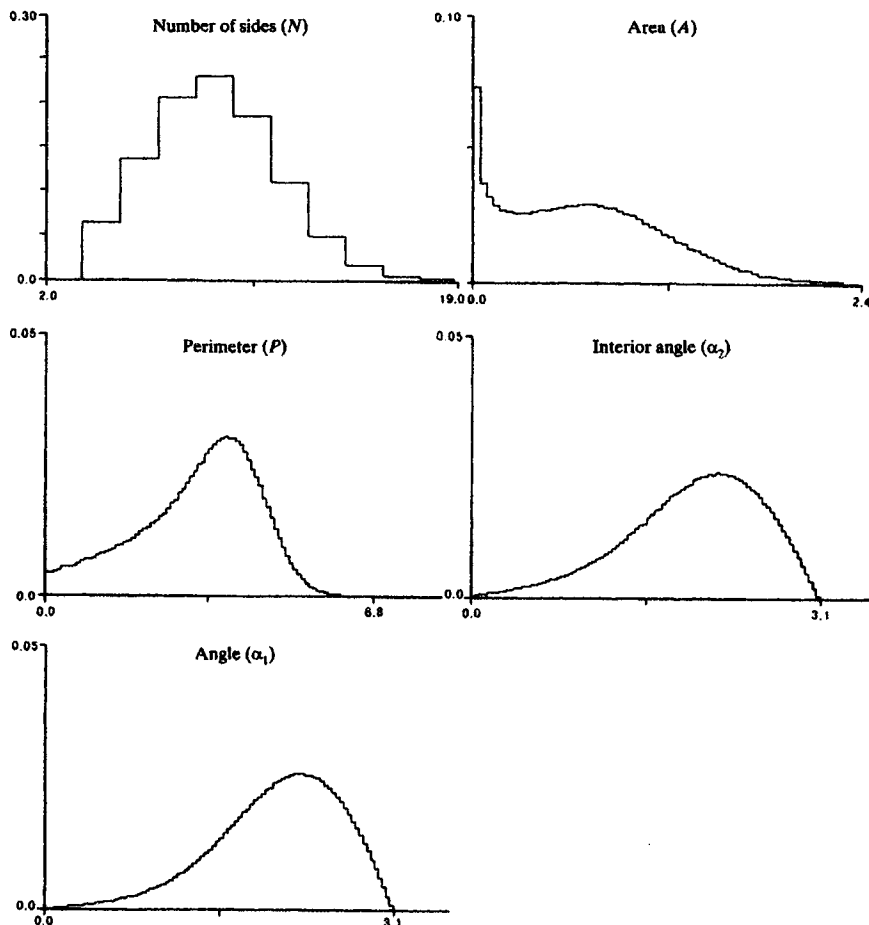


Figure 5.7.4 Normalized histograms of the number of vertices (edges) N , area A , perimeter P , interior angle α_2 of a typical sectional cell and the edge angle α_1 at a typical vertex for $\mathcal{V}_P(2, 3)$.

contemporaneous. In such instances we may assume that each generator p_i has both a location $x_i = (x_{i1}, x_{i2}, \dots, x_{im})$ in \mathbb{R}^m and an associated birth time, t_i (≥ 0). Once born, each point generates a cell which grows radially at a constant rate v . Interaction between growing cells is subject to the following conditions:

Condition JM1 If a point is born at a location which is already occupied by a growing cell, it disappears without trace.

Condition JM2 When radiating rays of two growing cells meet, both cease radiating so that the cell associated with a point is fully grown when growth ceases in all directions.

As we indicated in Section 3.1.2, this model can be considered equivalent to an (infinite) additively weighted Voronoi diagram in which the weight associated with p_i corresponds to t_i , since for the cell $C(p_i)$ that is generated by growth from p_i ,

$$C(p_i) = \left\{ \mathbf{x} \mid \left(t_i + \frac{\|\mathbf{x} - \mathbf{x}_i\|}{v} \right) \leq \left(t_j + \frac{\|\mathbf{x} - \mathbf{x}_j\|}{v} \right) \text{ for } p_j \in P, p_j \neq p_i \right\},$$

where $\|\mathbf{x} - \mathbf{x}_i\|$ and $\|\mathbf{x} - \mathbf{x}_j\|$ are the Euclidean distances from an arbitrary point p located at \mathbf{x} to p_i and p_j with location vectors \mathbf{x}_i and \mathbf{x}_j , respectively.

If we assume that both \mathbf{x}_i and t_i are generated by a Poisson point process, we have the *Johnson–Mehl* (J-M) (or *continuous nucleation*) model. This model was originally developed to study the growth of crystal aggregates (Kolmogorov, 1937; Johnson and Mehl, 1939; Avrami, 1939, 1940, 1941) and the surface film on metal (Evans, 1945). It has been independently rediscovered at least once since then (Glass, 1973, 1974; Armstrong, 1974; Jackson, 1974). The development of a tessellation over time in \mathbb{R}^2 according to the J-M model with a space–time homogeneous Poisson point process is illustrated in Figure 5.8.1. Such a tessellation is called a *Johnson–Mehl tessellation*. The rectangular window in Figure 5.8.1 was fully occupied by cells after 7 units of time. Suppose the intensity of the homogeneous Poisson point process is α per unit volume per unit time, i.e. the generators appear at a constant rate α . Chiu (1995c) showed that for each real number u , the time of complete tessellation T_L until the cube $[0, L]^m$ is fully occupied by cells of a J-M model (see Section 5.6.2) satisfies

$$\Pr \left\{ c^{m/(m+1)} (\alpha \omega_m v^m)^{1/(m+1)} T_L - c - \log \left[c^{1/(m+1)} \left(\frac{c + \log c}{m+1} \right)^{m-1} \right] \leq u \right\} \\ \rightarrow \exp \left(\psi_m \frac{(m+1)^{m-1}}{m^m} e^{-u} \right) \text{ as } L \rightarrow \infty,$$

where $c = \log(\alpha^m L^{m(m+1)} v^{-m} \omega_m^{-1})$, $\omega_m = \pi^{m/2}/\Gamma(m/2 + 1)$ is the volume of an m -dimensional sphere of unit radius and ψ_m is a constant given in equation (5.6.3). Furthermore,

$$\frac{\alpha \omega_m v^m T_L^{m+1}}{\log \alpha^m L^{m(m+1)}} \rightarrow 1 \text{ in probability as } L \rightarrow \infty.$$

Chiu also studied the time of complete tessellation for the following time-inhomogeneous Poisson point process. Suppose that the intensity measure of the Poisson point process on $\mathbb{R}^m \times [0, \infty)$ is $\ell \times \Lambda$, where ℓ is the Lebesgue measure in \mathbb{R}^m and Λ an arbitrary measure on $[0, \infty)$ such that $\Lambda([0, \infty)) > 0$ and

$$\lambda = \int_0^\infty \exp \left\{ -v^m \omega_m \int_0^\infty (t-s)^m \Lambda(ds) \right\} \Lambda(dt) < \infty.$$

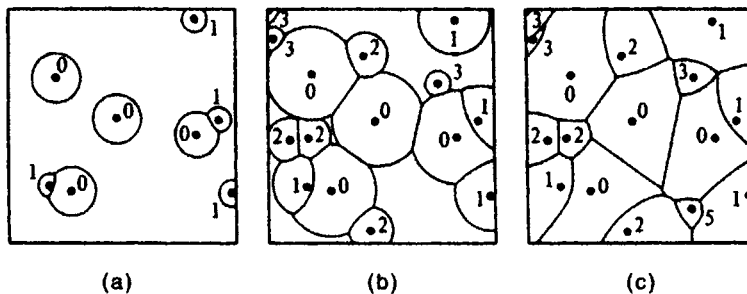


Figure 5.8.1 The Johnson–Mehl model for times (a) $t = 1$, (b) $t = 3$ and (c) $t = 7$.

The value λ is the intensity of cells formed according to the J–M model. Cowan *et al.* (1995) used $\Lambda(dt) = \alpha v e^{-\gamma t} dt$ to model the mechanism of the replication of a DNA molecule. This form of Λ can be interpreted as follows. The generators form a Poisson point process on \mathbb{R}^m . Each one starts to grow after an independent exponentially distributed random time, provided that its location has not yet been occupied by other cells.

Chiu and Quine (1997) showed that the total number of cell generators remaining within $[0, L]^m$ in a J–M model, after suitable normalization, follows the standard normal distribution, as $L \rightarrow \infty$ (see also Quine and Robinson, 1990; Holst *et al.*, 1996; Chiu, 1997). Quine and Robinson (1992) and Chiu *et al.* (1999) discussed the estimation of Λ and v in the case $m = 1$ while Molchanov and Chiu (2000) proposed estimation methods for an arbitrary m .

At time t , the union of all growing cells is indeed a Boolean model (see, for example, Stoyan *et al.*, 1995, Chapter 3) of m -dimensional spheres. Thus, the volume fraction of the region occupied by cells at time t is

$$X(t) = 1 - \exp \left\{ -\omega_m v^m \int_0^t (t-s)^{m-1} \Lambda(ds) \right\}.$$

For a large class of Λ , such as $\Lambda(dt) = \alpha t^{\beta-1} dt$, where $\alpha, \beta > 0$, $X(t)$ can be written as

$$X(t) = 1 - \exp \{-kt^n\}, \quad (5.8.1)$$

where, the parameters k and n are independent of t . Equation (5.8.1) is known as the *Kolmogorov–Johnson–Mehl–Avrami* (KJMA, JMAK, JMA, AJM, or Avrami) equation in the materials science literature. The parameter n is known as the *Avrami exponent* or *Avrami index*. The KJMA equation has been the standard tool to study crystallization kinetics (see, for example, Weinberg *et al.*, 1997).

A typical cell of the J–M tessellation in \mathbb{R}^m has been studied in detail by Evans (1945), Gilbert (1962) and Meijering (1953) for $m = 1, 2$ and 3 and by Møller (1992, 1999) for $m \geq 2$. The moments of several characteristics

have been derived. A typical cell of a J-M tessellation is non-convex, unless Λ is concentrated at a singleton, which gives the Poisson Voronoi diagram. The non-empty intersection of $m-k+1$ cells is called a k -face. A k -face is not necessarily connected, because of the non-convexity of cells. A connected component of an k -face is called a k -interface, which is a vertex, an edge and a cell face for $k = 0, 1$ and 2 , respectively. For each of the cases (i) $0 < k = l \leq m$, (ii) $1 \leq k = l + 1 \leq m$, (iii) $k = m$ and $l = 1$, and (iv) $1 \leq k \leq m$ and $l = 0$, the mean $(k-l)$ -contents, $\mu_{k,k-l}$, of $(k-l)$ -interfaces per unit volume in a k -dimensional hyperplane is given by

$$\begin{aligned}\mu_{k,k-l} = & v^{lm+n} c_{kn} \int_0^\infty \left\{ \int_0^t (t-s)^{m-1} \Lambda(ds) \right\}^{l+1} \\ & \times \exp \left\{ -v^n \omega_m \int_0^\infty (t-s)^m \Lambda(ds) \right\} dt,\end{aligned}$$

where $n = m - l$ and

$$c_{kn} = \frac{2^{l+1} \pi^{(l+1)m/2} \Gamma\left(\frac{ml+n+1}{2}\right) \Gamma\left(\frac{k+1}{2}\right)}{(l+1)! \Gamma\left(\frac{ml+n}{2}\right) \Gamma\left(\frac{m+1}{2}\right)^{l+1} \Gamma\left(\frac{k-l+1}{2}\right)}$$

(Møller, 1992, equation (4.2)). The cases (i), (ii) and (iv) concern vertices, edges and k -interfaces in the k -dimensional hyperplane, respectively, whilst case (iii) concerns cell faces in \mathbb{R}^m . Meijering (1953) and Miles (1972a) obtained the same results for some special cases. Møller (1992) also gave formulae for the intensity $I_p^{(k)}$ of p -interfaces in a k -dimensional hyperplane and the mean number of q -interfaces $N_{pq}^{(k)}$ contained in a typical p -interface in the hyperplane and the mean q -dimensional content $V_{pq}^{(k)}$ of the union of such q -interfaces ($0 \leq q \leq p \leq k \leq m$):

$$I_p^{(k)} N_{pq}^{(k)} = \binom{k-q+1}{p-q} I_q^{(k)}, \quad (5.8.2)$$

$$I_p^{(k)} V_{pq}^{(k)} = \binom{k-q+1}{p-q} \mu_{k,q}, \quad (5.8.3)$$

$$I_2^{(2)} = I_1^{(2)} - I_0^{(2)}, \quad (5.8.4)$$

and for $0 < k \leq m \leq 3$,

$$\sum_{i=0}^k (-1)^i I_i^{(k)} = 0. \quad (5.8.5)$$

Equations (5.8.2) and (5.8.3) yield

$$\begin{aligned}
I_m^{(m)} &= \lambda, & N_{m0}^{(m)} &= \frac{m+1}{\lambda} \mu_{m,0}, & V_{mp}^{(m)} &= \frac{m-p+1}{\lambda} \mu_{m,p}, \\
I_0^{(k)} &= \mu_{k,0}, & I_1^{(1)} = I_1^{(1)} &= \mu_{1,0}, & N_{10}^{(1)} &= 2, \\
V_{11}^{(1)} &= \frac{1}{\mu_{1,0}}.
\end{aligned} \tag{5.8.6}$$

Since the edges in the hyperplane do not necessarily contain vertices, equations (5.8.2)–(5.8.4) and (5.8.6) lead to a series of inequalities:

$$\begin{aligned}
I_1^{(k)} &\geq \frac{k+1}{2} \mu_{k,0}, & N_{21}^{(k)} &\geq N_{20}^{(k)}, & N_{10}^{(k)} &\leq 2, \\
V_{11}^{(k)} &\leq \frac{2}{k+1} \frac{\mu_{k,1}}{\mu_{k,0}}, & I_2^{(2)} &\geq \frac{\mu_{2,0}}{2}, & N_{21}^{(2)} &\leq 6, \\
V_{21}^{(2)} &\leq \frac{4\mu_{2,1}}{\mu_{2,0}}, & V_{22}^{(2)} &\leq \frac{2}{\mu_{2,0}}.
\end{aligned} \tag{5.8.7}$$

Furthermore, for $m = 3$,

$$N_{32}^{(3)} \geq 2 + \frac{2\mu_{3,0}}{\lambda}, \quad N_{31}^{(3)} \geq \frac{6\mu_{3,0}}{\lambda}. \tag{5.8.8}$$

In particular, for $m = 2$, we have

$$\begin{aligned}
I_2^{(2)} &= \lambda, & I_1^{(2)} &= 3\lambda, & I_0^{(2)} &= 2\lambda, \\
I_1^{(1)} = I_0^{(1)} &= \mu_{1,0}, & N_{21}^{(2)} = N_{20}^{(2)} &= 6, & N_{10}^{(2)} = N_{10}^{(1)} &= 2, \\
V_{22}^{(2)} &= \lambda^{-1}, & V_{21}^{(2)} &= \frac{2\mu_{2,1}}{\lambda}, & V_{11}^{(2)} &= \frac{\mu_{2,1}}{3\lambda}, \\
V_{11}^{(1)} &= \frac{1}{\mu_{1,0}},
\end{aligned} \tag{5.8.9}$$

whilst for $m = 3$, we get

$$\begin{aligned}
I_3^{(3)} &= \lambda, & I_2^{(3)} &\geq \lambda + \mu_{3,0}, & I_1^{(3)} &\geq 2\mu_{3,0}, \\
I_0^{(3)} &= \mu_{3,0}, & I_2^{(2)} &\geq \frac{\mu_{2,0}}{2}, & I_1^{(2)} &\geq \frac{3\mu_{2,0}}{2}, \\
I_0^{(2)} &= \mu_{2,0}, & I_1^{(1)} = I_0^{(1)} &= \mu_{1,0}, & N_{30}^{(3)} &= \frac{4\mu_{3,0}}{\lambda}, \\
N_{21}^{(3)} &\geq N_{20}^{(3)}, & N_{20}^{(3)} &\leq \frac{6\mu_{3,0}}{\lambda + \mu_{3,0}}, & N_{10}^{(3)} &\leq 2,
\end{aligned}$$

$$\begin{aligned}
N_{20}^{(2)} \leq N_{21}^{(2)} \leq 6, & \quad N_{10}^{(2)} \leq 2, & \quad N_{10}^{(1)} = 2, \\
V_{33}^{(3)} = \lambda^{-1}, & \quad V_{32}^{(3)} = \frac{2\mu_{3,2}}{\lambda}, & \quad V_{31}^{(3)} = \frac{3\mu_{3,1}}{\lambda}, \\
V_{22}^{(3)} \leq \frac{\mu_{3,2}}{\lambda + \mu_{3,0}}, & \quad V_{21}^{(3)} \leq \frac{3\mu_{3,1}}{\lambda + \mu_{3,0}}, & \quad V_{11}^{(3)} \leq \frac{\mu_{3,1}}{2\mu_{3,0}}, \\
V_{22}^{(2)} \leq \frac{2}{\mu_{2,0}}, & \quad V_{21}^{(2)} \leq \frac{4\mu_{2,1}}{\mu_{2,0}}, & \quad V_{11}^{(2)} \leq \frac{2\mu_{2,1}}{3\mu_{2,0}}, \\
V_{11}^{(1)} = \mu_{1,0}^{-1},
\end{aligned} \tag{5.8.10}$$

with equality in any one of the inequalities if and only if Λ is concentrated at a singleton, which leads to the Poisson Voronoi diagram (see also Møller, 1999). The mean number of full neighbours of a typical cell is

$$\begin{aligned}
E(C) = & \frac{4\pi^{m/2} v^m}{\lambda \Gamma\left(\frac{m}{2}\right)} \int_0^\infty \int_0^t \int_0^t (2t - t_1 - t_2)^{m-1} \\
& \times \exp\left\{-v^m \omega_m \int_0^\infty (t-s)^m \Lambda(ds)\right\} \Lambda(dt_1) \Lambda(dt_2) dt
\end{aligned}$$

(Møller, 1992, Theorem 4.5). In particular, if $m = 2$, then $E(C) = 4$. The mean k -dimensional content $V^{(k)}$ of a typical k -dimensional face in a k -dimensional hyperplane is bounded above by

$$\begin{aligned}
V^{(k)} < & \left\{ \frac{2\pi^{(m-k)/2} v^{m-k}}{\Gamma\left(\frac{m-k}{2}\right)} \int_0^\infty \int_0^t (t-u)^{m-k-1} \right. \\
& \left. \times \exp\left\{-v^m \omega_m \int_0^\infty (t-s)^m \Lambda(ds)\right\} \Lambda(du) dt \right\}^{-1}.
\end{aligned}$$

This is a generalization of the results obtained by Miles (1972a) for a J-M tessellation in \mathbb{R}^3 .

Second-order moments are much more complicated. Gilbert (1962) obtained the variance of the volume of a typical cell of a J-M tessellation in \mathbb{R}^3 generated by a homogeneous Poisson point process, i.e. $\Lambda(dt) = \alpha dt$, by numerical integration. Second-order moments of other characteristics can also be derived, but the results are too complicated to evaluate. Møller (1992) showed that the coefficients of variation, $CV(\mathcal{C}_k)$ and $CV(\mathcal{F}_k)$, of the k -dimensional content of a typical k -interface and k -face, respectively, satisfy

$$CV(\mathcal{C}_k) = \sqrt{\frac{C_k}{V_{kk}^{(k)}} - 1},$$

$$CV(\mathcal{F}_k) = \sqrt{\frac{C_k}{V^{(k)} - 1}},$$

where

$$C_k = \frac{4\pi^{(m+k-1)/2} v^{m+k}}{\Gamma\left(\frac{m-1}{2}\right) \Gamma\left(\frac{k}{2}\right)} \iiint_{\Omega_1} s^{m+k-1} J(r_1, R_1) \\ \times \exp \left[\frac{2\pi^{(m-1)/2} v^m s^m}{\Gamma\left(\frac{m-1}{2}\right)} \iiint_{\Omega_2} J(r_2, R_2) dr_2 dR_2 \Lambda(dt_2) \right] \\ \times ds dr_1 dR_1 \Lambda(dt_1),$$

with

$$J(r, R) = rR \left(\frac{r^2 + R^2 + r^2 R^2}{2} - \frac{1 + r^4 + R^4}{4} \right)^{(m-3)/2}.$$

The integrations are over Ω_1 , which is the range of all $s, r_1, R_1, t_1 \geq 0$ such that $r_1 + R_1 > 1$ and $|r_1 - R_1| < 1$, and Ω_2 , which is the range of all $r_2, R_2, t_2 \geq 0$ such that $r_2 + R_2 > 1$, $|r_2 - R_2| < 1$ and either $sR_2 + t_2 < sR_1 + t_1$ or $sr_2 + t_2 < sr_1 + t_1$ or both.

These moments for the time-homogeneous case $\Lambda(dt) = \alpha dt$ are summarized in Table 5.8.1. In order to facilitate a comparison with similar moments reported in Tables 5.5.1 and 5.5.3 for the Poisson Voronoi diagram, the numerical values in Table 5.8.1 are given in terms of the density of generator points per unit space after all cell growth has ceased rather than in terms of the birth rate α and the growth rate v . Note that inequalities arise in Table 5.8.1 because it is possible that the common edge (in \mathbb{R}^2) or the common face (in \mathbb{R}^3) between two cells may be interrupted by one or more smaller cells. Frost and Thompson (1987a) and Heinrich and Schüle (1995) have estimated the distributions of area, edge length and number of edges (vertices) of a typical cell in the time-homogeneous case using information from 10 000 and 20 000 cells, respectively, from a computer simulation.

Horálek (1988, 1989) and Møller (1992) studied the case

$$\Lambda(dt) = \alpha t^{\beta-1} dt, \text{ where } \alpha, \beta > 0, \quad (5.8.11)$$

in detail. Note that $\beta = 1$ gives the time-homogeneous J-M model while as $\beta \rightarrow 0$ the tessellation approaches \mathcal{V}_p . Møller (1995) estimated the distributions of area, perimeter, numbers of vertices, 0-faces with two vertices contained in a typical cell and full neighbours and minimal and maximal angles of a typical vertex in \mathbb{R}^2 and volume and numbers of cell face, vertices and closed edges in \mathbb{R}^3 for the case of equation (5.8.11) from simulations of 10 000 cells.

Frost and Thompson (1987a) used a simulation approach to study the J-M model in \mathbb{R}^2 with

$$\Lambda(dt) = \alpha e^{-\beta t} dt, \text{ where } \alpha, \beta > 0.$$

Table 5.8.1 The first and/or second-order moments of various characteristics of a space-time homogeneous Johnson–Mehl model.

Moment	Symbol	Exact value	Numerical value	Estimate [†]
<i>Two-dimensions</i>				
Intensity of cell centroids	λ	$(3/\pi)^{1/3}\Gamma(4/3)(\alpha/\nu)^{2/3}$	$0.879(\alpha/\nu)^{2/3}$	
Expected number of vertices/edges of a typical cell and its second moment	$E(N)$ $E(N^2)$	6 —	6 —	41.916
Expected number of full neighbours of a typical cell and its second moment	$E(C)$ $E(C^2)$	4 —	4 —	18.731
Expected area of a typical cell and its second moment	$E(A)$ $E(A^2)$	$[(\pi/3)^{1/3}\Gamma(4/3)](\nu/\alpha)^{2/3}$ —	λ^{-1} —	$1.703\lambda^{-2}$
Expected perimeter of a typical cell and its second moment	$E(P)$ $E(P^2)$	$[4(3/\pi)^{1/3}\Gamma(5/3)/\Gamma(4/3)](\nu/\alpha)^{1/3}$ —	$3.734\lambda^{-1/2}$ —	$17.460\lambda^{-1}$
Expected length of an edge of a typical cell	$E(L)$	$< [2(3/\pi)^{1/3}\Gamma(5/3)/\Gamma(4/3)](\nu/\alpha)^{1/3}$	$< 0.623\lambda^{-1/2}$	
<i>Three-dimensions</i>				
Intensity of cell centroids	λ	$[4\Gamma(5/2)/\pi^{5/2}]^{1/4}\Gamma(5/4)(\alpha/\nu)^{3/4}$	$0.896(\alpha/\nu)^{3/4}$	
Expected number of vertices of a typical cell and its second moment	$E(M)$ $E(M^2)$	$16\pi^{2/7}$ —	22.559 —	740.213
Expected number of edges of a typical cell	$E(E)$	$> 24\pi^{2/7}$	> 33.839	
Expected number of faces of a typical cell and its second moment	$E(F)$ $E(F^2)$	$> 8\pi^{2/7} + 2$ —	> 13.280 —	13.002 226.305
Expected number of full neighbours of a typical cell	$E(C)$	7	7	

Table 5.8.1 continued

Moment	Symbol	Exact value	Numerical value	Estimate [†]
Expected area of a volume cell and its second moment	E(V) E(V ²)	$[(\pi/3)^{1/4}\Gamma(5/4)](\nu/\alpha)^{3/4}$ —	λ^{-1} $2.236\lambda^{-2}$	
Expected surface area of a typical cell	E(S)	$[16\pi^{1/2}\Gamma(7/4)/[3^{3/2}\Gamma(5/4)]](\nu/\alpha)^{1/2}$	$5.143\lambda^{-2/3}$	
Expected total edge length of a typical cell	E(P)	$[3^{1/4}4\pi^{9/4}/[5\Gamma(5/4)]](\nu/\alpha)^{1/4}$	$14.71\lambda^{-1/3}$	
Correlation between the number of vertices and faces	corr(M, F)	—	—	0.9986
<i>Sections</i>				
Expected area of typical cell	E ⁽²⁾ (A)	$\{3^{1/2}5\Gamma(1/4)^{2/3}/[2^{4/3}\pi^2(5/4)^{2/3}]\}(\nu/\alpha)^{1/2}$	$0.816\lambda^{2/3}$	
Expected length of a typical line segment	E ⁽¹⁾ (L _{1,3})	$\{3^{1/4}\Gamma(1/4)^{1/3}/[2^{2/3}\pi^{1/4}\Gamma(3/4)\Gamma(5/4)^{1/3}]\}(\nu/\alpha)^{1/4}$	$0.778\lambda^{-1/3}$	

[†] Estimates from Monte Carlo simulation by Möller (1995).

α = birth rate.

ν = radial growth rate.

Sources: Evans (1945), Meijering (1953), Gilbert (1962) and Möller (1992, 1995).

In this case as $\beta \rightarrow 0$ we obtain the time-homogeneous J-M model, while $\beta \rightarrow \infty$ produces \mathcal{V}_p . Frost and Thompson (1987a) derived estimates of the distributions of the area, edge length and number of sides of a typical cell. They and Heinrich and Schüle (1995) also estimated the same distributions for situations in which the nucleation rate remains constant (i.e. time-homogeneous) but in which new generators are prohibited from being born at a distance δ from any edge of an existing cell (note that the Voronoi hard core models discussed in Section 5.12 may be considered as a limiting case of this modified J-M model). Heinrich and Schüle (1995) also estimated the distribution in the case when the generators form a cluster point process.

Another way to modify the J-M model to conform with certain empirical situations is to alter the growth rate v to vary over time. However, if v varies over time, we may have rather strange situations such as disconnected cells. Even worse, the resultant structure may not be a tessellation of \mathbb{R}^m at all. Chiu (1995c) showed such a pathological example in which the uncovered regions form a random fractal. Frost and Thompson (1987b) consider time-homogeneous situations in which the radial growth of a cell C_i at time t_i , $v_i(t)$, is proportional to a power of its radius $r_i(t)$ at that time. Thus,

$$v_i(t) \propto r_i(t)^\beta$$

which is equivalent to considering $r_i(t)$ as a function of the time elapsed $(t - t_i) = \Delta t$ since the birth of the cell's generator. In particular, they examine the distributions of the area and number of sides (vertices) of a typical cell in models with values of $\beta = -3, -2, -1, 0, 1$ (equivalent to Δt^ρ) ($\rho = 1/4, 1/3, 1/2, 1$) and $\exp(\Delta t)$, respectively. When $\beta = 0$ we have the basic J-M model while $\beta = -1$ yields a Voronoi power diagram (see Section 3.1.4) and $\beta = 1$ produces a multiplicatively weighted Voronoi diagram (see Section 3.1.1).

Because the J-M model has been of particular interest in materials science applications, there has been interest in the nature of one- and two-dimensional sections of the model in \mathbb{R}^3 . Horálek (1989, 1990) derived mean values for the length of the intercept through a typical cell and the area of a section of a typical cell for both the time-homogeneous J-M model and the J-M model with equation (5.8.11) (see Table 5.8.1 for these values for the time-homogeneous J-M model). Note that an exact value cannot be obtained for the area of a section of a typical cell because the star-shaped nature of the cells means that in two-dimensional sections it is possible to have subareas which are entirely surrounded by the planar section of an adjoining cell. Mahin *et al.* (1976, 1980) have used computer simulation to estimate the distribution of the cross-sectional area, intercept length and number of sides (vertices) of cells in sectional tessellations, while Saetre *et al.* (1986) have examined the distribution of the areas of cells in sections of J-M models with declining birth rates (a χ^2 distribution for t_i) and increasing birth rates (a Weibull distribution for t_i) and with growth rates declining over time.

Applications of the family of J-M models have been confined mainly to

the natural sciences and examples can be found in most of the references cited in this section. There are a huge number of studies of the application of the KJMA equation (5.8.1) and its generalizations or modifications on crystallization kinetics (see, for example, Christian, 1965; Crespo *et al.*, 1997; Weinberg *et al.*, 1997) and precipitation and the dissolution process (see, for example, Oguocha and Yannacopoulos, 1997). Hirsch *et al.* (1994) used the KJMA equation to study the kinetics of the mortality of fruit flies. The family of J-M models is also the basic framework of the geometric-probabilistic approach to heterogeneous chemical kinetics (Korobov, 1994, 1996). Additional astrophysical applications are presented by Zaninetti (1989, 1990, 1991b) who has used them in the study of supernovae explosions. Other applications include porphyroblasts (Carlson, 1991), microstructural evolution in thin films (Frost *et al.*, 1990), dynamic fragmentation (Grady and Kipp, 1985), plant ecology (Kenkel, 1990), recrystallization in cold rolled material (Marthinsen *et al.*, 1989; Furu *et al.*, 1990), and grain growth in metals (Srolovitz *et al.*, 1986). In the social sciences Boots (1973, 1975a) has used the models to explore the development of service areas associated with the provision of public, intercity bus services in England and Wales. These examples are applications of the J-M model in \mathbb{R}^2 and \mathbb{R}^3 . There are quite a number of biological applications of the J-M model in \mathbb{R} . Examples include unravelling the strands of a DNA molecule (Vanderbei and Shepp, 1988; Cowan *et al.*, 1995), release of neurotransmitter at neuromuscular synapses (Bennett and Robinson, 1990; Quine and Robinson, 1990, 1992), differentiation of cells into heterocysts in algae (Wolk, 1975) and lung carcinoma (Kayser and Stute, 1989).

5.9 HIGHER ORDER POISSON VORONOI DIAGRAMS

In Section 3.2 we generalized the basic concept of the ordinary Voronoi diagram by considering diagrams in which an individual cell is created with respect to a subset, $P_i^{(k)}$ of k points ($1 \leq k \leq n$) of the n points of P rather than an individual point of P . In the case of the order- k Voronoi diagram $\mathcal{V}^{(k)}$, an individual cell consists of all locations in \mathbb{R}^m for which the members of $P_i^{(k)}$ are the set of k nearest points while in the ordered order- k Voronoi diagram $\mathcal{V}^{(k)}$, we add the additional constraint that the k points are ordered so that all locations in a cell share the same first, second, ..., k th nearest points of P . When $\mathcal{V}^{(k)}$ and $\mathcal{V}^{(k)}$ are defined with respect to Θ_P we label them $\mathcal{V}_P^{(k)}$ and $\mathcal{V}_P^{(k)}$, respectively. Like \mathcal{V}_P , $\mathcal{V}_P^{(k)}$ is a normal tessellation while $\mathcal{V}_P^{(k)}$ is not. Figure 5.9.1 shows $\mathcal{V}_P^{(k)}$ in \mathbb{R}^2 for several different values of k .

Although Miles (1984, p. 311) has been able to derive an expression for the expectation $E_m V_s$ of the total s -dimensional content of the s -faces of an arbitrary cell of $\mathcal{V}_P^{(k)}$ in \mathbb{R}^m , which is analogous to expression (5.5.2) for \mathcal{V}_P , it has only proved possible to evaluate it for $m = 1, 2$. Thus, the known properties of $\mathcal{V}_P^{(k)}$ are limited to some first-order moments for $m = 2$. The same holds for $\mathcal{V}_P^{(k)}$. These values are given in Table 5.9.1.

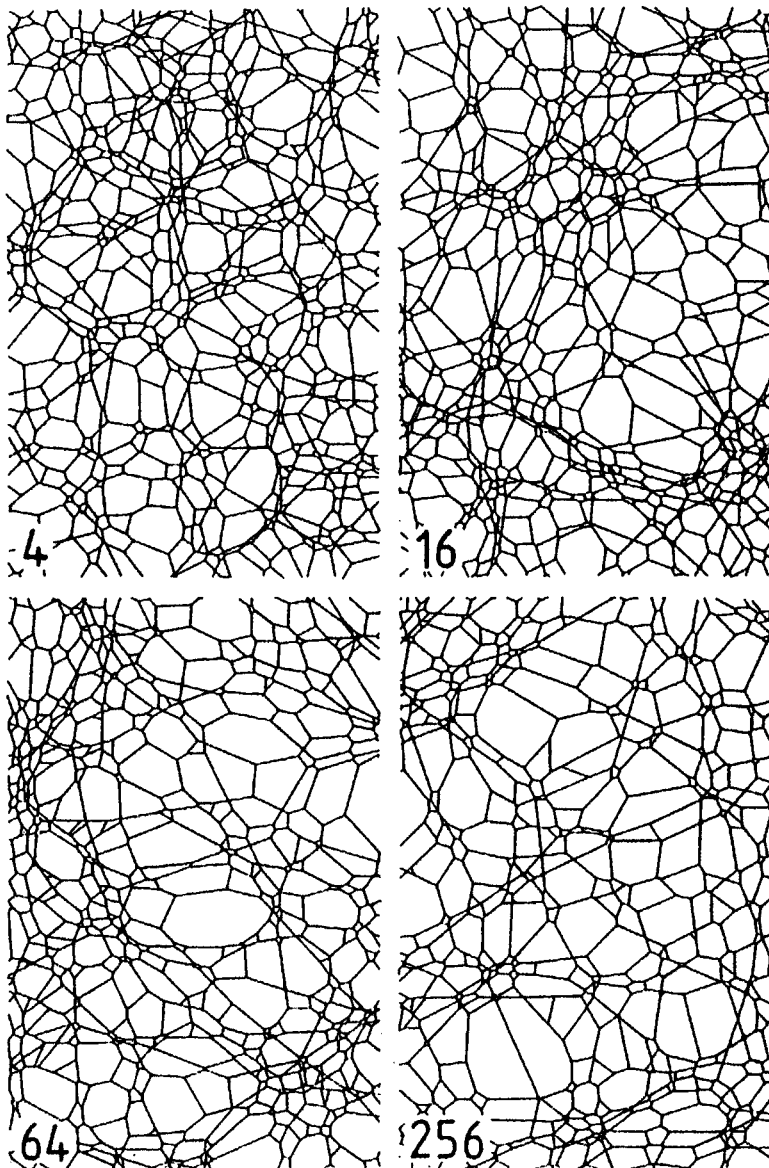


Figure 5.9.1 Portions of an order- k Poisson Voronoi diagram $\mathcal{V}_p^{(k)}$ for $k = 4, 16, 64, 256$. (Source: Miles and Maillardet, 1982, Figure 5.)

Table 5.9.1 The first and/or second-order moments of various characteristics of a typical cell of order- k and ordered order- k Poisson Voronoi diagrams in \mathbb{R}^2 .

Moment	Symbol	Exact value	Limit ($k \rightarrow \infty$)
<i>Order-k</i>			
Expected number of vertices (edges)	$E(N)$	6	
$E_2 N_0(E_2 N_1)$	$E(C)$	4	
Expected number of full neighbours	$E(A)$	λ^{-1}	
Expected area $E_2 V_2$	$E(P)$	$(2k)![k(k-1)!(2k-2)^{2k-3}\lambda^{1/2}]$	$4/(\pi k \lambda)^{1/2}$
<i>Ordered order-k</i>			
Expected number of vertices (edges)	$E(N)$	$[54\pi^2 k + 256(k-1)(k-2)]$ $\times [9\pi^2(2k-1) + 64(k-1)(k-2)]^{-1}$	4
$E_2 N_0(E_2 N_1)$	$E(N^2)$	$1/[k[2k-1+64(k-1)(k-2)/(9\pi^2)]\lambda]$	$(\pi^2 + 24)/2$
and its second moment $E_2[N_0^2](E_2[N_1^2])$	$E(A)$	$9\pi^2/(64k^3\lambda)$	
Expected area $E_2 V_2$	$E(A^2)$	$81\pi^6/(2^{13}k^6\lambda^2)$	
and its second moment $E_2[V_2^2]$	$E(P)$	$2\sum_{i=1}^k \{(2i)!/[i(i-1)!2^{2i-7}]\}$ $\times [k[2k-1+64(k-1)(k-2)/(9\pi^2)]\lambda^{1/2}]^{-1}$	$(3/4)[\pi^3/(\kappa^3)]^{1/2}$
Expected perimeter $E_2 V_1$	$E(P^2)$	$9\pi^3(\pi^2 + 4)/(128k^3\lambda)$	
and its second moment $E_2[V_1^2]$		=	intensity of Θ_p

Source: Miles (1964a, p. 904; 1970a, p. 114).

λ

Note that for both diagrams $E(N)$ is a consequence of the general result given in equation (5.5.6). Similarly, $E(A)$ for $\mathcal{V}_p^{(k)}$ holds for any underlying point process which is homogeneous and ergodic (Miles, 1986b, p. 569). This value is also a specific instance of the more general relationship (Miles, 1984, 1986a)

$$E_m V_m^{(2)} = \frac{2E_m V_m^{(1)}}{E_m N_{m-1}^{(1)}}, \quad (5.9.2)$$

where (k) refers to the order of $\mathcal{V}_p^{(k)}$, and $\mathcal{V}_p^{(1)} = \mathcal{V}_p$, which holds because of the one-to-one correspondence between the cells of $\mathcal{V}_p^{(2)}$ and the $(m-1)$ -faces of \mathcal{V}_p .

The values of $E(A)$ for $\mathcal{V}_p^{(k)}$ and $\mathcal{V}_p^{<k>}$ can be combined to define the expectation of the multiplicity w of a cell of $\mathcal{V}_p^{(k)}$ as the number of cells of $\mathcal{V}_p^{<k>}$ it comprises so that

$$E(w) = k \left(1 + \frac{64(k-1)(k-2)}{9\pi^2(2k-1)} \right), \quad (5.9.2)$$

which is asymptotically equal to $32k^2/(9\pi^2)$ as $k \rightarrow \infty$ (Miles, 1970a, p. 119; Santaló, 1976, p. 20).

For $\mathcal{V}_p^{<k>}$ in \mathbb{R}^2 , as $k \rightarrow \infty$, the proportion of cells with four vertices tends to unity (Miles, 1970a, p. 118) and $\mathcal{V}_p^{<k>}$ tends to become equivalent to the tessellation \mathcal{L} formed by an isotropic Poisson line process (see Section 1.3.3) of intensity $\tau = (8/3)(\lambda k^3/\pi)^{1/2}$. Such a process involves defining lines in terms of their polar coordinates (r, θ) representing the perpendicular distance and direction from the origin, respectively, where the range of (r, θ) is taken as $\Pi = \{(r, \theta); -\infty < r < \infty, 0 \leq \theta < \pi\}$. Then for $\tau > 0$, the Poisson point process of intensity τ/π in Π induces the Poisson line process of intensity τ in \mathbb{R}^2 (see Section 1.3.3). Thus, any values for the characteristics of an arbitrary cell of \mathcal{L} carry over asymptotically for $\mathcal{V}_p^{<k>}$. Knowledge of such characteristics is quite extensive with all the first- and second-order moments, together with some higher order moments and the correlation coefficients being known for N , A and P (Miles, 1964a,b, 1973). Crain and Miles (1976) have also estimated the distributions of N , A and P using Monte Carlo methods. The values of the moment measures are given in Table 5.9.1.

Very little is known about the distributions of the various cell characteristics although Miles and Maillardet (1982, p. 108) have derived an integral expression for the probability distribution of N for an arbitrary cell in terms of its size and shape. There are no triangles in $\mathcal{V}_p^{(k)}$ and, as Miles and Maillardet (1982, p. 109) demonstrated empirically for a cell with $N = 4$ and Miles (1995) proved heuristically for a very large cell, as $k \rightarrow \infty$, the vertices tend to circularity, with the sums of their opposite interior angles tending to π . This tendency can be observed in Figure 5.9.1. They also show that, for any given shape, the conditional ergodic distributions of A and P of the cells of $\mathcal{V}_p^{(2)}$ are both mixtures of gamma distributions of the type given in expression (5.5.33).

Table 5.10.1 The first moment of various characteristics of a typical cell in a Poisson Voronoi diagrams on the surface of a sphere.

Characteristic	Symbol	Exact value
Number of vertices (edges)	$E(N)$	$6(1-2/n)$
Area	$E(A)$	$4\pi/n$
Perimeter	$E(P)$	$\pi(n-1)! \sum_{i=0}^{n/2-1} [2^{n+2i-3} \times i!(i+1)!(n-2i-2)!]^{-1}$

n = number of points in the generator set.

Source: Miles (1971).

Finally, there has been some consideration of the tessellation $\mathcal{V}_p^{(k)}(s, m)$, created by an s -dimensional section of $\mathcal{V}_p^{(k)}$ in \mathbb{R}^m . Miles (1984, p. 326) has been able to derive an integral expression for the moments of the volume of an arbitrary cell but this has proved resistant to evaluation.

5.10 POISSON VORONOI DIAGRAMS ON THE SURFACE OF A SPHERE

One of the instances of Voronoi diagrams involving spaces which are not the Euclidean space, which was examined in Section 3.7, was that in which the members of the generator set were located on the surface of a sphere S with unit radius, centred at the origin. In this case the distance between two points is defined in terms of the length of the lesser arc on the great circle passing through the two points (see equation (3.7.17), Section 3.7.6). If the generator set consists of n points selected at random on S , the resulting Voronoi diagram is a random Voronoi diagram which we label \mathcal{V}_s . Knowledge of \mathcal{V}_s is limited to the first-order moments derived by Miles (1971) which are given in Table 5.10.1. Note that as $n \rightarrow \infty$, $E(N)$ tends to 6, which corresponds to $E(N) = 6$ for \mathcal{V}_p in \mathbb{R}^2 .

5.11 PROPERTIES OF POISSON DELAUNAY CELLS

As demonstrated in Section 2.2 the Poisson Delaunay tessellation \mathcal{D}_p can be considered the dual tessellation of \mathcal{V}_p in \mathbb{R}^m . Each Poisson Delaunay cell (PDC) of \mathcal{D}_p is an $(m+1)$ -dimensional simplex whose vertices p_0, \dots, p_m are points of Θ_p . For $m = 2$ and $m = 3$ the PDCs are triangles and tetrahedra, respectively. Any s -face of \mathcal{D}_p is an $(s+1)$ -dimensional simplex with vertices p_0, \dots, p_s , also points of Θ_p . Alternatively, an s -face can be considered as the convex hull of p_0, \dots, p_s . There are $\binom{m+1}{s+1}$ s -faces contained in a PDC. Because of the duality between \mathcal{V} and \mathcal{D} , there is a simple relationship between the intensities of their s -faces (Møller, 1989, equation (7.31)).

If $\lambda_s(\mathcal{D})$ and $\lambda_s(\mathcal{V})$ are the intensities of the s -faces of \mathcal{D} and \mathcal{V} , respectively, then

$$\lambda_s(\mathcal{D}) = \lambda_{m-s}(\mathcal{V}), \quad s = 0, \dots, m. \quad (5.11.1)$$

The major result relating to PDCs was derived by Miles (1970b, 1974) (see also Møller, 1989, Section 7; 1994, Section 4.3). Let c and r be the circum-centre and circumradius, respectively, of an $(m+1)$ -dimensional PDC in \mathbb{R}^m . Then the $(m+1)$ vertices of the cell are the points $\{c + r u_i\}$ where $\{u_i\}$ are the unit vectors ($i = 0, \dots, m$). The ergodic probability distribution of \mathcal{D}_P is completely specified by the joint probability density function (pdf)

$$f(r, u_0, \dots, u_m) = a(\lambda, m) \Delta_m r^{m^2-1} \exp(-\lambda \omega_m r^m), \quad (5.11.2)$$

where Δ_m is the volume of the $(m+1)$ -simplex with vertices u_0, \dots, u_m , $\omega_m = \pi^{m/2}/\Gamma(m/2 + 1)$ and

$$a(\lambda, m) = \frac{\pi^{(m^2+1)/2} \Gamma(m^2/2) \{2\lambda \Gamma[(m+1)/2]\}^m}{m^{m-2} \Gamma(m/2)^{2m+1} \Gamma[(m^2+1)/2]}. \quad (5.11.3)$$

The marginal pdf of r is given in equation (5.5.22) in Section 5.5. Furthermore, r , which may be considered a measure of the size of the $(m+1)$ -simplex, is independent of $\{u_0, \dots, u_m\}$ which represents the shape of the simplex. It was this independence that was exploited by Kendall (1989) in deriving a method of simulating individual $(m+1)$ -dimensional simplices (see Section 5.4). The pdf of r is a generalized gamma function (equation (5.5.32)) with $r = m$, $q = m^2$ and $b = \lambda_m$. Miles (1974) shows that equation (5.11.2) can be used to derive a general expression for the k th moment of the volume V_m of a typical PDC in \mathbb{R}^m :

$$\begin{aligned} E_m V_m^k &= \frac{(m+k-1)! \Gamma\left(\frac{m^2}{2}\right) \Gamma\left(\frac{m^2+mk+k+1}{2}\right) \Gamma\left(\frac{m+1}{2}\right)^{m-k+1}}{(m-1)! \Gamma\left(\frac{m^2+1}{2}\right) \Gamma\left(\frac{m^2+mk}{2}\right) \Gamma\left(\frac{m+k+1}{2}\right)^{m+1} (2^m \pi^{(m-1)/2} \lambda)^k} \\ &\quad \times \prod_{i=2}^{m+1} \left\{ \Gamma\left(\frac{k+i}{2}\right) / \Gamma\left(\frac{i}{2}\right) \right\} \text{ for } k = 1, 2, \dots \end{aligned} \quad (5.11.4)$$

(see also Møller, 1989, Corollary 7.6), where E_m denotes expectation with respect to the Palm distribution of the random tessellation with respect to the typical cell (see Møller, 1989, p. 47). When $m = 2$, this reduces to

$$E_2 V_2^k = \frac{\Gamma\left(\frac{3k+5}{2}\right) \Gamma\left(\frac{k}{2}+1\right)}{3\Gamma\left(\frac{k+3}{2}\right)^2 2^k \pi^{k-1/2} \lambda^k} \text{ for } k = 1, 2, \dots, \quad (5.11.5)$$

while for $m = 3$,

Table 5.11.1 Moments of various characteristics of a Poisson Delaunay diagram in \mathbb{R}^2 .

Moment	Symbol	Exact value	Numerical value
Intensity of cell vertices	λ_0	λ	
Intensity of mid-points of cell edges	λ_1	3λ	
Intensity of cell centroids	λ_2	2λ	
Expected total edge length per unit area	L_A	$32\lambda^{1/2}/(3\pi)$	$3.395\lambda^{1/2}$
Expected number of edges at a typical vertex	$E(E)$	6	
Expected number of cells at a typical vertex	$E(M)$	6	
Expected number of cells at a typical edge	$E(N)$	2	
Expected area of a typical cell, its second moment	$E(A)$	$1/(2\lambda)$	$0.5\lambda^{-1}$
and its k th moment	$E(A^2)$	$35/(8\pi^2\lambda^2)$	$0.443\lambda^{-2}$
Expected perimeter of a typical cell and its second moment	$E(A^k)$	$\Gamma(3k+5)/2)[\Gamma(k/2+1)/(3\Gamma(k+3)/2)]^2 2^{k-1/2}\pi^{k-1/2}\lambda^k$	—
Expected length of a typical edge, its second moment	$E(P)$	$32/(3\pi\lambda^{1/2})$	$3.395\lambda^{-1/2}$
and its k th moment	$E(P^2)$	$125/(3\pi\lambda)$	$13.263\lambda^{-1}$
Expected circumradius, its second moment	$E(L)$	$32/(9\pi\lambda^{1/2})$	$1.132\lambda^{-1/2}$
and its k th moment	$E(L^2)$	$5/(\pi\lambda)$	$1.592\lambda^{-1}$
Expected inradius	$E(L^k)$	$2^{k+3}\Gamma(k+5)/2)[3(k+2)\pi^{(k+1)/2}\lambda^{k/2}]$	—
and its second moment	$E(I)$	$1/(4\lambda^{1/2})$	$0.25\lambda^{-1/2}$
Expected circumradius, its second moment	$E(I^2)$	$1/(4\pi\lambda)$	$0.089\lambda^{-1}$
and its k th moment	$E(R)$	$3/(4\lambda^{1/2})$	$0.75\lambda^{-1/2}$
Expected angle spanned by two edges of a typical cell and its second moment	$E(R^2)$	$2l(\pi\lambda)$	$0.637\lambda^{-1}$
	$E(R^k)$	$\Gamma(k/2+2)(\pi\lambda)^{k/2}$	—
	$E(\alpha)$	$\pi/3$	1.047
	$E(\alpha^2)$	$(4\pi^2 - 15)/18$	1.360

λ = intensity of Θ_p .

Sources: Martin (1965) and Miles (1970a).

Table 5.11.2 Moments of various characteristics of a Poisson Delaunay diagram in \mathbb{R}^3 .

Moment	Symbol	Exact value	Numerical value
Intensity of cell vertices	λ_0	λ	
Intensity of mid-points of cell edges	λ_1	$(24\pi^2/35 + 1)\lambda$	7.768 λ
Intensity of centroids of cell faces	λ_2	$(48/35)\pi^2\lambda$	13.535 λ
Intensity of cell centroids	λ_3	$(24/35)\pi^2\lambda$	6.768 λ
Expected total face area per unit volume	S_v	$(200/27)\Gamma(2/3)(\pi/6)^{13}$	8.085 λ^{13}
Expected total edge length per unit area	L_v	$(24\pi^2/35)(2/3)(\pi/6)^{13}\Gamma(1/3)\lambda^{23}$	9.609 λ^{23}
Expected number of edges at a typical vertex	$E(E)$	$(3/4)^{13}\pi^{-13}\Gamma(1/3)\lambda^{23}$	
Expected number of faces at a typical vertex	$E(F)$	$(48\pi^2/35) + 2$	15.535
Expected number of cells at a typical vertex	$E(M)$	$(144/35)\pi^2$	40.606
Expected number of faces at a typical vertex	$E(G)$	$(96/35)\pi^2$	27.071
Expected number of edges at a typical vertex	$E(N)$	$(144\pi^2)(24\pi^2 + 35)$	5.228
Expected number of edges of a typical cell	$E(V)$	$(144\pi^2)(24\pi^2 + 35)$	5.228
Expected volume of a typical cell and its second moment	$E(V^2)$	$35/(24\pi^2)$	0.148 λ^{-1}
Expected volume of a typical cell and its k th moment	$E(V^k)$	$105/(286\pi^2\lambda^2)$ $35\pi^{12}(k+1)!(k+2)!(2k+4)!$ $\times [256\Gamma(k/2 + 2)^3\Gamma[(9+3k)/2](16\pi\lambda)^k]^{-1}$	0.037 λ^{-2}
Expected surface area of a typical cell and its second moment	$E(S)$	$[3500(3/4)^{25}\Gamma(2/3)]/[243\pi^{53}\lambda^{23}]$	—
Expected area of a typical face and its k th moment	$E(S^2)$	$[350(3/4)^{25}\Gamma(2/3)]/[243\pi^{53}\lambda^{23}]$	2.389 λ^{-23}
Expected total edge length of a typical cell and its second moment	$E(B)$	$E(A)$	6.934 λ^{-43}
Expected perimeter of a typical face and its second moment	$E(P)$	$E(A^k)$	0.597 λ^{-23}
Expected length of a typical edge and its k th moment	$E(L)$	$E(A^k)$	—
Expected mean breadth	$E(b)$	$E(B)$	7.422 λ^{-13}
Expected angle spanned by two edges of a typical face and its second moment	$E(\alpha)$	$E(B^2)$	57.760 λ^{-23}
	$E(\alpha^2)$	$E(P)$	3.711 λ^{-13}
		$E(P^2)$	14.640 λ^{-23}
		$E(L)$	1.237 λ^{-13}
		$E(L^k)$	—
		$E(b)$	1.118 λ^{-13}
		$E(\alpha)$	1.047
		$E(\alpha^2)$	1.270

λ = intensity of Θ_p .

Source: Miles (1970a), Muche (1999).

Table 5.11.3 The first moments of various characteristics of a Poisson Delaunay cell in \mathbb{R}^4 .

Characteristic	Exact first moment	Numerical value
Number of edges at a typical vertex	340/9	37.778
Number of triangles at a typical vertex	590/3	196.667
Number of tetrahedra at a typical vertex	2860/9	317.778
Number of cells at a typical vertex	1430/9	158.889
Number of triangles at a typical edge	177/17	10.412
Number of tetrahedra at a typical edge	429/17	25.235
Number of cells at a typical edge	286/17	16.824
Number of tetrahedra at a typical triangle	286/59	4.847
Number of cells at a typical triangle	286/59	4.487
Number of tetrahedra of a typical cell	2	2
Volume of a typical cell	$9/(286 \lambda)$	$0.031\lambda^{-1}$
Volume of a typical tetrahedron	$(2/\pi^2)^{3/4}(32/385)(14/13)^2(18!/17!)\Gamma(3/4)\lambda^{-3/4}$	$0.192\lambda^{-3/4}$
Area of a typical triangle	$2^{1/2}(2/13)(8/11)^2(17!/16!)\Gamma(1/2)\lambda^{1/2}$	$0.681\lambda^{-1/2}$
Length of a typical edge	$(2/\pi^6)^{1/4}(27/77)(16!/15!)\Gamma(1/4)\lambda^{-1/4}$	$1.3825\lambda^{-1/4}$

λ = intensity of Θ_p .

Source: Christ et al. (1982a, Tables 1 and 2).

Table 5.11.4 Correlation coefficients for the characteristics of a typical Poisson Delaunay cell in \mathbb{R}^2 .

Characteristic		P	I	R
Area	A	0.916	0.921	0.783
Perimeter	P	—	0.878	0.936
Inradius	I	—	—	0.694
Circumradius	R	—	—	—

Source: Miles (1970a, p.113).

$$\mathbb{E}_3 V_3^k = \frac{35\pi^{1/2}(k+1)!(k+2)!(2k+4)!}{256\Gamma\left(\frac{k}{2}+2\right)^3 \Gamma\left(\frac{9+3k}{2}\right)(16\pi\lambda)^k} \quad \text{for } k=1, 2, \dots \quad (5.11.6)$$

Values of $\mathbb{E}_2 V_2^k$ and $\mathbb{E}_3 V_3^k$ for $k = 1, 2$ are given in Tables 5.11.1 and 5.11.2, respectively.

For $m = 2$, Miles (1970a) has also derived the first- and second-order moments of a number of characteristics of a typical PDC (see Table 5.11.1). In addition, the relationship described in equation (5.11.1) allows the derivation of other moment measures for \mathcal{D}_p in \mathbb{R}^2 , \mathbb{R}^3 and \mathbb{R}^4 which are reported in Tables 5.11.1, 5.11.2 and 5.11.3, respectively. Correlation coefficients for pairs of selected characteristics of PDCs in \mathbb{R}^2 have also been obtained by Miles (1970a, Table 1) and are given in Table 5.11.4.

Probability distributions of PDC characteristics are mathematically more tractable than those of PVC characteristics considered in Section 5.5.

Rathie (1992) showed that the moments given in equation (5.11.4) determined the distribution of the volume of a typical PDC uniquely (see Rao, 1973, p. 106) and obtained the pdf $f_{\lambda V_m}$ for the standardized volume (λV_m) of a typical PDC:

$$f_{\lambda V_m}(v) = A_m (2\pi i v)^{-1} \int_Y \nabla_m(k) (B_m v^2)^{-k} dk, \quad v > 0, \quad (5.11.7)$$

where $i = \sqrt{-1}$, Y encloses all the poles of the integrand,

$$A_m = \frac{2^{m-1/2} (m+1)^{m^2/2} \Gamma\left(\frac{m^2}{2}\right) \Gamma\left(\frac{m+1}{2}\right)^m}{\pi m^{(m^2-1)/2} \Gamma(m) \Gamma\left(\frac{m^2+1}{2}\right) \prod_{i=2}^m \Gamma\left(\frac{i}{2}\right)},$$

$$B_m = \left[\frac{2^{m-1} \pi^{(m-1)/2} m^{m/2} \Gamma\left(\frac{m+1}{2}\right)}{(m+1)^{(m+1)/2}} \right]^2,$$

$$\nabla_m(k) = \frac{\prod_{r=2}^m \Gamma\left(\frac{r}{2} + k\right) \prod_{r=0}^m \Gamma\left[\frac{m^2 + 1 + 2r}{2(m+1)} + k\right]}{\prod_{r=1}^{m-1} \Gamma\left(\frac{m}{2} + \frac{r}{m} + k\right) \Gamma\left(\frac{m+1}{2} + k\right)^{m-1}}.$$

The integral in equation (5.11.7) can be evaluated as the sum of the residues at the poles of $\nabla_m(k)$. As a result, $f_{\lambda V_m}(v)$ can be expressed as an infinite series involving gamma, psi and zeta functions (see also Pederzoli, 1995). Rathie also developed a computer program for the numerical calculation of the density and the distribution functions.

In particular, when $m = 2$, the density given in equation (5.11.7) reduces to

$$f_{\lambda V_2}(v) = \left(\frac{8}{9}\right) \pi v K_{1/6}^2 \left(\frac{2\pi v}{3\sqrt{3}}\right), \quad v \geq 0, \quad (5.11.8)$$

where $K_{1/6}$ is the modified Bessel function of order 1/6:

$$K_{1/6}(x) = \sqrt{\pi} \left(\frac{x}{2}\right)^{1/6} \Gamma\left(\frac{2}{3}\right)^{-1} \int_1^\infty \exp(-xt)(t^2 - 1)^{-1/3} dt.$$

See Figure 5.11.1(a).

For $m = 3$, the density for the standardized volume derived from equation (5.11.7) involves a sequence of complicated analytical functions. Muche (1996b), using Miles' formula (5.11.2), obtained the following three-fold integral form for this density, which is more suitable for numerical evaluation:

$$f_{\lambda V_3}(v) = \frac{35}{2} \int_0^{2\pi} \int_0^{2\pi - \alpha_1} \int_0^\pi v \sin \beta \times \exp\left(\frac{-2\pi v}{g(\alpha_1, \alpha_2)(1 + \cos \beta) \sin^2 \beta}\right) d\beta d\alpha_2 d\alpha_1, \quad v \geq 0, \quad (5.11.9)$$

where

$$g(\alpha_1, \alpha_2) = \sin \frac{\alpha_1}{2} \sin \frac{\alpha_2}{2} \sin \frac{\alpha_1 + \alpha_2}{2}. \quad (5.11.10)$$

See Figure 5.11.1(b). He also obtained a two-fold integral expression for the density of the standardized area of a typical PDC in \mathbb{R}^2 given in equation (5.11.8):

$$f_{\lambda V_2}(v) = \frac{\pi v}{6} \int_0^{2\pi} \int_0^{2\pi - \alpha_1} \frac{1}{g(\alpha_1, \alpha_2)} \exp\left(\frac{-\pi v}{2g(\alpha_1, \alpha_2)}\right) d\alpha_2 d\alpha_1, \quad v \geq 0,$$

where the function g is given in equation (5.11.10). The equivalent radius R_m is defined to be the radius of an m -dimensional sphere with volume V_m . The pdfs of R_m for $m = 2$ and $m = 3$ are given in Muche (1996b):

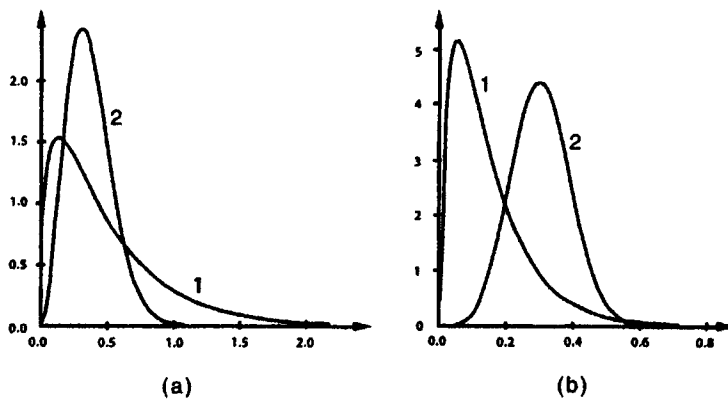


Figure 5.11.1 Probability density functions of (a) (1) the area V_2 and (2) the equivalent radius R_2 of a typical two-dimensional Poisson Delaunay cell; (b) (1) the volume V_3 and (2) the equivalent radius R_3 of a typical three-dimensional Poisson Delaunay cell ($\lambda = 1$). (Source: Muche, 1996b, Figures 1 and 5.)

$$f_{R_2}(r) = \frac{\pi^3 \lambda^2 r^3}{3} \int_0^{2\pi} \int_0^{2\pi - \alpha_1} \frac{1}{g(\alpha_1, \alpha_2)} \exp\left(\frac{-\lambda\pi^2 r^2}{2g(\alpha_1, \alpha_2)}\right) d\alpha_2 d\alpha_1, \quad r \geq 0,$$

$$f_{R_3}(r) = \frac{280\pi^2 \lambda^2 r^5}{3} \int_0^{2\pi} \int_0^{2\pi - \alpha_1} \int_0^\pi \sin \beta \times \exp\left(\frac{-8\pi^2 \lambda r^3}{3g(\alpha_1, \alpha_2)(1 + \cos \beta) \sin^2 \beta}\right) d\beta d\alpha_1 d\alpha_2, \quad r \geq 0,$$

respectively (see Figure 5.11.1). The k th moments are also obtained:

$$E_2 R_2^k = \frac{\Gamma\left(\frac{k+4}{4}\right) \Gamma\left(\frac{3k+10}{4}\right)}{3 \cdot 2^{k/2} \pi^{k-1/2} \Gamma\left(\frac{k+6}{4}\right)^2 \lambda^{k/2}},$$

$$E_3 R_3^k = \frac{35 \cdot 3^{k/3} \Gamma\left(\frac{k}{3} + 2\right) \Gamma\left(\frac{k}{3} + 3\right) \Gamma\left(\frac{2k}{3} + 5\right)}{2^{2k+8} \pi^{2k/3-1/2} \Gamma\left(\frac{k}{6} + 2\right)^3 \Gamma\left(\frac{k+9}{2}\right) \lambda^{k/3}}.$$

A *Gabriel edge* is an edge of a Delaunay cell which intersects the interface between the two Voronoi cells. The length of a typical Gabriel edge E follows a generalized gamma distribution, the density of which is:

$$f_L(l) = \frac{m\lambda\omega_m l^{m-1}}{2^m} \exp\left(-\frac{\lambda\omega_m l^m}{2^m}\right), \quad l > 0,$$

where $\omega_m = \pi^{m/2}/\Gamma(m/2 + 1)$ is the volume of an m -dimensional sphere of unit radius.

Knowledge of the probability distributions of other PDC characteristics is limited to $m = 3$ and $m = 2$. Miles' formula (5.11.2) plays a fundamental role in the derivation of them. For $m = 2$, the pdfs for the perimeter of a typical cell P (Muche, 1996b) and the length of a typical edge L (Collins, 1968; Muche, 1996b) are

$$f_P(p) = \frac{\pi\lambda^2 p^3}{12} \int_0^{2\pi} \int_0^{2\pi-\alpha_1} \frac{g(\alpha_1, \alpha_2)}{\left(\sin \frac{\alpha_1}{2} + \sin \frac{\alpha_2}{2} + \sin \frac{\alpha_1 + \alpha_2}{2}\right)^4} \times \exp\left(\frac{-\lambda\pi p^2}{4\left(\sin \frac{\alpha_1}{2} + \sin \frac{\alpha_2}{2} + \sin \frac{\alpha_1 + \alpha_2}{2}\right)^2}\right) d\alpha_2 d\alpha_1, \quad p \geq 0,$$

$$f_L(l) = \frac{\lambda\pi l}{3} \left(\lambda^{1/2} l \exp\left(\frac{-\lambda\pi l^2}{4}\right) + \frac{2}{\sqrt{\pi}} \int_{(\lambda\pi)^{1/2} l/2}^{\infty} \exp(-x^2) dx \right), \quad l \geq 0,$$

where g is given in equation (5.11.10). See Figure 5.11.2. The k th moments can now be evaluated:

$$\begin{aligned} E(P^k) &= \frac{2^{k+1} \Gamma\left(2 + \frac{k}{2}\right)}{3\pi^{k/2+1} \lambda^{k/2}} \int_0^{2\pi} \int_0^{2\pi-\alpha_1} g(\alpha_1, \alpha_2) \\ &\quad \times \left(\sin \frac{\alpha_1}{2} + \sin \frac{\alpha_2}{2} + \sin \frac{\alpha_1 + \alpha_2}{2}\right)^k d\alpha_2 d\alpha_1, \\ E(L^k) &= \frac{2^{k+1} (k+1)(k+3) \Gamma\left(\frac{k+1}{2}\right)}{3(k+2)\pi^{k+1/2} \lambda^{k/2}}. \end{aligned}$$

Mecke and Muche (1995) showed that the length of an edge emanating from a typical vertex has the same distribution as L . Drouffe and Itzykson (1984) have also estimated $E(L|N)$, the average length of an edge emanating from a vertex, as a function of the number of edges incident at the vertex, which they find grows approximately as $N^{1/2}$.

The joint pdf of the interior angles of a typical PDC was obtained by Miles (1970a):

$$f_{\alpha, \beta}(\alpha, \beta) = \frac{8\pi}{3} [\sin \alpha \sin \beta \sin(\alpha + \beta)], \quad \alpha \geq 0, \beta \geq 0, \alpha + \beta < \pi. \quad (5.11.11)$$

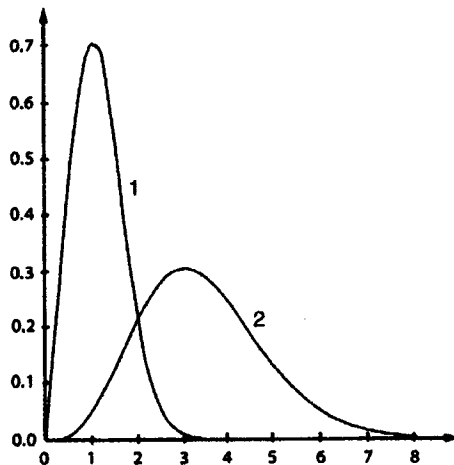


Figure 5.11.2 Probability density functions of (1) the length of an edge L and (2) the perimeter P of a typical two-dimensional Poisson Delaunay cell ($\lambda = 1$). (Source: Muche, 1996b, Figure 6.)

This density attains its maximum at $\alpha = \beta = \pi/3$, which indicates that the most likely triangle in \mathcal{D}_p is an equilateral one. From equation (5.11.11) the marginal density can be derived:

$$f_\alpha(\alpha) = \frac{4}{3\pi} [\sin \alpha + (\pi - \alpha) \cos \alpha] \sin \alpha, \quad 0 \leq \alpha < \pi, \quad (5.11.12)$$

which is the density of a randomly selected angle of a typical triangle of \mathcal{D}_p . This density is illustrated in Figure 5.11.3. Equation (5.11.12) was also obtained by Collins (1968), and the mode of it is at $\alpha = 0.89489$ radians ($51^\circ 16' 24''$). The first two moments are given in Table 5.11.1. Problems in using equation (5.11.12) in empirical applications led to the use of Miles' approach to derive both the densities of the minimum, middle and maximum angles, $f_{\alpha_{\min}}$, $f_{\alpha_{\text{mid}}}$ and $f_{\alpha_{\max}}$, respectively, of a typical PDC. Mardia *et al.* (1977) derived

$$f_{\alpha_{\min}}(\alpha) = \frac{2}{\pi} [(\pi - 3\alpha) \sin 2\alpha + \cos 2\alpha - \cos 4\alpha], \quad 0 \leq \alpha < \frac{\pi}{3}, \quad (5.11.13)$$

and Boots (1986) gave

$$f_{\alpha_{\max}}(\alpha) = \begin{cases} \frac{2}{\pi} [(3\alpha - \pi) \sin 2\alpha - \cos 2\alpha + \cos 4\alpha], & \frac{\pi}{3} \leq \alpha < \frac{\pi}{2}, \\ \frac{4}{\pi} [\sin \alpha + (\pi - \alpha) \cos \alpha] \sin \alpha, & \frac{\pi}{2} \leq \alpha < \pi. \end{cases} \quad (5.11.14)$$

Muche (1999) obtained that

$$f_{\alpha_{\text{mid}}}(\alpha) = \begin{cases} \frac{8}{\pi} [2 \sin^3 \alpha - \sin \alpha + \alpha \cos \alpha] \sin \alpha, & 0 \leq \alpha < \frac{\pi}{3}, \\ \frac{4}{\pi} [\pi - 2\alpha + \sin 2\alpha] \sin 2\alpha, & \frac{\pi}{3} \leq \alpha < \frac{\pi}{2}. \end{cases} \quad (5.11.15)$$

These densities are illustrated in Figure 5.11.3.

Further understanding of the angular properties of \mathcal{D}_p in \mathbb{R}^2 is provided by Kendall (1983) whose approach involves an examination of the shape of Delaunay triangles. Kendall's theory of shape involves associating a triad of labelled points from a pattern with a location in a shape space (for an overview of how this is achieved see Stoyan *et al.*, 1995, pp. 255–273 or Small, 1988, 1996). The particular shape space derived by Kendall is represented as a flat, curvilinear triangle referred to as the spherical blackboard. This is illustrated in Figure 5.11.4(a) which also shows triangles of representative shapes located at the appropriate positions. Figure 5.11.4(b) shows the shapes of 5000 PDCs obtained by Kendall using the simulation procedure described in Section 5.4. This clearly illustrates the dominance of more equilateral shapes.

For $m = 3$, Kumar and Kurtz (1994b) derived the pdf of the angle α in a typical face spanned by two of its edges:

$$f_\alpha(\alpha) = \frac{4}{3\pi^2} [2(\pi - \alpha)(2 + \cos 2\alpha) + 3 \sin 2\alpha] \sin^2 \alpha, \quad 0 \leq \alpha \leq \pi,$$

which was again obtained by Muche (1996b; 1999), who also derived the pdfs for the minimum, middle and maximum interior angles of a typical face, $f_{\alpha_{\min}}$, $f_{\alpha_{\text{mid}}}$ and $f_{\alpha_{\max}}$, respectively:

$$f_{\alpha_{\min}}(\alpha) = \frac{8}{\pi^2} [(\pi - 3\alpha)(3 - 2 \sin^2 \alpha) - (16 \sin^4 \alpha - 9) \sin \alpha \cos \alpha] \sin^2 \alpha, \quad 0 \leq \alpha < \pi/3,$$

$$f_{\alpha_{\text{mid}}}(\alpha) = \begin{cases} \frac{16}{\pi^2} [\alpha(3 - 2 \sin^2 \alpha) - (3 - 8 \sin^4 \alpha) \sin \alpha \cos \alpha] \sin^2 \alpha, & 0 \leq \alpha < \pi/3, \\ \frac{16}{\pi^2} [(\pi - 2\alpha)(3 - 2 \sin^2 \alpha) - 2(4 \sin^4 \alpha - 3) \sin \alpha \cos \alpha] \sin^2 \alpha, & \pi/3 \leq \alpha < \pi/2, \end{cases}$$

$$f_{\alpha_{\max}}(\alpha) = \begin{cases} \frac{8}{\pi^2} [(3\alpha - \pi)(3 - 2 \sin^2 \alpha) - (9 - 16 \sin^4 \alpha) \sin \alpha \cos \alpha] \sin^2 \alpha, & \pi/3 \leq \alpha < \pi/2, \\ \frac{8}{\pi^2} [(\pi - \alpha)(3 - 2 \sin^2 \alpha) + 3 \sin \alpha \cos \alpha] \sin^2 \alpha, & \pi/2 \leq \alpha < \pi. \end{cases}$$

These densities are illustrated in Figure 5.11.5.

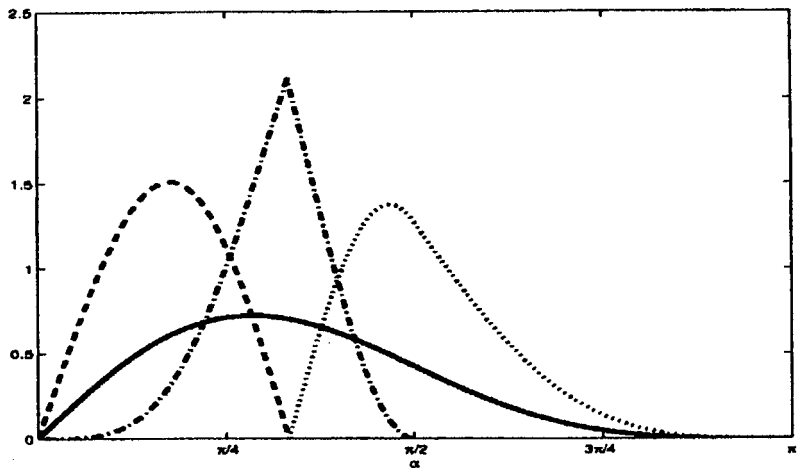


Figure 5.11.3 Probability density functions of interior angles of a typical PDC in \mathbb{R}^2 : — randomly selected angle α ; - - - minimum α_{\min} ; · · · middle α_{mid} ; · · · · maximum α_{\max} of the three angles of a typical cell.

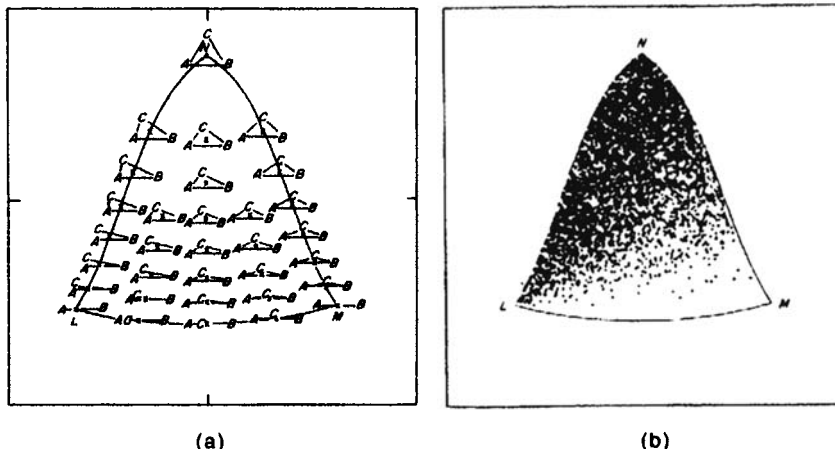


Figure 5.11.4 (a) The spherical blackboard showing 32 triangles located according to their shapes. (b) 5000 Poisson Delaunay cells in \mathbb{R}^2 located on the spherical blackboard. (Source: (a) Kendall, 1981; (b) Kendall, 1983.)

Muche (1996b, 1999) also established the pdfs for the surface area S , the total edge length B and the mean breadth \bar{b} of a typical PDC in \mathbb{R}^3 , the area A and the perimeter P of a typical face, and the length L of a typical edge. Denote by p_0, p_1, p_2 and p_3 the four vertices of a PDC in \mathbb{R}^3 and by c the centre of the sphere on whose surface the vertices lie. Consider the spherical coordinate system (distance, polar angle, amplitude). The locations of the vertices relative to c can be expressed in terms of seven parameters:

$$\begin{aligned} p_0 - c &= \left(r, \beta, -\frac{\alpha_1}{2} \right), & p_1 - c &= \left(r, \beta, \frac{\alpha_1}{2} \right), \\ p_2 - c &= \left(r, \beta, \frac{\alpha_1}{2} + \alpha_2 \right), & p_3 - c &= (r, \cos^{-1}(\cos \beta - h), \eta). \end{aligned}$$

Denote the corresponding unit vectors by $\mathbf{u}_i = (p_i - c)/r$. Let $t_{ij} = \|\mathbf{u}_i - \mathbf{u}_j\|$, $i, j = 0, 1, 2, 3$, $i \neq j$, be the distance between \mathbf{u}_i and \mathbf{u}_j , and $a_i = a_i(\mathbf{u}_i, \mathbf{u}_k, \mathbf{u}_l)$, where i, j, k, l are distinct elements from $\{0, 1, 2, 3\}$, be the area of the triangle spanned by $\mathbf{u}_j, \mathbf{u}_k, \mathbf{u}_l$. Furthermore, let κ_{ij} , $i, j = 0, 1, 2, 3$ and $i \neq j$, be the angle between the normal vectors of these two faces adjacent to the edge spanned by p_i and p_j . The pdfs are

$$\begin{aligned} f_S(s) &= \frac{70\lambda^3}{9} \int_0^{2\pi} \int_0^{2\pi-\alpha_1} \int_0^\pi \int_0^{2\pi} \int_0^{1+\cos\beta} \frac{hs^{7/2} g(\alpha_1, \alpha_2)^2 \sin^5 \beta}{(a_0 + a_1 + a_2 + a_3)^{9/2}} \\ &\quad \times \exp\left(-\frac{4\pi\lambda}{3} \frac{s^3/2}{(a_0 + a_1 + a_2 + a_3)^{3/2}}\right) dh d\eta d\beta d\alpha_2 d\alpha_1, \quad s \geq 0, \end{aligned}$$

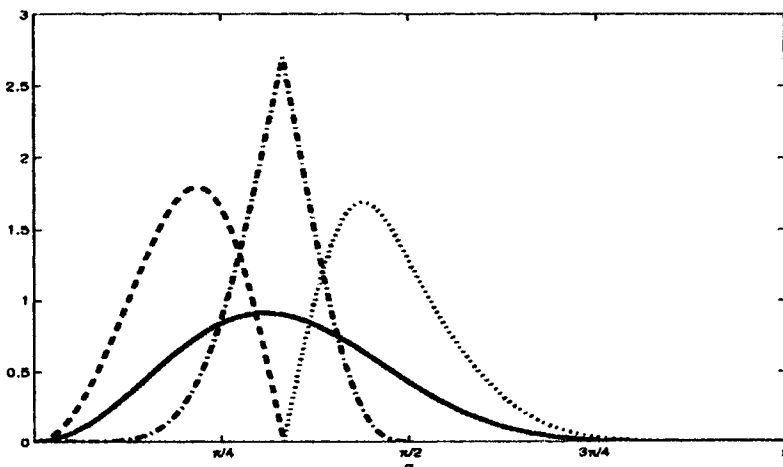


Figure 5.11.5 Probability density function of interior angles of a typical face of a PDC in \mathbb{R}^3 : — randomly selected angle α ; - - - minimum α_{\min} ; · - middle α_{mid} ; . . . maximum α_{\max} of the three interior angles of a typical face.

$$\begin{aligned}
f_B(b) &= \frac{140\lambda^3}{9} \int_0^{2\pi} \int_0^{2\pi-\alpha_1} \int_0^\pi \int_0^{2\pi} \int_0^{1+\cos\beta} \frac{hb^8 g(\alpha_1, \alpha_2)^2 \sin^5 \beta}{(t_{01} + t_{02} + t_{03} + t_{12} + t_{13} + t_{23})^9} \\
&\quad \times \exp\left(-\frac{4\pi\lambda}{3} \frac{b^3}{(t_{01} + t_{02} + t_{03} + t_{12} + t_{13} + t_{23})^3}\right) dh d\eta d\beta d\alpha_2 d\alpha_1, \quad b \geq 0, \\
f_{\bar{b}}(\bar{b}) &= \frac{140(4\pi^9)\lambda^3}{9} \int_0^{2\pi} \int_0^{2\pi-\alpha_1} \int_0^\pi \int_0^{2\pi} \int_0^{1+\cos\beta} \frac{h(\bar{b})^8 g(\alpha_1, \alpha_2)^2 \sin^5 \beta}{\left(\sum_{i,j=0,\dots,3, i \neq j} t_{ij} \kappa_{ij}\right)^9} \\
&\quad \times \exp\left(-\frac{(4\pi)^4 \lambda}{3} \frac{(\bar{b})^3}{\left(\sum_{i,j=0,\dots,3, i \neq j} t_{ij} \kappa_{ij}\right)^3}\right) dh d\eta d\beta d\alpha_2 d\alpha_1, \quad \bar{b} \geq 0, \\
f_A(a) &= \frac{35\pi\lambda^3}{72\sqrt{2}} \int_0^{2\pi} \int_0^{2\pi-\alpha_1} \int_0^\pi \frac{a^{7/2} (1 + \cos\beta)^2}{g(\alpha_1, \alpha_2)^{5/2} \sin^4 \beta} \\
&\quad \times \exp\left(\frac{-\sqrt{2} \pi \lambda a^{3/2}}{3g(\alpha_1, \alpha_2)^{3/2} \sin^4 \beta}\right) d\beta d\alpha_2 d\alpha_1, \quad a \geq 0, \\
f_p(p) &= \frac{35\pi\lambda^3}{2^7 \cdot 9} \int_0^{2\pi} \int_0^{2\pi-\alpha_1} \int_0^\pi \frac{p^8 g(\alpha_1, \alpha_2)^2 (1 + \cos\beta)^2}{\sin^4 \beta \left(\sin \frac{\alpha_1}{2} + \sin \frac{\alpha_2}{2} + \sin \frac{\alpha_1 + \alpha_2}{2}\right)^9} \\
&\quad \times \exp\left(\frac{-\lambda \pi p^3}{6 \sin^3 \beta \left(\sin \frac{\alpha_1}{2} + \sin \frac{\alpha_2}{2} + \sin \frac{\alpha_1 + \alpha_2}{2}\right)^3}\right) d\beta d\alpha_2 d\alpha_1, \quad p \geq 0, \\
f_L(l) &= \frac{35\pi^2 \lambda^3}{2^7 \cdot 9} \int_0^{\pi/2} \int_0^{\pi/2} \frac{l^8 (2 - \sin^2 \beta) (3 - 2 \sin^2 \phi)}{\sin^4 \beta \sin^7 \phi} \\
&\quad \times \exp\left(\frac{\pi \lambda l^3}{6 \sin^3 \beta \sin^3 \phi}\right) d\phi d\beta, \quad l \geq 0,
\end{aligned}$$

where g is given in equation (5.11.10). See Figure 5.11.6.

Muche (1998) derived an equivalent one-fold integral form for f_L in the case $m = 3$:

$$\begin{aligned}
f_L(l) &= \frac{35\pi\lambda l^2}{2^8} \left[\left(\frac{\pi\lambda l^3}{4} + \frac{5}{2} \right) \exp\left(-\frac{\pi\lambda l^3}{6}\right) \right. \\
&\quad \left. - \frac{\pi\lambda l^2}{3} \int_{1/2}^{\infty} \left(1 + \frac{\pi\lambda l^2 x}{6} \right) \exp\left(-\frac{4\pi\lambda x^3}{3}\right) dx \right], \quad l \geq 0.
\end{aligned}$$

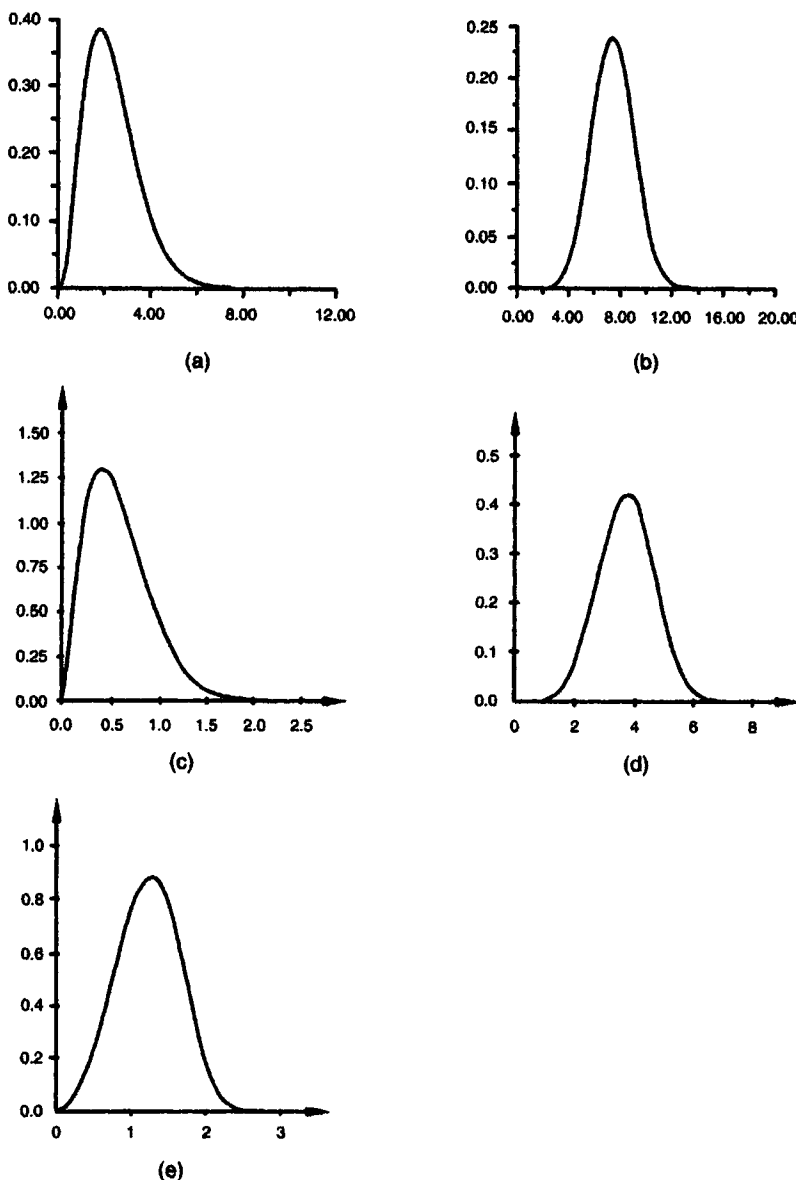


Figure 5.11.6 Probability density functions of (a) the total surface area S ; (b) the total edge length B of a typical cell; (c) the area A ; (d) the perimeter P of a typical face; (e) the length L of a typical edge of a three-dimensional Poisson Delaunay tessellation ($\lambda = 1$). (Sources: (a), (b) Muche, 1999; (c)–(e) Muche, 1996b, Figures 2, 3 and 4.)

The k th moments of A and L can be derived from their densities:

$$\begin{aligned} E(A^k) &= \frac{35 \cdot 3^{2k/3} (k+4) \Gamma\left(\frac{2k}{3} + 3\right) \Gamma(k+3) \Gamma\left(\frac{3k}{2} + 4\right)}{2^{10k/3+9} \pi^{2k/3-1/2} \Gamma\left(\frac{k}{2} + 2\right)^3 \Gamma\left(k + \frac{9}{2}\right) \lambda^{2k/3}}, \\ E(L^k) &= \frac{35}{32} \frac{(k+8)(k+6)}{(k+7)(k+5)(k+3)} \Gamma\left(3 + \frac{k}{3}\right) \left(\frac{6}{\pi\lambda}\right)^{k/3}, \end{aligned}$$

whilst the first and/or second moments of S , B , \bar{b} , P and α are given in Table 5.11.2. As in the case $m = 2$, the length of an edge emanating from a typical vertex has the same distribution as L (Mecke and Muche, 1995).

Kumar and Kurtz (1994b) simulated 1.2 million PDCs in \mathbb{R}^3 . They found that the distributions of the volume V and surface area S of a typical cell, and the face area A of a typical face, can be approximated by a gamma distribution, whilst those of the total edge length of a typical cell and the perimeter of a typical face can be approximated by a normal distribution.

With regard to an s -dimensional section of \mathcal{D}_p in \mathbb{R}^m , which is denoted by $\mathcal{D}_p(s, m)$, note that $\mathcal{D}_p(2, 3)$ consists of triangles and quadrilaterals while $\mathcal{D}_p(3, 4)$ consists of polyhedra with four and five faces and that the plane section of $\mathcal{D}_p(3, 4)$ contains polygons with three, four and five sides (Miles, 1986a, p. 153).

So far the only work on the nature of \mathcal{D} from the various generalizations of \mathcal{V} discussed in Section 3.7 has been that of Miles (1971) on the nature of the Delaunay tessellation \mathcal{D}_s for p random points distributed on the surface of a sphere of unit radius and centred at the origin o in \mathbb{R}^3 . In this case \mathcal{D}_s has $2p-4$ triangular faces and $3p-6$ edges. The expected area of a typical face $E(A)$ is given by

$$E(A) = \frac{2\pi}{p-2}. \quad (5.11.16)$$

In addition, Miles (1971, p. 167, equation (7.6)) derived an expression for the probability distribution of \mathcal{D}_s but was not able to evaluate it.

5.12 OTHER RANDOM VORONOI DIAGRAMS

If, as a result of comparing the characteristics of an empirical tessellation with those of the Poisson Voronoi diagram, \mathcal{V}_p , we determine that the latter is inappropriate as a model of the former or if we have other evidence that supports this viewpoint, we may wish to consider other random tessellations as models. One approach is to modify the properties of the homogeneous Poisson point process Θ_p (see Section 1.3.3) which provides the generator set for \mathcal{V}_p . For example, the independent scattering property of Θ_p means that

there is no constraint on interpoint distances, while in empirical situations inhibitive or repulsive effects may limit how closely individual points can be located with respect to others. If such limits are imposed, the locations of the points in \mathbb{R}^m are more dispersed than they would be in Θ_p . Following established convention in point pattern analysis (see Section 8.1), we label the resulting pattern of points as regular. In some areas of application in the natural sciences such patterns are also referred to as ordered. Alternatively, we may permit the intensity of the point process to vary spatially or randomly according to certain distributions, i.e. we consider an inhomogeneous point process or a compound point process (see Section 1.3.3). The resulting pattern of points is one in which there is a relative concentration of points in some regions of \mathbb{R}^m and a relative absence in others. Again following convention, we refer to such patterns as disordered.

In this section we briefly review different point processes which have been used to create generator sets for Voronoi diagrams. We do not report results for these diagrams although Table 5.12.1 provides a summary of the studies known to the authors together with a listing of the characteristics examined in them. We also note that, with the exception of those studies by Finney (1970a, 1975a), where the point locations are measured from laboratory models of sphere packings in \mathbb{R}^3 , and Lemaître *et al.* (1991, 1992, 1993) and Gervois *et al.* (1992) which involve hard discs moving on an air table, all studies report estimates from Monte Carlo simulations.

We begin by considering processes that produce point patterns which are more regular than those generated by Θ_p . A common feature of many of these processes is that a minimum interpoint distance r is specified. In one group of processes, collectively known as *hard core processes*, this constraint is imposed on points generated by Θ_p . The process is equivalent to a random packing of equal discs or spheres in \mathbb{R}^2 and \mathbb{R}^3 , respectively, if the resulting points are considered to be the centres of non-intersecting discs or spheres of diameter r (see Section 7.1). If we are concerned with a bounded region, B , of \mathbb{R}^3 , hard core processes terminate when either a previously specified number of points has been located in B or it is no longer possible to add more points in B without violating the minimum interpoint distance. The latter case is referred to as *complete random packing*. In either case the process can be characterized by the *packing density* which is the proportion of B that is occupied by discs or spheres. Hard core processes may take a variety of forms. In the *simple sequential inhibition (SSI) process* (Hasegawa and Tanemura, 1980; Tanemura and Hasegawa, 1980; Lotwick, 1982; Hanson, 1983) also referred to as *random sequential adsorption (or addition) (RSA)* (Feder, 1980), discs of fixed diameter r are located sequentially in B until the specified number of discs is obtained (or complete random packing is achieved). At each step the location of the centre of the next disc is chosen uniformly at random from those points which ensure that no two discs overlap. Voronoi diagrams of points located by SSI processes have been used in various applications. These include use as models of non-periodic micro-structure in examinations of the effects of defects on elastic and compressive

Table 5.12.1 Studies of other random Voronoi and Delaunay cells.

Study	R ^m	Model type	Characteristics
Boots (1977)	2	CP SSI	N
Boots (1982)	2	CP	N
Boots (1984)	2	DL	N
Burger <i>et al.</i> (1988)	2	CA DL	A N L _D
Finney (1970a)	3	HC	A F N V
Finney (1975a)	3	RA	R N
Fraser (1991)	2	RA	A L N
Fraser <i>et al.</i> (1990)	2	RA	L N
Fraser <i>et al.</i> (1991)	2	RA	L
Frost and Thompson (1987a)	2	SSI	A L N α
Frost and Thompson (1987b)	2	SSI	A N
Gervois <i>et al.</i> (1992)	2	RA	$A_n m_n$
Gotoh (1983)	3	RA SSI TL	A
Hanson (1983)	3	SSI	F M N V
Hasegawa and Tanemura (1980)	2	SSI	L _D
Heinrich and Schüle (1995)	2	PC TP	A N P
Hermann <i>et al.</i> (1989)	2	TP	A
Hutchings and Discombe (1986)	2	DL PC	A L _D
Icke and van de Weygaert (1987)	2	SSI SC	A L N P α
Kumar <i>et al.</i> (1997)	2	DL TP	N
	3	DL	F
Le Caér and Ho (1990)	2	RM	A L N P A _D L _D P _D
Lemaître <i>et al.</i> (1991)	2	RA	L _D α_D
Lemaître <i>et al.</i> (1992)	2	RA SSI	N
Lemaître <i>et al.</i> (1993)	2	RA	A N P
Lorz and Hahn (1993)	3	PC TP	B E F M N S V \bar{b} f_3 g_3 α_3
Marcelpoil and Usson (1992)	2	DL	A P
Møller <i>et al.</i> (1989)	3	TP	M S V h
Moukarzel and Herrmann (1992)	2	DL	A N P L _D
Mulheran and Blackman (1995)	2	TP	A
Smalley (1966)	2	SSI	N
Szeto and Tam (1995)	2	DL	A P
Tanemura and Hasegawa (1980)	2	SSI	A N L P α
van de Weygaert (1994)	3	PC SSI	A B E F L M N P S V j_2 j_3 α_1 α_3
Vincent and Howarth (1982)	2	TP	N L _D α_D
Wilkinson (1988a)	2	CA	A
Zaninetti (1992)	2	RM SO	A
	3	SO	V
Zhang <i>et al.</i> (1996)	2	SSI	L _D

Model type:

CA Cluster amplification
 CP Compound Poisson
 DL Displaced lattice
 HC Hard core
 PC Poisson cluster
 RA Re-arrangement

RM Random matrix
 SC Sequential clustering
 SO Sobol
 SSI Simple sequential inhibition
 TL Thinned lattice
 TP Thinned Poisson

Table 5.12.1 cont.**Characteristics:***Three Dimensions*

Voronoi cells:

<i>A</i>	Area/face	<i>V</i>	Volume
<i>B</i>	Total edge length/cell	<i>b̄</i>	Mean breadth
<i>E</i>	Edges/cell	<i>h̄</i>	Mean height
<i>F</i>	Faces/cell	<i>f₃</i>	Cell shape factor $6V/(\pi b^3)$
<i>L</i>	Edge length	<i>g₃</i>	Cell shape factor $6\sqrt{\pi} V/S^{3/2}$
<i>M</i>	Vertices/cell	<i>j₂</i>	Face shape factor $4\pi A/S^2$
<i>N</i>	Edges/face	<i>j₃</i>	Cell shape factor $36\pi V^2/S^3$
<i>P</i>	Total edge length/face	α_1	Dihedral angle on a typical edge
<i>S</i>	Surface area	α_3	Randomly selected dihedral angle between adjacent faces

Two Dimensions

Voronoi cells:

<i>A</i>	Area
<i>L</i>	Edge length
<i>N</i>	Vertices
<i>P</i>	Perimeter
α	Interior angle
A_n	Area of an <i>n</i> -edged cell
m_n	Vertices of a neighbouring cell of an <i>n</i> -edged cell

Delaunay cells:

<i>A_D</i>	Area
<i>L_D</i>	Edge length
<i>P_D</i>	Perimeter
α_D	Interior angle

failure properties (Silva and Gibson, 1997; Silva *et al.*, 1995), granular structure of rocks in microfracturing (Malan and Napier, 1995), porous cellulose acetate membrane (Jafferali *et al.*, 1996), spatially non-differentiated tissue such as that found in the liver (Blackburn and Dunckley, 1996), and populations of anchorage-dependent animal cells developing on surfaces (Lim and Davies, 1990). Such Voronoi diagrams have also been used as initial states for two-dimensional models of soap froth (Weaire and Kermode 1984; Weaire and Lei, 1990; Kermode and Weaire, 1990) and dry foams (Herdle and Aref, 1992).

An alternative approach involves *thinning processes* in which first a specified number of points is generated in *B* using Θ_p and then points are removed in various ways until the minimum interpoint distance constraint is satisfied for all remaining points (Vincent and Howarth, 1982; Hermann *et al.*, 1989; Lorz and Hahn, 1993; Heinrich and Schüle, 1995).

Another hard core process involves a *re-arrangement process* (Finney, 1975a; Fraser, 1991). Initially, a set of points is generated by Θ_p . Then, for any pair of points separated by a distance less than *r*, the points are moved apart along a line passing through them until their interpoint distance is equal to *r*. This procedure is repeated until the minimum interpoint distance condition is met. Fraser *et al.* (1990, 1991) use a variant of this process to define the initial state for a solid-liquid transition model.

As discussed in Section 1.3.3, a Gibbs point process can produce a hard core process with minimum interpoint distance *r* if the pair potential is infinite when the distance between two points is less than *r*. Davy and Guild

(1988) use the Voronoi diagram generated by such a Gibbs point process to study composite materials consisting of spherical filler particles. Kuroda and Tanemura (1992) establish limit theorems for the Voronoi diagram generated by a more general Gibbs point process in which the pair potential function is non-negative.

Hasegawa *et al.* (1981) propose a variant of the SSI version of the hard core process which they label *Voronoi polygonal areal random packing*. It involves defining a minimum size, a , for the Voronoi polygon associated with a point. Initially, three points are located in B according to Θ_p . A new point is then selected at random and the Voronoi diagram of the points is generated. The new point is retained only if the sizes of individual Voronoi polygons exceed a . This procedure is continued until no additional points can be located in B without violating the minimum size constraint.

An alternative way of generating point patterns which are more regular than those resulting from Θ_p is to take a completely ordered situation such as the point lattices described in Section 8.1 and to introduce a random component. One way of doing this is to use a thinning process in which lattice points are deleted randomly according to a specified probability (Gotoh, 1993). Mulheran and Blackman (1995) use the Voronoi diagram of a randomly thinned square lattice to model the growth of a surface film.

Another way involves *displaced lattice processes*. If d is the distance separating neighbouring points on a lattice, a displaced lattice process involves moving each lattice point a distance $\alpha\beta d$ in a random direction ϕ ($0 \leq \phi < 2\pi$) where β is a displacement function and α is a random value ($0 < \alpha < 1$). As $\beta \rightarrow 1$, the points of the displaced lattice tend to Θ_p . Most applications of Voronoi diagrams for displaced lattice points involve triangular or square lattices in \mathbb{R}^2 and include using such structures in analyses of polycrystalline materials. For example, they have been used to explore the effects on such materials of monotonic and cyclic loadings (Cannmo *et al.*, 1995), to consider how disorder in local conductances and in local connectivity affects global conductance (Priolo *et al.*, 1992), to model zinc oxide varistors (Bartkowiak and Mahan, 1995), and as the basis of a two-phase model of ferritic-austenitic stainless duplex steel (Werner *et al.*, 1994). Applications involving lattices in \mathbb{R}^3 include the study of the large-scale distribution of galaxies (SubbaRao and Szalay, 1992) (see also Section 7.2).

Le Caér and Ho (1990) provide another point process in \mathbb{R}^2 which is more regular than Θ_p and which is associated with the eigenvalues of random matrices. For an ensemble of asymmetric $(n \times n)$ complex random matrices, M_n , in which the real and imaginary parts of the matrix elements are independently and identically distributed according to a Gaussian distribution with mean, μ , and standard deviation, $\sigma/\sqrt{2}$, the eigenvalues of $M_n/n^{1/2}$ are distributed uniformly over a disc of radius σ . The eigenvalues also display an inhibitive effect since the probability of finding two identical eigenvalues in such matrices is zero. Furthermore, this process is unique in the statistical sense, isotropic whatever the value of n and homogeneous when $n \rightarrow \infty$ (see Section 1.3.3 for a discussion of isotropy and homogeneity in point processes).

These properties led Le Caér and Ho (1990) to suggest that the resulting Voronoi diagram, which they label the *random matrix Voronoi diagram*, could be used in the same normative fashion as V_p .

Another process which is more regular than Θ_p involves *Sobol points* (Zaninetti, 1992). The locations of the points are determined by a Sobol sequence which generates numbers between 0 and 1 directly as binary fractions of length w from a set of w special binary fractions, $V_i = 1, 2, \dots, w$, called *direction numbers*.

Less effort has been expended on Voronoi diagrams associated with point patterns more disordered than those resulting from Θ_p . Disordered point patterns can be generated by inhomogeneous or compound point processes. One example is provided by the *negative binomial process* in which the intensity of Θ_p is random and follows a gamma distribution. In such a process the number of points in a subarea follows a negative binomial distribution. We can further allow the intensity to vary spatially in a negative binomial process. Divide \mathbb{R}^m into many non-overlapping subsets. The random intensities in such subsets are independent and follow the same gamma distribution. Then the intensity of the point process varies spatially and in each arbitrary region the number of points still follows a negative binomial distribution. Boots (1977, 1982) reports on Voronoi diagrams for point processes generated in this way in \mathbb{R}^2 .

An alternative way of making Θ_p more disordered occurs in *Poisson cluster processes*. Such processes involve three steps. First, a set of locations for cluster centres in B is defined using Θ_p . Then a random variable describing the number of points in each cluster is generated from a specified probability distribution. Finally, the points in each cluster are distributed with respect to the cluster centre according to some spatial process. Hutchings and Discombe (1986), Hermann *et al.* (1989), Lorz and Hahn (1993), and Heinrich and Schüle (1995) describe characteristics of Voronoi diagrams for points generated by a Poisson cluster process where the number of points in a cluster has a Poisson distribution and where the points are distributed according to Θ_p over a circle (or sphere) of fixed radius centred on the cluster centre.

Burger *et al.* (1988) and Wilkinson (1988a) use the opposite of the thinning process described above to generate points which are more disordered than those of Θ_p . We label this a *cluster amplification process*. First a set of points is generated by Θ_p with intensity λ . Then any point which is farther than a critical distance, $\alpha\lambda^{1/2}$ ($0 < \alpha < 1$), from any other point is removed. The points removed in this way are replaced by an equivalent number of points located in B according to Θ_p . These steps are then repeated until the critical distance condition is satisfied. Note that as $\alpha \rightarrow 1$, the cluster amplification process tends to Θ_p .

Finally, we note that Icke and van de Weygaert (1987) describe a *sequential clustering process* in which an initial point is located at random in B and then each subsequent point is located at a distance $r = -\alpha \log d$ ($\alpha \geq 0$), where d is a random number ($0 \leq d \leq 1$), and a random direction ϕ ($0 \leq \phi < 2\pi$) from the previous point. As $\alpha \rightarrow \infty$, the process approaches Θ_p .

Voronoi diagrams generated by different point process are rather similar. For example, they are all regular and normal (see Property IV5 in Section 5.1). The first moments of cell characteristics may not vary too much (see Table 5.1.1 in Section 5.1). It may be desirable to have some statistical methods to distinguish different Voronoi diagrams. A natural way is to recognize the generator of each Voronoi cell by using Property V15 in Section 2.3 and then spatial point process statistics (see, for example, Diggle, 1983; Ripley, 1988; Cressie, 1991; Stoyan *et al.*, 1995) can be applied. However, empirical situations involving three-dimensional structures are often studied by means of planar sections (see Section 5.7). Since we are not able to construct the three-dimensional point process of the generators from a planar section of a Voronoi diagram, Krawietz and Lorz (1991) and Hahn and Lorz (1994) propose using stereological methods. Several tests are suggested to test whether a given Voronoi diagram is a Poisson Voronoi diagram or not. They find empirically that it is easier to distinguish a Poisson Voronoi diagram from a more disordered Voronoi diagram than from a more regular one. Among the tests they consider, the most powerful one is based on the variance of the cell areas of sectional Voronoi diagrams.